universität wien

DISSERTATION

Titel der Dissertation

"Structural characterization and interaction studies of myopodin isoform A with Z-disc binding partners"

Verfasser

Eduardo Henrique Salviano Bezerra

angestrebter akademischer Grad

Doctor of Philosophy (PhD)

Wien, 2015

Studienkennzahl lt. Studienblatt:	A 794 685 490
Dissertationsgebiet lt. Studienblatt:	Molekulare Biologie
Betreuerin:	Univ. Prof. Dr. Kristina Djinovic-Carugo

Table of contents

ACKNOWLEDGEMENTS

First, I would like to express my gratitude to my supervisor, Prof. Kristina Djinovic-Carugo, who gave me the opportunity to work in her group and who guided throughout my PhD. Her intensive support and scientific knowledge were precious for the success of my work and keep my enthusiasm for structural biology all these years.

Thanks to all the members of the laboratory for the pleasant working atmosphere. Especially Irina Grishkovskaya for her pacience and guidance in my experiments, Euripedes Ribeiro, Nikos Pinotsis and Gustavo Bezerra for the technical advices and scientific discussions.

I would like to thank to my PhD committee members, Prof. John Victor Small, Prof. Robert Konrat, and Prof. Dieter Fürst. They provided helpful advice and critical suggestions to the development of my work.

I would like to thank to my thesis reviewers, Prof. Matthias Wilmanns, and Prof. Marie-Louise Bang. I am really grateful for assigning your precious time to evaluate my thesis.

I would like to thank to my thesis examiners, Prof. Robert Konrat, Prof. Tim Clausen and Prof. Marie-Louise Bang for their participation in my defense.

I would like to acknowledge my collaborators. Georg Kontaxis and Prof. Robert Konrat for the kindly help with the NMR work. I thank Prof. Dieter Fürst and Peter van der Ven in Bonn University, Germany, for their support and discussions in the interpretation of my work in the light of cell biology.

Finally, I thank for the strength and education my parents provide me. I am sincerely grateful for the hard work and fighting spirit inherited from them. Denise, I thank you for your never-ending patience, understanding and support. Without you beside me I could not have reached so far. My family, fundamental pillar of my life.

Abstract

Myopodin is a member of the Podin family, a group of proteins widely expressed in muscle cells. Expression of myopodin has been observed at the early stages of the myofibrillogenesis process. In differentiated muscle cells myopodin is extensively found in the Z-discs, where it associates with several other fundamental components of the Z-disc, such as actin, α-actinin 2 and filamin C. Myopodin interacts with these proteins mostly through its central domain, a region conserved for all myopodin isoforms. The longest isoform of myopodin expressed in cardiomyocytes, myopodin A, possesses a PDZ domain at the N-terminus. This region of myopodin is responsible for its binding to the C-terminus of α-actinin-2, intermediate filament protein synemin and VPS18. The main aim of my thesis was to structurally and biochemically characterize the binding of myopodin to the selected binding partners and thus understand the function of myopodin in muscle cells. In this respect, by using ITC, I was able to measure differences in the affinities between PDZ domain of myopodin and C-terminal peptide of synemin, VPS18 and α-actinin 2. These complexes were successfully crystallized and their structures solved non-conventional binding of the peptide to the myopodin's PDZ has been observed in all structures. In addition, the data obtained from X-ray structure models of the individual complexes helped to uncover the structural determinants responsible for different binding affinities of the studied binding partners. Furthermore, while studying the biochemical properties of myopodin with SEC-MALLS at reducing and oxidizing conditions, differences in oligomeric state of the myopodin were observed. As this suggests, the actin bundling activity of myopodin central domain is achieved by two independent F-actin binding sites. We observed a dissociation constant of 2.0 μM using MST experiments for myopodin central domain and filamin C Ig d18-21 complex. However, it was suggested that phosphorylation of three serine sites of myopodin central domain regulates this interaction. In order to evaluate the phosphorylation effect, a phosphomimetic mutant of the myopodin central domain was generated. The binding affinity of filamin C fragment for the mutant was found to be dramatically reduced, suggesting down-regulation of the interaction by phosphorylation. Characterization of myopodin "hot spot" interaction sites, PDZ and central domain, can explain the dynamic that drives myopodin in different cell events based on the interaction with different binding partners with different binding affinities.

Zusammenfassung

Myopdin ist ein Mitglied der Podinfamilie, eine Gruppe von Proteinen, die in Muskelzellen exprimiert wird. Die Expression von Myopodin wurde in früheren Stadien der Myofibrillogenese beobachtet. In differenzierten Muskelzellen findet man Myopodin in den Z-Scheiben, wo es mit einigen fundamentalen Komponenten der Z-Scheibe interagiert wie Aktin, α-Aktinin-2 und Filamin C. Myopodin interagiert mit diesen Proteinen hauptsächlich über ihre zentrale Domäne, eine Region, die in allen Isoformen konserviert ist. Die längste in Kardiomyozyten exprimierte Isoform von Myopodin, Myopodin A, enthält auch eine PDZ-Domäne am N-Terminus. Dieser Teil von Myopodin ist verantwortlich für die Bindung an den C-Terminus von α-Aktinin-2, an das Intermediärfilament Synemin und VPS18. Das Hauptziel dieser Arbeit war, die Bindung von Myopodin mit ausgewählten Bindepartner strukturell und biochemisch zu charakterisieren um so die Funktion von Myopodin in Muskelzellen zu verstehen. Vor diesem Hintergrund war es mir möglich, Unterschiede in den Affinitäten zwischen der PDZ-Domäne von Myopodin und den C-terminalen Peptiden von Synemin, VPS18 und α-Aktinin-2 mittels ITC zu messen. Diese Komplexe wurden auch erfolgreich kristallisiert und deren Struktur gelöst. In allen Strukturen wurde die nicht-konventionelle Art der Bindung zwischen den Peptiden und der PDZ-Domäne von Myopodin beobachtet. Zusätzlich halfen diese Modelle der einzelnen Komplexe die strukturellen Determinanten aufzudecken, die verantwortlich für die unterschiedlichen Affinitäten der untersuchten Bindepartner sind. Unterstützt werden diese Ergebnisse durch Untersuchung der biophysikalischen Eigenschaften mit SEC-MALLS in sowohl reduzierender als auch oxidierender Umgebung. Es wurden auch Unterschiede in der Oligomerisierung von Myopodin beobachtet. Diese Anhaltspunkte deuten darauf hin, dass die Aktin-Bündelungsaktivität der zentralen Domäne von Myopodin von zwei unabhängigen F-Aktin Bindungsstellen verwirklicht werden. Wir verzeichneten eine Dissoziationskonstante von 2.0 μM in MST Experimenten mit der zentralen Domäne und Filamin C Ig d18-21. Allerdings wurde auch ein Regulationsmechanismus dieser Interaktion in Form von Phosphorylierung an drei Serinen von Myopodin vorgeschlagen. Um den Effekt der Phosphorylierung zu untersuchen wurden phosphorylierungsnachahmende Mutanten von Myopodin A generiert. Die Affinität des Filamin C Fragments zu der phosphorylierungsnachahmenden Mutanten sank dramatisch, was eine Herabregulierung der Interaktion durch Phosphorylierung

andeutet. Basierend auf den Interaktionen mit unterschiedlichen Bindepartnern und deren unterschiedlichen Affinitäten, kann die Charakterisierung der Myopodin Interaktions-”Hotspots” die Dynamiken erklären, die Myopodin in den verschiedenen Zellvorgängen antreiben.

Abbreviations

ABD - Actin-binding domain

ACTN2 - α-actinin 2

ALP - Actinin-associated LIM protein

bHLH - Basic helix-loop-helix motif

CASA - Chaperone-assisted selective autophagy

CHAP - Cytoskeletal heart-enriched actin-associated protein

E – Embryonic days

EHN - Enigma-like homolog

EST – Expressed Sequence Tag

FLNc - filamin C

GDP– guanosine 5'-diphosphate

GTP - Guanosine-5'-triphosphate

Hfp – Hours postfertilization

HOPS - Homotypic fusion and vacule protein sorting

IFs - Intermediate filaments

Ig - Immunoglobulin like domains

K_d - dissociation constant

LIC - Ligation independent cloning

MLP - Muscle LIM protein

MRF4 - Muscle-specific regulatory factor 4

MST - Microscale thermophoresis

MYF5 - Myogenic factor 5

MYOD - Myoblast determination protein

NMR - Nuclear magnetic resonance

PBF - PDZ-binding motif

PCR - Polymerase chain reaction

PCT - pre-crystallization test

P_i - Inorganic phosphate

PSD-95 - postsynaptic density protein 95

SAW - Surface acoustic wave

SEC-MALLS - size exclusion chromatography - multi-angle laser light scattering

SLS - Static light scattering

SYN - synemin

Tm - Melting temperature

VPS18 - Vacuolar protein sorting protein 18

ZO-1 - zonula occludens

1. Introduction

1.1. Cytoskeleton

The cytoskeleton is based on the combination of several complex protein-protein interactions and the collective behavior of molecules. It has organization as the main role of the cell environment. A dynamic scaffold to support cell shape on a large scale (several micrometers to a millimeter) from protein arrangements to cell compartments (Karsenti, Nedelec et al. 2006). The cytoskeleton is composed of three fundamental components: microfilaments, intermediate filaments and microtubules. It constitutes a unique organelle, which is physically rigid and at the same time flexible, that allows sustainability and transport in cells (Guharoy, Szabo et al. 2013).

1.1.1. Microtubules

Microtubules are a component of the cytoskeleton, found throughout the cytoplasm. Microtubules are long tubes (up to 50 μm) with a diameter of 25 nm (Karsenti, Nedelec et al. 2006). Microtubules are polymers of the protein tubulin found in all dividing eukaryotic cells and in most differentiated cell types. A dynamic arrangement of microtubules is formed during cell division, called the mitotic spindle, to physically segregate the chromosomes and to orient the plane of cleavage. In non-dividing cells, microtubules organize the position of the nucleus and organelles. These structures are also physically robust polymers, with an intrinsic resistance to bending and compression (Desai and Mitchison 1997). Microtubules are composed heterodimers α- and β-tubulin subunits, which make up the subunit of a microtubule. These subunits have 50% homology (Burns 1991), and each has 50 kDa. Tubulin heterodimers are arranged in linear protofilaments that associate laterally to form 25 nm wide hollow cylindrical polymers. *In vitro*, the protofilament from mammalian spontaneously assembled brain tubulin varies between 10 and 15, with the vast majority having 14 protofilaments. However, *in vivo* microtubules and nucleated *in vitro* from centrosomes and axonemes have predominantly 13 protofilaments (Evans, Mitchison et al. 1985). Heterodimers of α- and β-tubulin assemble polar structures by the head-to-tail association (Amos and Klug 1974), generating microtubule nucleus. Nucleation is followed by elongation of the microtubule at both ends to form a cylinder

(figure 1.1), where αβ heterodimers are oriented with their β-tubulin subunit pointing toward the plus end facing the solvent, and α-tubulin is exposed at the minus end of the microtubule (Desai and Mitchison 1997). A dynamic instability is generated by the microtubule polymerizing and depolymerizing. GTP-tubulin is incorporated at the polymerizing microtubule ends, the bound GTP is hydrolyzed during or soon after polymerization, and Pi is subsequently released. In this way, most of the microtubule polymer is composed of GDP-tubulin. The microtubule end containing tubulin-bound GTP or GDP–Pi is stable against depolymerization. The hydrolysis of tubulin-bound GTP and the release of Pi from the cap region induces conformational changes in the tubulin molecules, resulting in catastrophe and shortening of the microtubule (Inoue and Salmon 1995, Jordan and Wilson 2004).

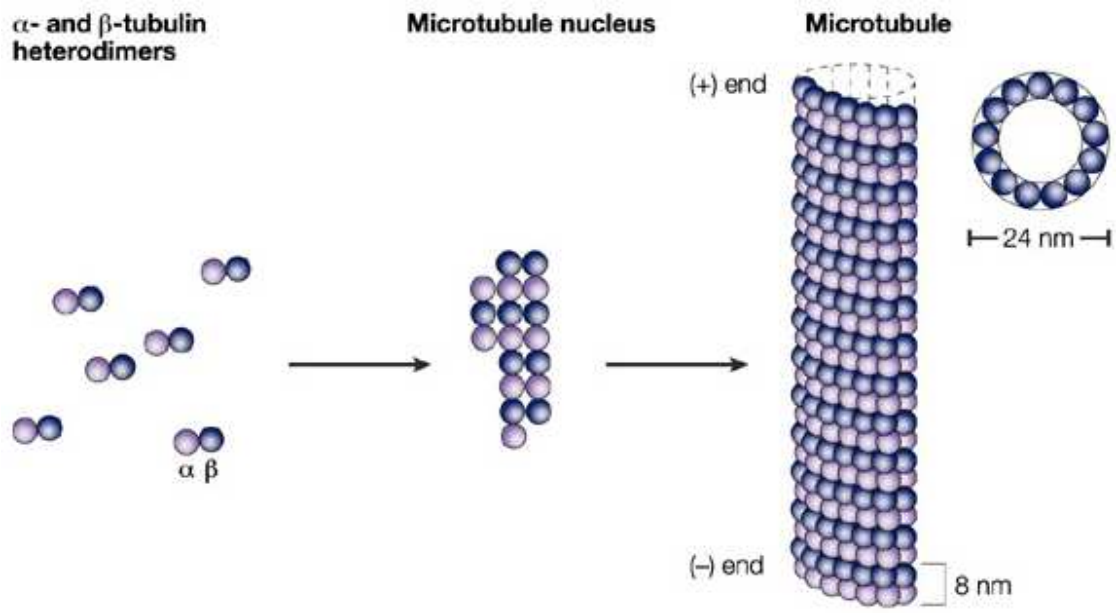

Figure 1.1: Polymerization of microtubules. Arrangement of α- and β-tubulin monomers for the microtubules formation adapted from (Jordan and Wilson 2004).

1.1.2. Intermediate filaments (IFs)

IFs are dynamic elements of vertebrate cells cytoskeleton. IFs have been recognized as a superfamily of 10-nm fibers ubiquitous in multicellular eukaryotes. The name of the IF serves to emphasize the intermediate diameter size in between the other cytoskeletal fibers such as microfilament (7 nm) and microtubules (25 nm) (Ishikawa, Bischoff et al. 1968). IFs can be found in the cytoplasm and the nucleus. In

the nucleus, IFs play an important role in the formation of nuclear cytoskeleton (Dey, Togra et al. 2014). The intermediate filament family is divided into six sequence homology classes, which have different tissue expression patterns (Fuchs and Weber 1994). Despite the great diversity of intermediate filaments, they all have the same conserved organization which is a central α-helical domain (rod) flanked by a non-α-helical N-terminal (head) and C-terminal (tail) domains. The rod domain α-helices are the key point for the dimerization, which occurs *via* formation of a parallel coiled coil. Two dimers interact in an antiparallel way to form a tetramer. Tetramer units pack together laterally to form a sheet of eight parallel protofilaments that are supercoiled into a tight bundle, twisted in a rope-like manner to form an intermediate filament (Dey, Togra et al. 2014).

IFs are involved in several important cellular processes (table 1.1): mechanical strength, Ifs interacts and links with actin and microtubules (Lammerding, Schulze et al. 2004); tissue growth, presenting a differential local expression in damaged cells (DePianto and Coulombe 2004); cell organization and adhesion control, playing a fundamental role for the lysosomes transport (Styers, Kowalczyk et al. 2005) and involvement in the attachment of cell membrane, desmosomes and hemidesmosomes adhesion areas (Colucci-Guyon, Portier et al. 1994).

Table 1.1

The intermediate filament protein multigene family.

Member name	Sequence homology class	c-DNA deduced mass in kDa	Typical occurrence in mammals/notable features
Assembly group 1			*Cytoplasmatic*
Acidic cytokeratins*	I	40–64	All epithelia; heteropolymer with a type II CK
CK9–20			
Basic cytokeratins*	II	52–68	All epithelia; heteropolymer with a type I CK
CK1–8			
Assembly group 2			*Cytoplasmatic*
Vimentin	III	55	Mesenchymal cells
Desmin	III	53	Muscle cells
Glial fibrillary acidic protein (GFAP)	III	50–52	Glia cells, astrocytes, stellate cells of liver
Peripherin	III	54	Diverse neuronal cells
Synemin	[III/V]	182	Muscle cells; copolymer with desmin and/or vimentin
Paranemin	IV/I	178	Muscle cells; copolymer with desmin and/or vimentin
Nestin	VI	240	Neuroepithelial stem cells, muscle cells; copolymer with vimentin and/or a-internexin
α-Internexin	IV	56	Neurons
Neurofilament triplet proteins	IV		Neurons
NF-L		68	
NF-M		110	Neurons; copolymer with NF-L
NF-H		130	Neurons; copolymer with NF-L
Assembly group 3			*Nuclear*
Lamins			
type A/C	V	62–72	Most differentiated cells
type B		65–68	All cell types

Adapted from (Herrmann and Aebi 2000)

1.1.3. Microfilaments

Microfilaments or actin filaments are the thinnest filaments of the cytoskeleton (7 nm diameter), a structure found in the cytoplasm of eukaryotic cells, and most plentiful in muscle cells. They have the ability to change their shape to adapt to their environment, to move along narrow spaces or to divide. These versatilities are the result of the special assembly of the microfilaments and depend on actin

polymerization in different types of organization: branched and cross-linked networks, parallel bundles, and anti-parallel contractile structures (Blanchoin, Boujemaa-Paterski et al. 2014). The assembly of actin cytoskeletal depends on the regulated transition of cellular actin between its globular monomeric (G-actin) and filamentous (F-actin) states. Actin is an ATPase, and nucleotide hydrolysis by actin is a critical factor regulating the transition between the G- and F-actin states. These filaments are polar polymers with a right-handed helical twist and two ends called barbed and pointed ends and these extremities have different elongation dynamics. The barbed end is the more active end of the actin filament and elongates 10 times faster than the pointed end, at a rate of 11.6 $\mu M^{-1} \cdot s^{-1}$ (Pollard 1986). In a cellular environment in which concentrations of actin can be more than 300 μM, actin filament barbed ends can assemble as fast as 3,000 subunits/s, meaning that an actin filament can reach length scales relevant to the cell (10 μm) in <2 s (Pollard, Blanchoin et al. 2000). These polymerization dynamics are fundamental for the cell's movement. End-capping proteins such as CapZ prevent the addition or loss of monomers at the filament end where actin elongation is unfavorable, such as in the muscle apparatus (Caldwell, Heiss et al. 1989).

The formation of actin cytoskeleton is the primary condition for several functions in the cell, such as adhesion, motility, signal transduction, cell shape changes and protein sorting (van der Flier and Sonnenberg 2001). For the participation and function of actin in these processes, actin filament polymerization and the crosslinking into bundles or networks are necessary. A number of actin-binding proteins mediate this process.

A plethora of actin-binding proteins regulate the cellular activity of actin, these proteins can be organized in seven groups: Cross-linking proteins (e.g. a-actinin), motor proteins (e.g. the myosin), monomer-sequestering proteins (e.g. thymosin beta4, DNase I), stabilizing proteins that prevent actin depolymerization (e.g. tropomyosin), severing proteins (e.g. gelsolin), filament-depolymerizing proteins (e.g. CapZ, cofilin) and capping proteins (e.g. CapZ) (dos Remedios, Chhabra et al. 2003).

1.2. Striated muscle cells

Striated muscles cells or myocytes are long, tubular cells and because of their highly elongated shape they are also termed myofibers. These cells are composed of

an internal organization of myofilaments. Myocytes are covered by a plasma membrane called sarcolemma and this membrane includes the sarcoplasm and myofibrils.

Skeletal muscle cells (myocytes) are the most abundant muscle type in the body, responsible for all movements under voluntary control. Myocites are multinucleated and can be 2–3 cm long and 100 μm in diameter in an adult human.

In striated muscle cells, the intermediate filaments desmin and vinculin have proved to be important players for myocytes sarcoplasm architecture. Desmin is shown to be present in both skeletal and cardiac Z-disc, in longitudinal myofibrils sections showed by immunofluorescence (Lazarides and Hubbard 1976). Desmin surrounds myofibril Z-discs, and is extended as far as the costamers, where it is anchored by vinculin. In myocytes, vinculin is associated with the sarcolemma, forming bands orientated in longitudinal axis of the cell. These bands work as lateral attachments of myofibrils to the plasma membrane along the whole of its length (Pardo, Siliciano et al. 1983).

Myocytes are composed of bundles of myofibrils, which are very long chains of sarcomeres, the contractile units of the cell. The major filament proteins in sarcomeres are actin, myosin and titin. Cardiomyocytes have a branching myofiber morphology with a central nucleus; they also have an increased capillary irrigation and high mitochondrial density, making them highly resistant to fatigue (Alberts, Johnson et al. 2002).

Actin and myosin myofilaments are organized in such a way that they partially overlap in a repeated arrangement. Dark A bands and light I bands are the result of the overlap and non-overlap regions respectively of myofilaments forming the sarcomeres. Titin (connectin), the third filamentous system in striated muscle cells required for sarcomere assembly. Titin is a protein that extends from the Z-disc to the M-band. Titin first 200 residues span the Z-disc, while its C-terminus is anchored to the M-band, delimiting the dimension of the sarcomere and its organization (Kontrogianni-Konstantopoulos, Ackermann et al. 2009).

Sarcomeres are the basic contractile units of striated muscle, and consist of Z-disc, M-line, I-band and A-band (figure 1.2). A-band spans the length of myosin thick filaments cross-linked by myomesin dimers in the sarcomeric M-line (Lange, Himmel et al. 2005, Lange, Ehler et al. 2006). The Z-discs are localized in the boundaries of the sarcomeres, in a zigzag pattern connecting the ends of actin filaments cross-linked

by α-actinin molecules (Luther 1991), and this basic scaffold is the anchor point for several proteins involved in muscle development (Wang, Shaner et al. 2005).

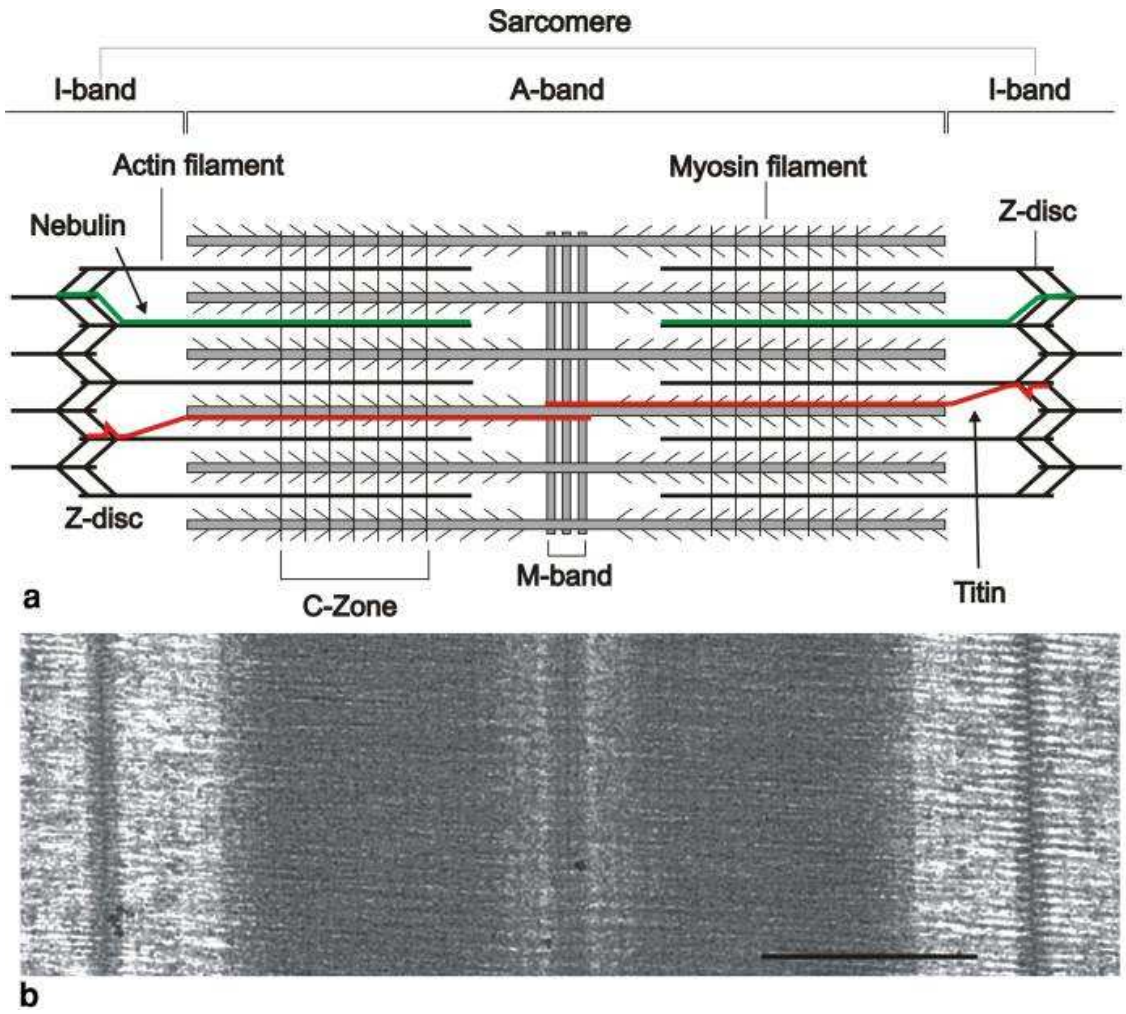

Figure 1.2: Striated muscle sarcomere. (a) Schematic representation of a sarcomere diagram with its main elements. (b) Electron micrograph of a longitudinal section of the sarcomere. Scale bar = 500 nm. Adapted from (Luther 2009).

1.3. Myofibrillogenesis

Muscle fibers are developed from a differentiation process of mononucleate myoblast cells fusion, forming multinucleated nascent myotubes (Wakelam 1985). This differentiation to mature myotubes is regulated by specific transcription factors, the myogenic regulatory factors (MRF). This process is ruled by 4 main factors: myogenic factor 5 (MYF5), muscle-specific regulatory factor 4 (MRF4), myoblast determination protein (MYOD) and myogenin. All these factors contain a basic helix-loop-helix (bHLH) motif (figure 1.3) (Lassar, Skapek et al. 1994, Braun and Gautel 2011).

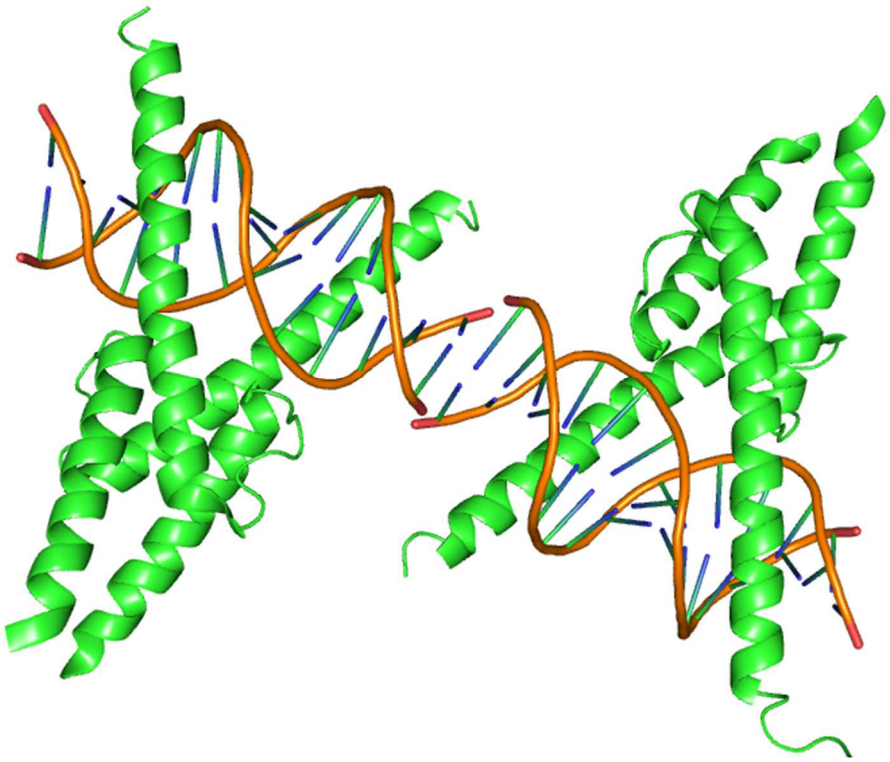

Figure 1.3: MyoD bHLH domain. Crystal structure of MyoD bHLH domain (green)-DNA complex (PDB entry: 1MDY) (Ma, Rould et al. 1994).

With a posterior cell morphology, change can be observed in a specific organization of the cytoskeleton. The formation of the myofibrils organized in sarcomeres is called myofibrillogenesis. Several studies using different models have investigated the myofibrils assembly and identify the sequence of events involved in myofibrillogenesis (Sanger, Kang et al. 2005).

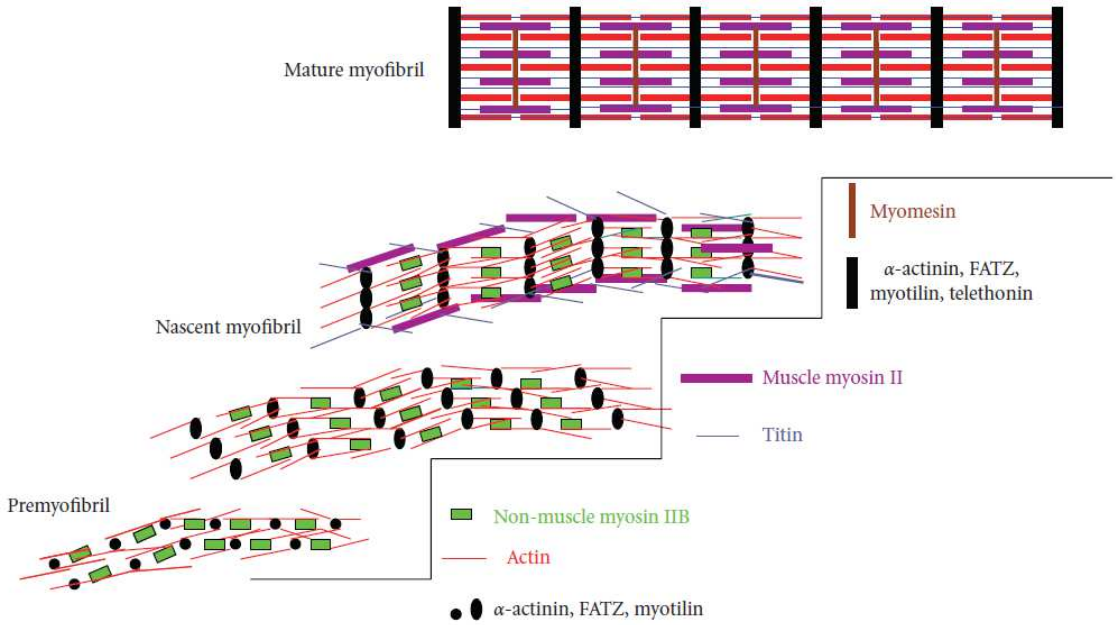

Figure 1.4: Premyofibril model. Premyofibrils are made up of minisarcomeres, nonmuscle myosin II aligned with actin filaments embedded in the Z-bodies. Nascent myofibrils have muscle myosin II and Z-bodies become aligned in adjacent fibrils. Furthermore, in mature myofibrils the fusion of the Z-bodies in Z-discs, alignment of the muscle myosin II in the A-band and complete absence of nonmuscle myosin can be observed. Figure modified from (Sanger, Wang et al. 2010).

Premyofibrils consist of minisarcomeres at the edges of muscle cells. They are composed of nonmuscle myosin II and thin actin filament, which contain Z-bodies in their boundaries. The Z-bodies are enriched with muscle α -actinin which interact with the barbed ends of actin filaments. The premyofibrils start to align among and then become thicker. At this moment, the presence of titin and muscle myosin II can be observed. At this stage, the Z-bodies start to align and the fibrils are classified as nascent myofibrils. In the progression from nascent to mature myofibrils, the nonmuscle myosin is not present anymore. The muscle myosin II overlaps in thick filaments, and C-protein and myomesin are incorporated in the A-band and Z bodies transform and become aligned to Z-lines or Z-bands (figure 1.4) (Du, Sanger et al. 2008, Sanger, Wang et al. 2010).

1.4. Z-disc

Z-discs delineate the lateral borders of sarcomeres. They consist of actin filaments coming from adjacent sarcomeres cross-linked by α-actinin homodimers organized in an antiparallel fashion. In recent years, an increasing number of proteins have been identified as components of the Z-disc interaction network (figure 1.5). Several of these proteins play fundamental roles, not only in structural function, but also in signaling pathways (Frank, Kuhn et al. 2006). The muscle stretch sensing potential of the Z-disc is one important discussion point. Cardiomyocites under mechanical stress can have their gene expression modulated and present cellular hypertrophy (Knoll, Hoshijima et al. 2002).

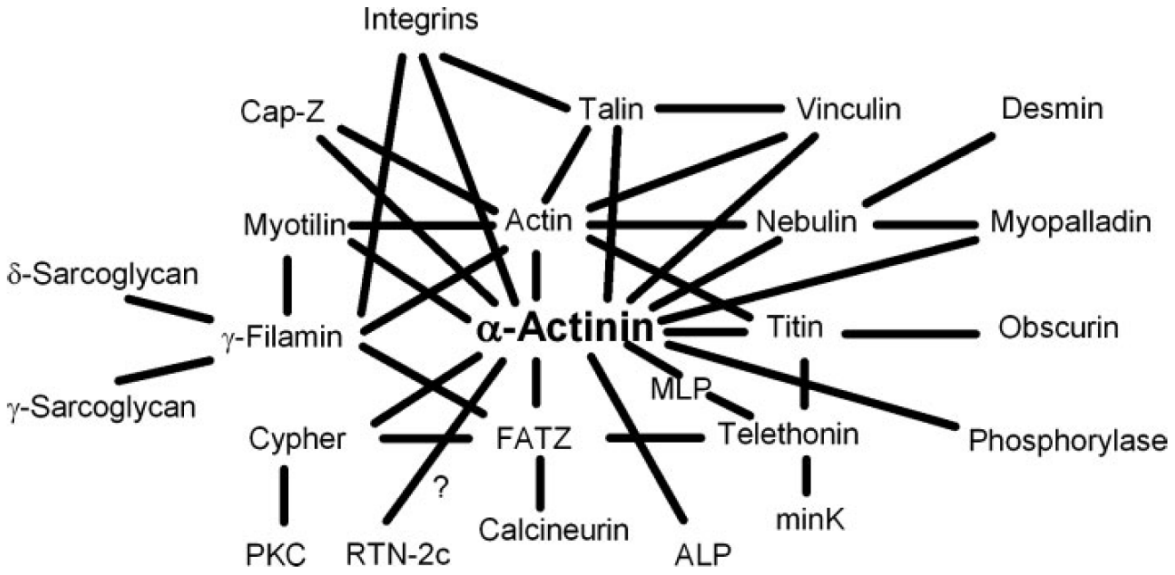

Figure 1.5: Z-disc protein interaction net. Map of α-actinin direct and indirect interactions with several elements of muscle cells. Figure adapted from (Wang, Shaner et al. 2005).

Despite the variety of proteins that compose the Z-disc, several of them contain common domains involved in protein-protein interactions.. Some of these domains are frequently present, like LIM and PDZ domains. LIM domains consist of cysteine-rich consensus sequences that comprise tandem zinc finger protein motifs. They can be found in zyxin, MLP, ALP, enigma and ZASP, also mediating several protein-protein interactions in the Z-disc. In addition, some of these proteins have been reported to shuttle to the nucleus, and are a possible connection between the sarcomeric stretching sensor mechanism and nuclear transcriptional regulation from cardiac cells

(Frank and Frey 2011). Some of these LIM proteins share a PDZ domain (PDZ-LIM proteins), including ZASP, enigma, EHN (enigma-like homolog) and the actinin-associated LIM protein (ALP) family. PDZ domains are present in membrane proteins, receptors and enzymes (Hillier, Christopherson et al. 1999, Kim and Sheng 2004). In muscle cells, these domains mediate many protein-protein interactions. ZASP PDZ domain interacts with Z-disc structural components, as the C-terminus of α-actinin 2 and other members, such as myotilin and FATZ (Zhou, Ruiz-Lozano et al. 1999, von Nandelstadh, Ismail et al. 2009). PDZ domain from ALP and enigma family display conserved residues involved in α-actinin binding (Katzemich, Liao et al. 2013).

1.5. The Podin family

The podin family of proteins consists of 3 members: synaptopodin, myopodin (synaptopodin 2 or fesselin), and tritopodin (CHAP or synaptopodin 2-like). Each family member has at least 3 isoforms that are produced by alternative splicing. Podin family members are proline rich proteins. Predicted to be predominantly intrinsically disordered. Podin family members have multiple binding partners including actin and other actin-binding proteins. Several members of the Podin family have been shown to stimulate actin polymerization and to bundle actin filaments either on their own or in collaboration with other proteins (Chalovich and Schroeter 2010). Synaptopodin was first discovered as an actin-associated protein in kidney podocytes and postsynaptic densities of telencephalic synapses (Mundel, Heid et al. 1997). Other members of the podin family were discovered in avian smooth muscle (Leinweber, Fredricksen et al. 1999) and in heart and skeletal muscle (myopodin, genethonin-2, synaptopodin 2 or fesselin) (Weins, Schwarz et al. 2001). The last member of the synaptopodin family of proteins, the synaptopodin 2-like protein, is found in heart and skeletal muscle tissue and is better known by the name tritopodin (Claeys, van der Ven et al. 2009).

1.5.1. Synaptopodin

Synaptopodin is a protein encoded by the gene SYNPO, and expressed mostly in telencephalic dendritic cells and renal podocytes. Mundel et al. described the first discovered member of the podin family synaptopodin in 1997. It is a proline-rich protein and this characteristic promotes an intrinsically unstructured and disordered molecule. It has 2 PPXY motifs involved in the interaction for WW domains of other postsynaptic proteins, thus potentially mediating the interaction of these proteins and actin cytoskeleton(Patrie, Drescher et al. 2002). In dendritic cells, synaptopodin expression is restricted to postsynaptic densities where it co-localizes with actin microfilaments associated dendritic spines for telencephalic synapses. Renal podocytes present synaptopodin expression during cell differentiation and are also colocalized with microfilaments during foot processes, an extension of the podocyte and increase of the surface area. In both cases, synaptopodin has a potential role in modulating cell actin-based motility (Mundel, Heid et al. 1997). Furthermore, it has been found that synaptopodin occurs in three different isoforms: synaptopodin short isoform (685 amino acids), synaptopodin long isoform (903 amino acids), and Synpo-T (181 amino acids) (Asanuma, Kim et al. 2005). The synaptopodin long isoform possesses a central domain with conserved podin homology region and a C-terminal region, which binds both actin and α-actinin 2. Since different binding sites for actin and α-actinin 2 have been observed, it is possible that there might be simultaneous interaction of both proteins and a modulation of the interaction between then. This makes synaptopodin an important player in cytoskeleton formation of the dendritic spine apparatus (Kremerskothen, Plaas et al. 2005).

1.5.2. Myopodin

Myopodin is the second member of the podin family, and is also called synaptopodin 2 or fesselin. Leinweber et al. first identified the avian homologue in 1999. It was initially found in smooth and skeletal muscle cells Z-discs and dense bodies. This protein, termed fesselin, has the ability to interact and induce cross-linking of the actin filaments. Fesselin shares a unique sequence homology with human and murine synaptopodin, evidence that these proteins could be related and be associated

with actin in cells and colocalized with α-actinin (Leinweber, Fredricksen et al. 1999). In mouse and human muscle library screens a new member of the podin gene family, with an identity of 87.5% between human and mouse myopodin and an overall homology of 47.7 % to synaptopodin has been identified. Myopodin shows a specific distribution in the muscle cell during the differentiation process. In undifferentiated myoblasts, myopodin is heavily expressed in the nucleus and has a very weak presence in the cytoplasm, but during differentiation myopodin can be found in both compartments. In differentiated myotubes myopodin can be clearly observed in the Z-discs and is no longer in the nucleus. A single 3.6 kB myopodin mRNA has been detected in skeletal muscle and heart, with the expression in the skeletal muscle being more evident than in the heart. Through western blot analysis of cytosolic extracts of mouse skeletal and heart muscle, a 110 kDa band corresponding to synaptopodin has been found in both tissues and myopodin was observed as a band with apparent molecular weight of 80 kDa in skeletal muscle and 95 kDa in the heart (Weins, Schwarz et al. 2001).

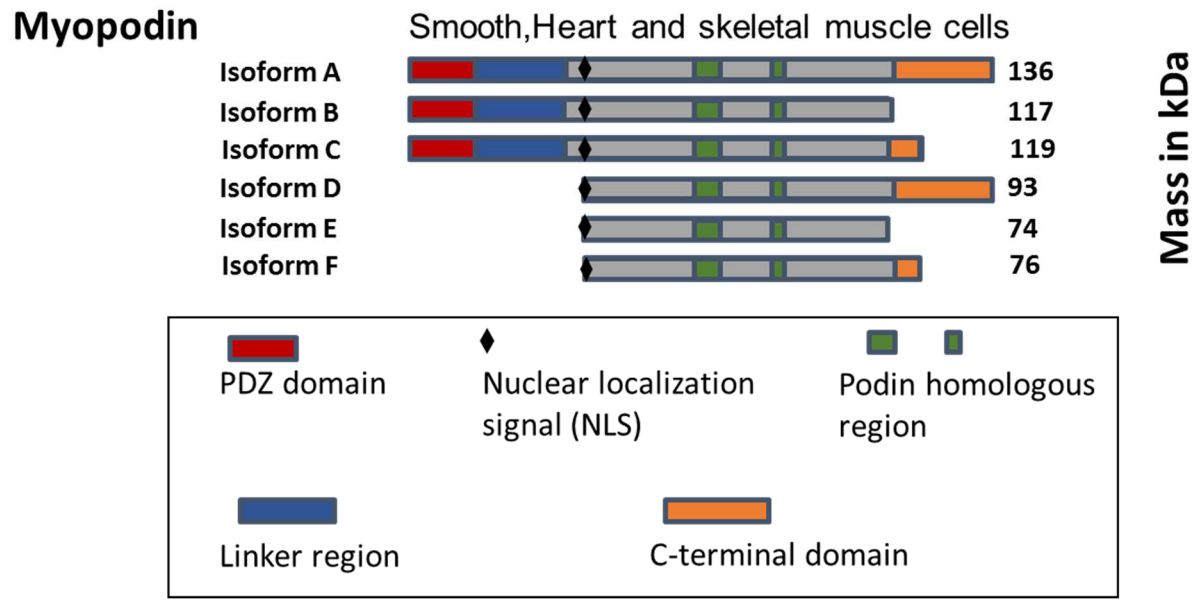

Figure 1.6: Representation of myopodin isoforms. Protein isoforms calculated from the amino acid composition of molecular weight for human and murine myopodin. Two homologous regions identified in all podin family and in the long isoforms PDZ domain are present.

Alternative splicing events result in at least three different protein variants of myopodin. They have been described as 3 isoforms that can be differentiated by an

alternative splicing of the C-terminal region. These isoforms (myopodin long isoforms) have been termed myopodin A (136 kDa – 1261 aa), myopodin B (117 kDa – 1093 aa) and myopodin C (119 kDa – 1109 aa). Myopodin long isoforms contain a predicted PDZ domain close to their N-terminus (De Ganck, De Corte et al. 2008). Analysis of the human prostate indicates the existence of shorter mRNA transcripts. An EST database analysis also provided evidence for an alternative transcriptional start site in the exon 3 of the gene SYNPO2 and the generation of additional isoforms, where the N-terminal portion including the PDZ domain is missing (Lin, Yu et al. 2001). Myopodin short isoforms are expressed in 3 additional isoforms: myopodin D (93 kDa – 866 aa), myopodin E (74 kDa – 698 aa) and myopodin F (76 kDa – 714 aa) (figure 1.6). An analysis using isoform-specific antibodies has shown different isoform expression patterns in different muscle types. In skeletal muscle, the expression of myopodin isoform E can be observed as well as a weak expression of the long isoform variant myopodin isoform A. In cardiomyocytes, the presence of long myopodin isoforms can be observed by Western blot. On the protein level, proteins with N-terminal PDZ domain and variants encoded by exon 6 region were also detected. This suggests that, the Myopodin isoforms A and B are expressed, particularly in the heart. In smooth muscle-rich tissues the presence of long myopodin isoform A can be observed, as well as the expression of short isoforms as myopodin isoform E. The short isoform present in the prostate is related to myopodin isoform F, due to the different migration behavior in the SDS gel electrophoresis, which has an apparent bigger molecular weight (Linnemann 2010).

It has been proposed that myopodin could be involved in several structural and signaling processes in the Z-disc (Weins, Schwarz et al. 2001). It has also been suggested that myopodin avian homolog, referred to as fesselin, might be associated with the process of actin filament organization and binds with a reasonable affinity (K : 2×10^6 M^{-1}) determined by co-sedimentation with F-actin. Fesselin does not only bind to actin but also enhances the actin polymerization (Weins, Schwarz et al. 2001). The affinity of Ca^{2+}-calmodulin to the fesselin F-actin complex was approximately 10^8 M^{-1}.Calmodulin binding to fesselin appeared to be functionally significant. In the presence of fesselin and calmodulin, the polymerization of actin was Ca^{2+}-dependent. Ca^{2+}-free calmodulin either had no effect or enhanced the ability of fesselin to accelerate actin polymerization (Schroeter and Chalovich 2004). Myopodin can play a role as a tumor suppressor gene implicated in the metastatis of prostate cancer cells. Inactivation of

myopodin may have a negative impact on a patient's clinical outcome, providing a potential target for clinical intervention (Yu, Tseng et al. 2006).

1.5.2.1. PDZ domains

PDZ domains are very common protein-protein interaction motifs. They were first described as GLGF repeats found in discs-large homology region. This domain has also been observed in postsynaptic density protein 95 (PSD-95), is involved in the regulation of synaptic function, and also in zonula occludens (ZO-1), scaffolding proteins providing the structural basis for the assembly of multiprotein complexes at the cytoplasmic surface of intercellular junctions. PDZ is the acronym for these three proteins (PSD-95, iscs-large homology region and ZO-1) where this domain was first observed (Kennedy 1995). It can be found in a large variety of organisms, in different cells and participating in innumerous cell process as cell signaling. PDZ motifs are present in invertebrate and vertebrate, but PDZ homologous domains are also present in plants, yeast and bacterial proteins (Ponting 1997).

Being a relatively ancient class of binding domain, PDZ domains primarily recognize the C-terminal extreme of the binding partner proteins in the canonical binding mode(Doyle, Lee et al. 1996, Saras and Heldin 1996, Remaut and Waksman 2006). In addition, some PDZ domain interactions recognize internal motifs. These interactions are distinct from canonical PDZ-peptide interactions, and they do not recognize of a C-terminal sequence on partner protein (Cowburn 1997, Hillier, Christopherson et al. 1999). PDZ domains are usually 80-100 amino acid residues long and adopt a similar topology.

Structural studies have revealed that canonical PDZ domains are essentially globular domains composed of five or six β-strands (βA– βF) and a short α-helix (αA) and a long α-helix (αB) arranged into what has been described as a "β sandwich" (Fanning and Anderson 1996, Lee and Zheng 2010). The PDZ binding site groove is composed of three structural elements: α-helix B (αB), β-strand B (βB) (figure 1.7 a) and the carboxylate-binding loop. The carboxylate-binding site is a loop located in the groove between the α-helix B and the β-strand B, and this loop has highly conserved characteristic residues. The loop is represented by X-Φ-G-Φ motif, where X is any amino acid residue and Φ is hydrophobic residue. This loop sequence allows 3 amide groups to serve as the H-bonding donors for two carboxylate oxygens from the C-

terminal residue of the PDZ-binding motif (PBF) from the carboxyl terminus, and a water molecule. The PDZ β-sheet composed of βB, βB and βD is augmented by the binding partner's C-terminus (PDZ-binding motif) in an antiparallel fashion with the βB, promoting an extension of the β-sheet.

PDZ domains display a hydrophobic pocket to accommodate the ligand hydrophobic side-chain of the of the C-terminal residue. This pocket composition could have a slight variation in hydrophobic groups, but this raises the interesting possibility of a selectivity mechanism based on the volume of the hydrophobic pocket (Doyle, Lee et al. 1996). In addition, PDZ binding motif side chains grant additional specificity to the protein–protein interaction (Doyle, Lee et al. 1996, Fanning and Anderson 1996, Remaut and Waksman 2006). PDZ domains can be classified by the C-terminal sequence of the ligand PDZ binding motif or peptide. This classification places the last 4 residues (P-3, P-2, P-1 and P0) in 3 classes (table 2.): class I domains, which recognize the motif -X-[S/T]-X-Φ; class II domains, which recognize the motif -X-Φ-X-Φ; and class III domains, which recognize the motif -X-[D/E]-X-Φ (where Φ is a hydrophobic residue) (table 1.2) (Hillier, Christopherson et al. 1999, Jelen, Oleksy et al. 2003).

In several crystal structures PDZ domains assume an auto-inhibited form, where the protein C-terminus is the PMF of its own PDZ domain causing the auto-inhibition. The C-termini of PDZ itself (auto-inhibited) or the PBM to construct extensions of PDZ domains greatly assists in the formation of PDZ domain crystals, with each PDZ domain binding the C-terminus of an adjacent molecule in the crystal lattice (Elkins, Papagrigoriou et al. 2007). The structure of GRASP PDZ in an auto-inhibited form was determined by Sugi *et al.* 2007 showing 4 molecules in the asymmetric unit. Two molecules present a proper canonical binding, but the other two display an unusual perpendicular non-canonical binding mode, where only the last residue P0 is observed in the binding pocket (Sugi, Oyama et al. 2007). A similar conformation can also be observed by nuclear magnetic resonance (NMR) with X11/Mint PDZ domains auto-inhibited in a perpendicular binding mode (Long, Feng et al. 2005).

Table 1.2

Classification of PDZ domains based on the C-terminal sequence of their binding partners.

Class	C-terminus of the partner protein	Interacting partner	Exemple of PDZ domain
Class I -X-[S/T]-X-Φ	EDTV	Shaker K^+ channel	PSD-95 (PDZ2)
	ESDV	NMDA receptor subunits NR2A/B	PSD-95 (PDZ2)
	TTRV	neuroligin	PSD-95 (PDZ3)
	TSVF	ILR-5α	syntenin (PDZ1, PDZ2)
	ESLV	PMCA4b	PSD-95 (PDZ1,2 and 3)
	QSAV	voltage-gated Na^+ channel	syntrophin
	DSSL	protein kinase C-α	PICK1
	DTRL	β_2-adrenergic receptor	NHERF (PDZ1)
	QTRL	CFTR	NHERF (PDZ1)
	SSTL	GKAP	Shank/ProSAP
	PTRL	metabotrophic glutamate receptor subunit mGluR5	Shank/ProSAP
		GRK6A	
Class II -X-Φ-X-Φ	SVKI	AMPA receptor subunit GluR2	PICK2, GRIP (PDZ5)
	EYFI	glycophorin C	erytrocite p55
	EYYV	neurexin	CASK
	EFYA	syndecan-2	CASK, syntenin (PDZ2)
	YYKV	ephrin B1	PICK2, GRIP (PDZ6), syntenin (PDZ2)
	DVPV	receptor tyrosine kinase ErbB2	erbin
Class III -X-[D/E/K/R]-X-Φ	VDSV	melatonin receptor	nNOS
	GEPL	KIF17	mLIN10/Mint1/X11
	FEEL	merlin	syntenin (PDZ1)
	K/RYV	synthesized peptide	engineered from AF6

Adapted from (Jelen, Oleksy et al. 2003)

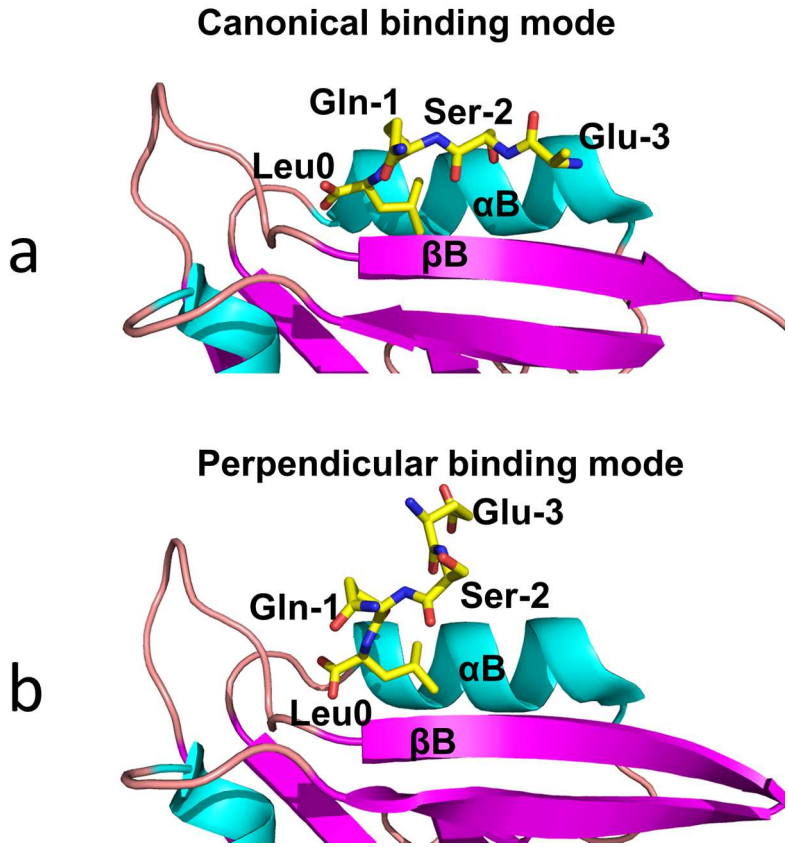

Figure 1.7: Canonical and perpendicular PDZ binding modes. Binding modes of tamalin to the binding partner C-terminus in a canonical (A) and perpendicular (B) conformation (PDB code: 2EGK) (Sugi, Oyama et al. 2007)..

1.5.2.1.1. Myopodin PDZ domain and synemin

Synemin is a type VI intermediate filament protein colocalized with desmin and vimetin in the Z-disc. Differing from the other intermediate filaments, which can form homopolymeric dimers, synemin is unable to self-assemble into filaments. For this to occur, synemin needs to interact with another intermediate filament. It has already been described how synemin can interact *via* rod domain with desmin, vimetin and vinculin tail, while synemin C-terminal tail domains is able to interact with α-actinin 2 head and rod domain (figure 1.8) (Bellin, Sernett et al. 1999). This suggests that synemin could possibly play a crosslinking role between the Z-disc and the costamers (Bellin, Huiatt et al. 2001). A model has been put forward to show how heteropolimeric intermediate filaments, formed by synemin and desmin, encircle and pack together nearby myofibrils in striated muscle cells and anchor these myofibrils to the sarcolemma costamers (Bellin, Huiatt et al. 2001, Lund, Kerr et al. 2012). This process happens through IF's synemin tail interaction with the Z-disc α-actinin 2 from

neighboring myofibrils in the other hand the IF's are anchored to the constamers *via* by interactions between synemin and vinculin and/or α-actinin (Bellin, Huiatt et al. 2001).

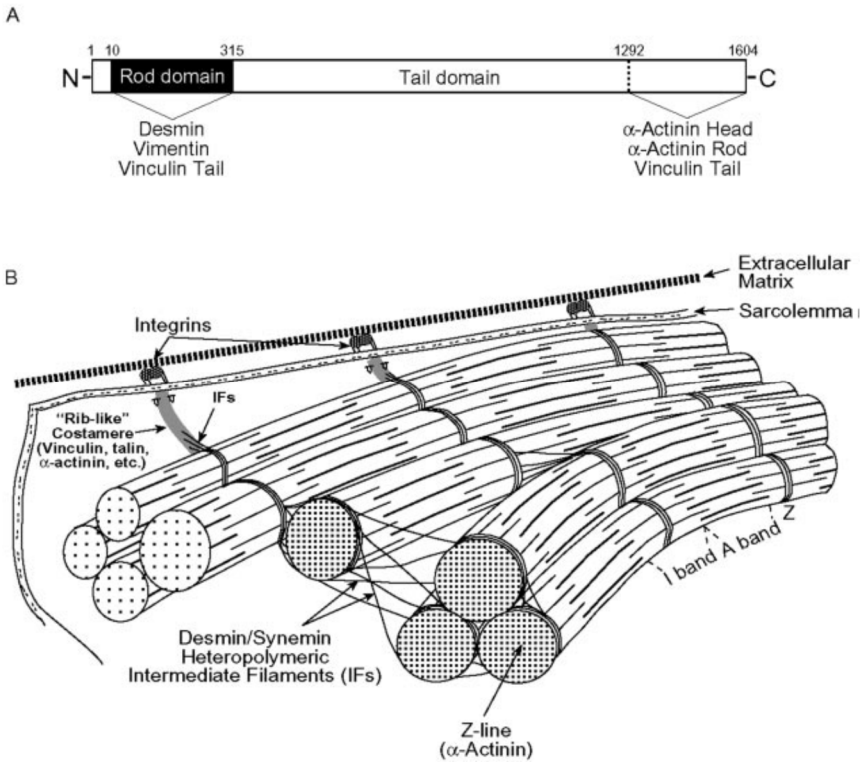

Figure 1.8: Sumary of synemin interactions. (A) synemin map of interactions. (B) Diagram that explain the proposed role of synemin in striated muscle cells (Bellin, Huiatt et al. 2001).

As myopodin long isoforms are also present in sarcomere Z-disc from cardiomyocites and are colocalized with α-actinin and synemin, the capacity of PDZ domain from myopodin to interact with synemin was investigated. Using yeast two-hybrid, myopodin interaction to fragments containing sequences from the C-terminal portion of synemin was observed. A western blot overlay demonstrated that the C-terminal portion of synemin specifically interacts with the PDZ domain of myopodin (Vakeel 2006).

1.5.2.1.2. Myopodin PDZ domain and VPS18

Myopodin PPPY motif interaction with the WW domain of BAG3 has recently been described. BAG3 protein is involved in chaperone-assisted selective autophagy (CASA) complex which mediates autophagy of the Z-disc components pathway, such as filamin C (figure 1.9). Myopodin PDZ domain also interacts with the C-terminal

portion of vacuolar protein sorting protein 18 (VPS18), a protein that participates in the homotypic fusion and vacuole protein sorting (HOPS) tethering complex (Ulbricht, Eppler et al. 2013).

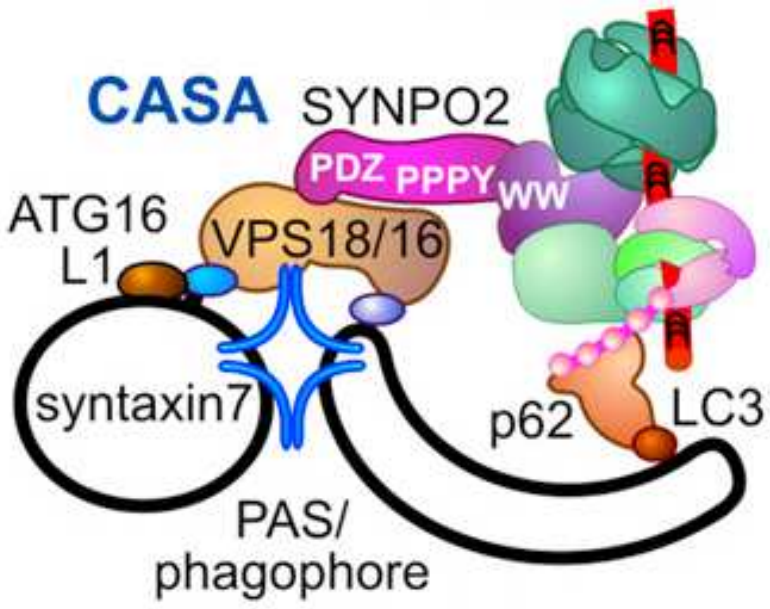

Figure 1.9: CASA complex. Myopodin (SYNPO2) mediating the interaction between the HOPS and CASA complexes. Adapted from (Ulbricht, Eppler et al. 2013).

BAG-3 in CASA complex is responsible for a proteostasis mechanism of Z-disc maintenance, as autophagic degradation essential for maintaining Z-disc integrity and muscle contractility. Degradation might be initiated by a BAG-3-facilitated release of damaged components from the Z-disc, like the release of the Z disc protein filamin C. In addition, BAG-3 sequesters YAP/TAZ inhibitors (LATS1/2 and AMOTL1/2 PPxY motifs) mediated by BAG-3 WW domain, which are free to activate the expression of filamin C. Myopodin, which is a filamin binding protein, seems to play a role in this scenario, since it also interacts with CASA complex *via* BAG-3 WW domain (Arndt, Dick et al. 2010, Ulbricht, Eppler et al. 2013). It was shown in the filamin degradation process that only myopodin isoforms which present in the N-terminal PDZ domain form a stable complex with CASA, suggests that the myopodin PDZ domain is fundamental in Z disc proteostasis. Since this myopodin PDZ domain interacts with VPS18, a core HOPS component, it can be presumed that it works in membrane fusion complexes to direct proteins into different cell compartments in autophagosome formation. Myopodin apparently links the client-processing CASA chaperone machinery to a membrane

tethering and fusion complex that provides autophagosome membranes (Brocker, Kuhlee et al. 2012, Ulbricht, Eppler et al. 2013).

1.5.2.1.3. Myopodin PDZ domain and α-actinin 2

α-actinins are members of the spectrin actin-binding family with important structural and maintenance function. All α-actinin isoforms share a domain topology consisting of an actin-binding domain (ABD), a central rod domain and a C-terminal calmodulin-like domains composed by two pairs of EF hand motifs (EF hand 1-2 and EF hand 3-4) (Blanchard, Ohanian et al. 1989). α-actinin 2 (ACTN2) is the isoform present in muscles and can be found in the Z-discs from striated muscle cells, as an antiparallel dimer crosslinking actin. α-actinin 2 rod domain dimer possesses 4 spectrin repeats, composed of 3 α-helices in a coiled-coil assembly. In addition to the actin-binding domain, the spectrin repeats also serves as an anchoring point for several Z-disc proteins, such as the ALP/ENIGMA family (spectrin 2-4), FATZ (spectrin 3-4), myotilin (spectrin 3-4) or myopodin (spectrin 3-4) (Djinovic-Carugo, Gautel et al. 2002, Linnemann, van der Ven et al. 2010).

α-actinin 2 EF hand 3-4 C-terminal domain contains the PDZ binding motif belonging to class I, based on the C-terminal 4 residues (-E-S-D-L-**COOH**). It is thought that ALP and ENIGMA family motifs cooperate in the Z-disc assembly through their interactions with α-actinin 2 *via* the PDZ domains. Based on sequence analysis, it was found that putative PDZ domain candidates with N-terminal PWGFRLxGG motif which are able to bind to α-actinin 2, myopodin long isoforms, have highly similar PDZ domains to ALP and ENIGMA family and are able to interact (Katzemich, Liao et al. 2013).

1.5.2.2. Myopodin central domain

Analysis of myopodin avian homolog primary sequence and CD spectroscopy demonstrated its native unfolded nature and the presence of multiple actin-binding sites (Leinweber, Fredricksen et al. 1999) (Weins, Schwarz et al. 2001, Khaymina, Kenney et al. 2007). The central domain of myopodin (664-916 aa of long isoforms and 240-521 aa of short isoforms) is intrinsically disordered (figure 1.10) and is a

multiadapter domain capable of binding to several binding partners as actin, α-actinin 2 and filamin C (Linnemann, van der Ven et al. 2010).

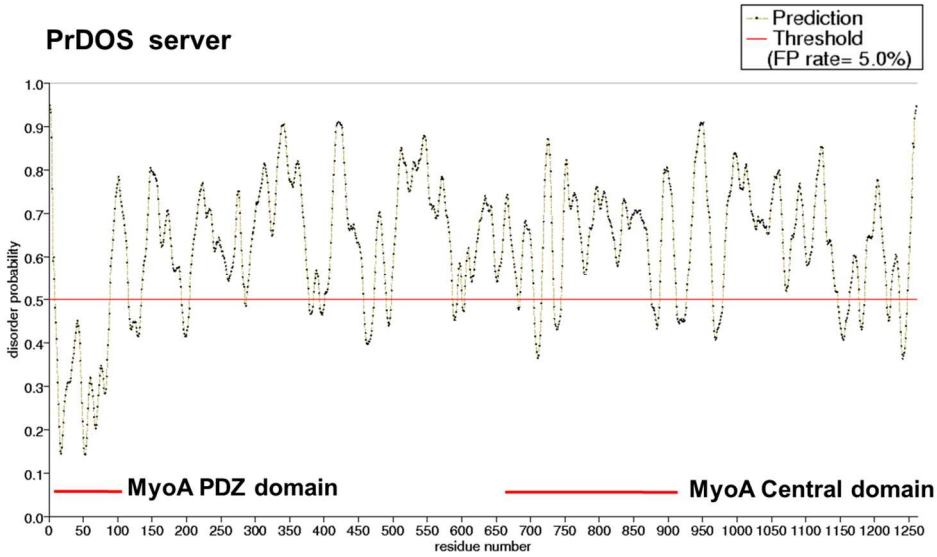

Figure 1.10: Disorder prediction of myopodin by PrDOS server (Ishida and Kinoshita 2007). The values above 0.5 in disorder probability indicate disorder residues. The red bars represent myopodin PDZ domain and Central domain extension.

1.5.2.2.1 Myopodin central domain and filamin C

Three members compose the filamin family in humans: filamin A, filamin B and filamin C. All filamin family members share a common domain organization. This is an ABD domain containing two calponin-like domains in the N-terminal extremity followed by 24 immunoglobulin like (Ig) domains interrupted twice by 2 flexible hinges between the 2 rod regions. These hinges occur between the Ig domain d15 and d16, and between Ig domains d23 and d24. Filamins are homodimers mediated by the Ig d24 dimerization domain (Baldassarre, Razinia et al. 2012, Sawyer and Sutherland-Smith 2012). Filamin C (FLNc), or γ-filamin is found in skeletal and cardiac muscle (Thompson, Chan et al. 2000). In the Z-disc, filamin C plays a fundamental role in mechanotransduction, intercalating discs under mechanical strain, and in cell development, interacting with a great diversity of proteins colocalized in Z-disc (van der Ven, Obermann et al. 2000). Filamin C interacts with sarcolemma-associated proteins as integrin (Gontier, Taivainen et al. 2005), sarcoglycan (Thompson, Chan et al. 2000) and structural Z-disc proteins (figure 1.11), such as myotilin (van der Ven, Wiesner et al. 2000), FATZ (Gontier, Taivainen et al. 2005), xin (van der Ven, Ehler et

al. 2006), KY-protein (Beatham, Romero et al. 2004) and in the heart filamin C interacts with nebulette (Holmes and Moncman 2008). The interaction with myopodin central domain with the Ig domains d20-21 of filamin C has recently been mapped by Linnemann *et al*. 2010.. Moreover, the determinated dissociation constant of 1.9×10^{-6} ± 0.8×10^{-6} M to myopodin central domain was obtained by surface acoustic wave.

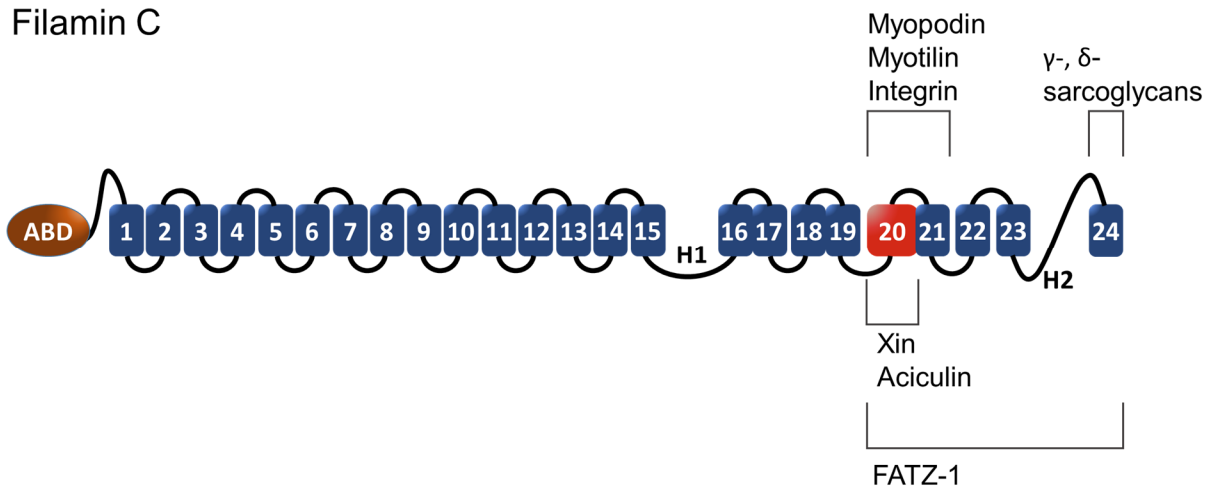

Figure 1.11: Schematic representation of a filamin C. Filamin C 24 Ig domains and the ABD domain mapped with its protein–protein interaction sites.

1.5.3. Tritopodin

Tritopodin, also termed synaptopodin 2-like or CHAP (cytoskeletal heart-enriched actin-associated protein), is the third member of the podin family. Encoded by the gene SYNPO2L, tritopodin was revealed by database searches and shares an extended sequence homology with the other members of the podin family (Claeys, van der Ven et al. 2009). It can be expressed in two different isoforms: the long isoform tritopodin a (CHAPa) (978 aa) and the short isoform tritopodin b (CHAPb) (749 aa). Tritopodin b shows a significant sequence homology of 31% to myopodin (synaptopodin 2) and 30% to synaptopodin; it has been identified and characterized in several models (zebrafish, chick, mouse and human) It is conserved among vertebrates and presents an important role in muscle cells (Beqqali, Monshouwer-Kloots et al. 2010, van Eldik, Beqqali et al. 2011). In both isoforms the podin homology region that binds to α-actinin 2 is conserved. In addition, the long isoform also

possesses a N-terminal PDZ domain with conserved residues among PDZ domains in Z-disc proteins, that putatively binds to α-actinin 2 C-terminal (Katzemich, Liao et al. 2013). Tritopodin is expressed during heart and skeletal muscle cell development. During the early mouse embryonic days, CHAPb is the dominant expressed isoform present in the cardiac crescent and somites, and by embryonic day (E) 12.5 it is already possible to detect CHAPb in limb muscle, CHAPa is upregulated in adult heart and skeletal muscle. Due to the shift of the isoform expression CHAPb is not expressed in adult muscle cells. This information implies that tritopodin is muscle-specifc and stage-dependent on different isoforms (Beqqali, Monshouwer-Kloots et al. 2010). Tritopodin is colocalized with α-actinin and actin in embrionic cardiomyocytes, adult cardiac and skeletal muscle. Using immunoprecipitation only direct interaction to tritopodin C-terminal domain with α-actinin 2 was observed. Zebrafish model proved to be an excellent vehicle to understand the importance of tritopodin *in vivo*, where 2 genes *chap1* and *chap2*, analogues of tritopodin, were found. In both genes the PDZ domain and the C-terminal actin-association domain were conserved. *Chap1* expression can be observed from the beginning of the cardiomyocyte differentiation and is no longer detected at 48 hours postfertilization (hpf). *Chap2* expression is expressed only in somites until 36 hpf when it shows cardiac expression. The Knockdown of *chap1* and *chap2* promotes a decreased cardiac contractility and loop defect, enlarged pericardial sac, myofibrillar disarray and disruption of somite boundaries. This shows that it has an essential role in cardiac and skeletal muscle development and function (Beqqali, Monshouwer-Kloots et al. 2010).

2. The aim of the study

Muscles are remarkable biomechanical machineries, and this is a reflex of complex and organized protein-protein interactions in muscle cells. A single myofibril is composed of many minimum contractile units, known as sarcomeres. The proteins at the junctions between sarcomeres form the Z-disc. The Z-discs are a very crowded environment, but extremely organized. This is where we can observe the main structural components, α-actinin and actin, forming the base outline for anchoring proteins. The podin family proteins to be colocalized with actin and their interaction sites have been described (Mundel, Heid et al. 1997, Weins, Schwarz et al. 2001, Kremerskothen, Plaas et al. 2005) . It has been proposed that myopodin can bind and bundle actin filaments thus playing an important role in the actin network formation (Leinweber, Fredricksen et al. 1999), but how this mechanism of interaction works has not so far been elucidated. In addition, the myopodin central domain and its interaction with filamin C, a protein with an important role in muscle cell development as signal transduction processes, actin organization and mechanosensing activities (van der Ven, Obermann et al. 2000, Razinia, Makela et al. 2012, Furst, Goldfarb et al. 2013). Longer myopodin isoforms host a PDZ domain in their N-terminus (De Ganck, De Corte et al. 2008). This PDZ domain is homologous to other PDZ domains in the Z-disc with a predicted binding to α-actinin (Katzemich, Liao et al. 2013) as well as to synemin and VPS18 as identified *via* two hybrid screen.

The aim of my study is to elucidate the structural basis for different affinities of myopodin PDZ domain to binding partners peptides (synemin, VPS18 and α-actinin) The second aim of the study was to understand how myopodin binding/bundling is related to its molecular architecture, in particular its oligomeric state. The third aim was to evaluate how phosphorylation of myopodin central domain modulates its interaction with filamin C.

The characterization of myopodin and its interactions by a combination of structural, biophysical and biochemical methods shall enlighten the understanding of the role of myopodin and its interactions within the ultrastructural model of Z-disc.

3. Results

3.1. Myopodin PDZ domain

3.1.1. Myopodin PDZ domain construct design

The PDZ domain construct named MyoA PDZ was designed to contain the N-terminal myopodin PDZ domain (amino acid residues 5-86) (figure 3.1) to investigate the interaction with synemin, VPS18 and α-actinin 2.

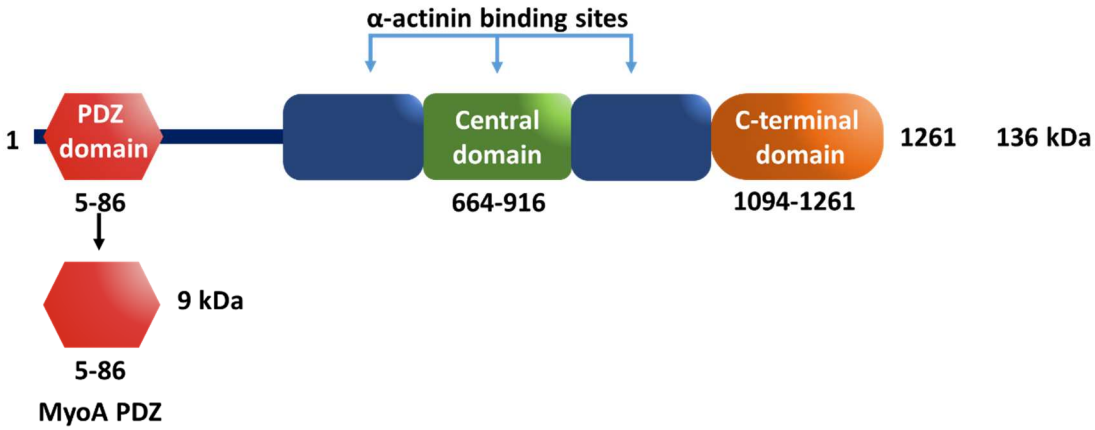

Figure 3.1. **Schematic illustration of myopodin A, an isoform with 1261 residues and 136 kDa**. The MyoA PDZ construct contains the PDZ domain located in the amino-terminus (5-86).

3.1.2. Purification of recombinant myopodin PDZ domain constructs

MyoA PDZ construct was expressed in BL21 (DE3) competent *E. coli* cells. Protein samples were initially purified by affinity chromatography HisTrap FF crude column (GE Healthcare) (figure 3.2a). After His-tag cleavage by 3C protease, samples were applied again to a HisTrap FF crude column (GE Healthcare) (figure 3.2b). Unbound fractions were collected and further purified using a Superdex 75 16/60 gel filtration column (GE Healthcare) (Figure 3.2c). The fractions of the peak corresponding to the MyoA PDZ were collected and further analyzed by SDS-PAGE in order to measure the purity of samples (figure 3.2).

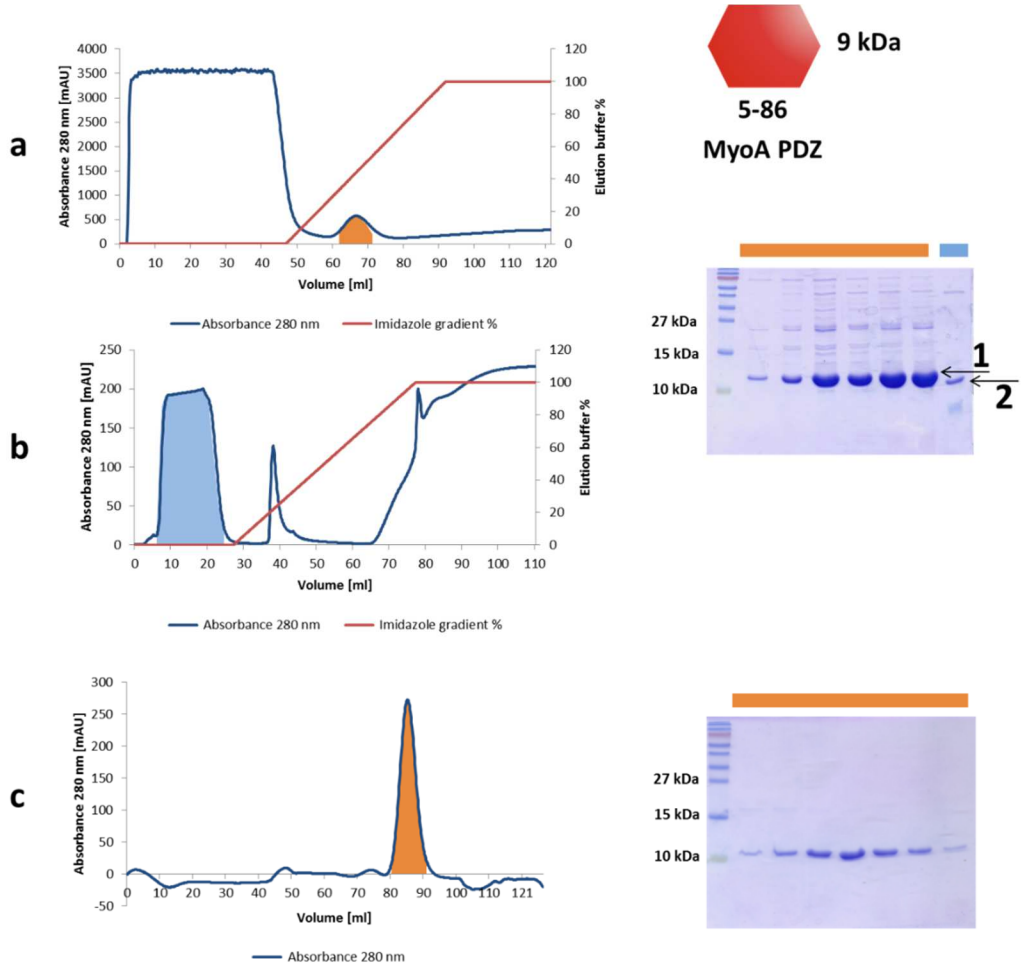

1

Figure 3.2: Purification of MyoA PDZ. (a) Elution profile of HisTrap with MyoA PDZ collected in the retained fraction (1). (b) Second HisTrap run with cleaved MyoA PDZ collected in the flow through fraction (2). (c) Cleaved sample was applied to a superdex 75 16/600 and eluted at 85 ml volume. The protein fractions from different purification stages were analyzed by SDS-PAGE (18% of acrylamide).

3.1.3. Thermal stability (Thermofluor)

Thermofluor was carried out to understand the thermal stability of MyoA PDZ under different conditions (table 3.1). Accordingly, among the tested conditions, a significant increase in the melting temperature (Tm) in the range of the potassium phosphate pH 7.0 was observed. The conditions B1, C1 and F1 (table 3.1) present the highest Tm value of 54º C (figure 3.3).

Table 3.1

Thermofluor master pH and ionic strength screen

	1	2	3	4	5	5	7	8	9	10	11	12
A	Potassium phosphate **pH 7.**	Hepes **pH 7.0**	Ammonium acetate **pH 7.3**	Sodium phosphate **pH 7.5**	Tris **pH 7.5**	Imidazole **pH 8.0**	Hepes **pH 8.0**	Tris **pH 8.0**	Bicine **pH 8.0**	Tris **pH 8.5**	Bicine **pH 9.0**	Water
B	Potassium phosphate **pH 7.** + 100 mM NaCl	Hepes **pH 7.0** + 100 mM NaCl	Ammonium acetate **pH 7.3** + 100 mM NaCl	Sodium phosphate **pH 7.5** + 100 mM NaCl	Tris **pH 7.5** + 100 mM NaCl	Imidazole **pH 8.0** + 100 mM NaCl	Hepes **pH 8.0** + 100 mM NaCl	Tris **pH 8.0** + 100 mM NaCl	Bicine **pH 8.0** + 100 mM NaCl	Tris **pH 8.5** + 100 mM NaCl	Bicine **pH 9.0** + 100 mM NaCl	100 mM NaCl
C	Potassium phosphate **pH 7.** + 500 mM NaCl	Hepes **pH 7.0** + 500 mM NaCl	Ammonium acetate **pH 7.3** + 500 mM NaCl	Sodium phosphate **pH 7.5** + 500 mM NaCl	Tris **pH 7.5** + 500 mM NaCl	Imidazole **pH 8.0** + 500 mM NaCl	Hepes **pH 8.0** + 500 mM NaCl	Tris **pH 8.0** + 500 mM NaCl	Bicine **pH 8.0** + 500 mM NaCl	Tris **pH 8.5** + 500 mM NaCl	Bicine **pH 9.0** + 500 mM NaCl	500 mM NaCl
D	Potassium phosphate **pH 7.** + 100 mM KCl	Hepes **pH 7.0** + 100 mM KCl	Ammonium acetate **pH 7.3** + 100 mM KCl	Sodium phosphate **pH 7.5** + 100 mM KCl	Tris **pH 7.5** + 100 mM KCl	Imidazole **pH 8.0** + 100 mM KCl	Hepes **pH 8.0** + 100 mM KCl	Tris **pH 8.0** + 100 mM KCl	Bicine **pH 8.0** + 100 mM KCl	Tris **pH 8.5** + 100 mM KCl	Bicine **pH 9.0** + 100 mM KCl	100 mM KCl
E	Potassium phosphate **pH 7.** + 500 mM KCl	Hepes **pH 7.0** + 500 mM KCl	Ammonium acetate **pH 7.3** + 500 mM KCl	Sodium phosphate **pH 7.5** + 500 mM KCl	Tris **pH 7.5** + 500 mM KCl	Imidazole **pH 8.0** + 500 mM KCl	Hepes **pH 8.0** + 500 mM KCl	Tris **pH 8.0** + 500 mM KCl	Bicine **pH 8.0** + 500 mM KCl	Tris **pH 8.5** + 500 mM KCl	Bicine **pH 9.0** + 500 mM KCl	500 mM KCl
F	Potassium phosphate **pH 7.** + 100 mM (NH4)2SO4	Hepes **pH 7.0** +100 mM (NH4)2SO4	Ammonium acetate **pH 7.3** + 100 mM (NH4)2SO4	Sodium phosphate **pH 7.5** + 100 mM (NH4)2SO4	Tris **pH 7.5** +100 mM (NH4)2SO4	Imidazole **pH 8.0** + 100 mM (NH4)2SO4	Hepes **pH 8.0** + 100 mM (NH4)2SO4	Tris **pH 8.0** + 100 mM (NH4)2SO4	Bicine **pH 8.0** + 100mM (NH4)2SO4	Tris **pH 8.5** + 100 mM (NH4)2SO4	Bicine **pH 9.0** + 100 mM (NH4)2SO4	100 mM (NH4)2SO4
G	Potassium phosphate **pH 7.** +10% Glycerol	Hepes **pH 7.0** +10% Glycerol	Ammonium acetate **pH 7.3** +10% Glycerol	Sodium phosphate **pH 7.5** +10% Glycerol	Tris **pH 7.5** +10% Glycerol	Imidazole **pH 8.0** +10% Glycerol	Hepes **pH 8.0** +10% Glycerol	Tris **pH 8.0** +10% Glycerol	Bicine **pH 8.0** +10% Glycerol	Tris **pH 8.5** +10% Glycerol	Bicine **pH 9.0** +10% Glycerol	10% Glycerol
H	Potassium phosphate **pH 7.** +20% Glycerol	Hepes **pH 7.0** +20% Glycerol	Ammonium acetate **pH 7.3** +20% Glycerol	Sodium phosphate **pH 7.5** +20% Glycerol	Tris **pH 7.5** +20% Glycerol	Imidazole **pH 8.0** +20% Glycerol	Hepes **pH 8.0** +20% Glycerol	Tris **pH 8.0** +20% Glycerol	Bicine **pH 8.0** +20% Glycerol	Tris **pH 8.5** +20% Glycerol	Bicine **pH 9.0** +20% Glycerol	20% Glycerol

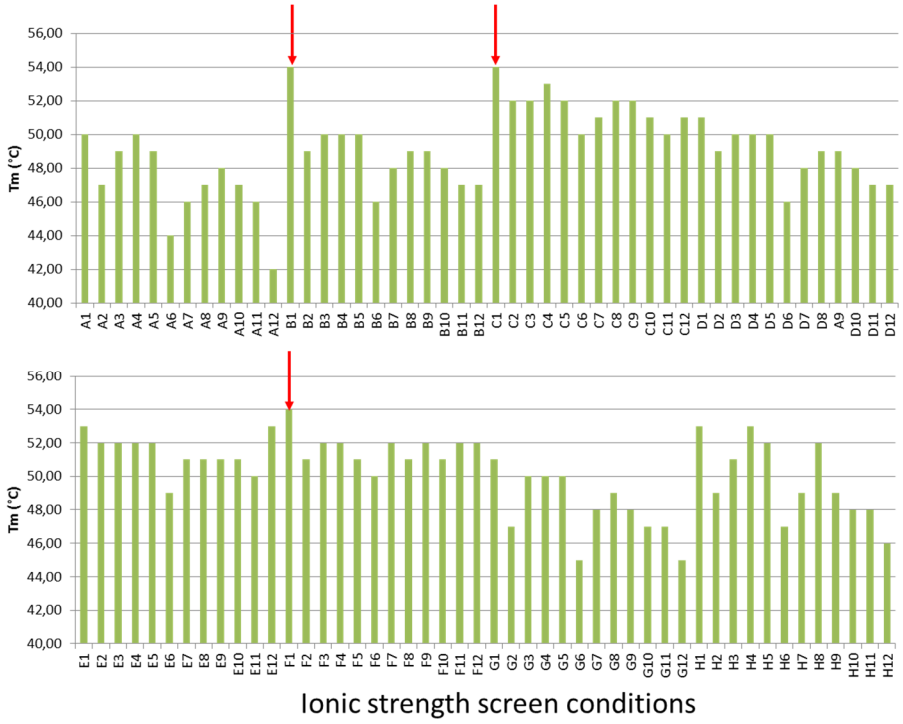

Figure 3.3: **Changes in the unfolding transition temperature were calculated for measurements on ionic strength screen.** Thermofluor melting temperature profile of MyoA PDZ. The highest Tm value is indicated by a red arrow.

The potassium phosphate pH 7.0 and 100 mM NaCl condition (Table 3.1 B1) used in the screening showed optimal results and was kept for subsequent peptide interaction experiments.

We further investigated how MyoA PDZ s binding partner's peptides modulate the Tm value for the MyoA PDZ. C-terminal peptide of the binding partners in complex with MyoA PDZ promoted a melting peak shift to 56º C, 57º C and 59º C for α-actinin 2, VPS18 and synemin peptides, (figure 3.4) corresponding to 2º,3º and 5º C increase, respectively. These pieces of evidence show that the peptide increase the stability of the PDZ domain to different levels as seen from different Tm.

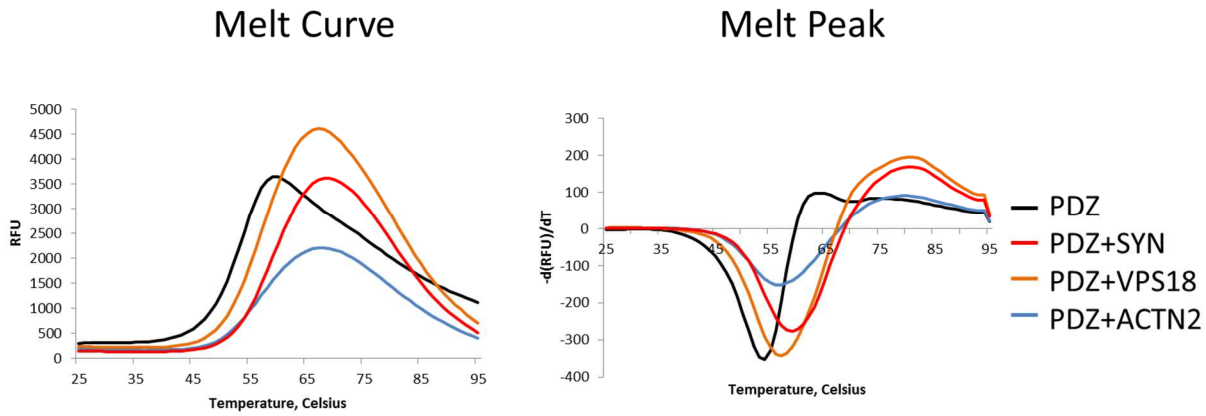

	Tm (°C)
PDZ	54
PDZ+SYN 8aa peptide	59
PDZ+VPS18 8aa peptide	57
PDZ+ACTN2 8aa peptide	56

Figure 3.4: Thermal shift for apo PDZ domain and in complex with peptides. A Tm value increase signifies that the peptide has a stabilizing effect.

3.1.4. Myopodin PDZ domain crystallization

Prior to crystallization experiments the pre-crystallization test (PCT) Hampton Research was performed, which determines the appropriate sample concentration for crystallization screening following the PCT protocol. MyoA PDZ in storage buffer (20 mM tris pH 8.0, 300 mM NaCl, 1.0 mM EDTA, 1.0 mM DTT and 5% glycerol) was initially used for this test. It was found that 30 mg/ml was the optimal concentration for the crystallization assays. We started to consider new solutions to solubilize the

protein, due to the high concentration of protein obtained in the first PCT trail. Performing the PCT experiment with the protein solubilized in water, an optimal concentration of 10 mg/ml was obtained. In addition, microcrystals at the PCT condition A1 were observed after 30 minutes and crystals (figure 3.5) were observed in these same drops overnight. MyoA PDZ was crystallized using a vapor diffusion method (hanging-drop) at 22 °C. The protein sample was mixed with an equal volume of the crystallization solution, the same as the one used in the A1 condition from PCT, 100 mM tris pH 8.5, 2.0 M ammonium sulfate. Crystals were transferred to the crystallization solution containing 25% glycerol and flash frozen in liquid nitrogen. Diffraction data were collected using the beamline ID23-1 at ESRF (Grenoble,France). The structure was solved by molecular replacement using MOLREP (Lebedev, Vagin et al. 2008); using MyoA PDZ/synemin complex structure as a search model.

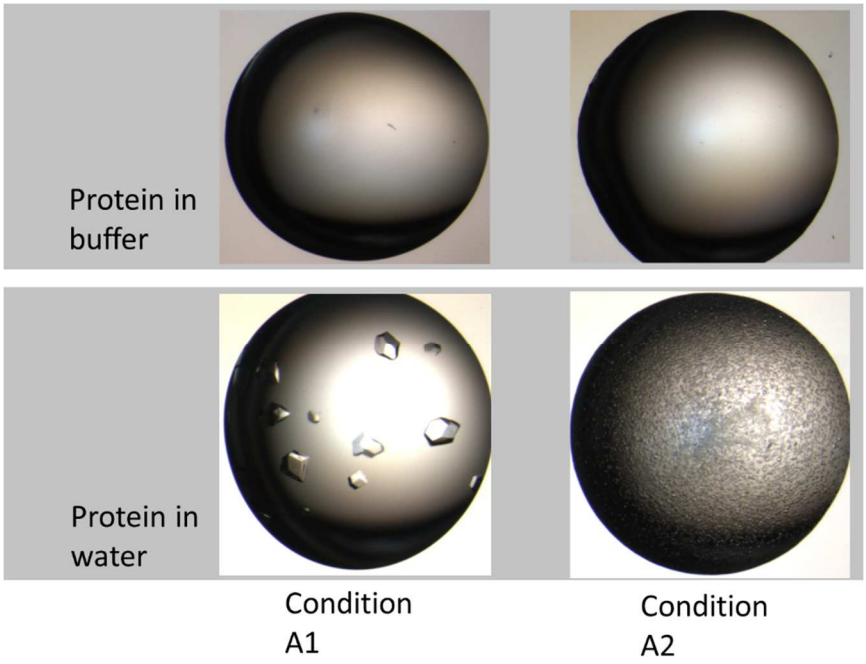

Figure 3.5: Pre-crystallization test. MyoA PDZ crystals formed after overnight in a hanging drop vapor diffusion experiment. The protein concentration is 10 mg/ml in water. Crystals grew already in the PCT condition A1 (100 mM tris pH 8.5, 2.0 M ammonium sulfate).

Table 3.2 Data collection and refinement statistics of MyoA PDZ

DATA COLLECTION	
Source	ESRF
Wavelength (Å)	0.933
Resolution (Å)	55.94 – 2.15 (2.27 – 2.15)
Space group	$I4_122$
Unit cell (Å)	a = b = 79.11, c = 60.49
Molecules / a.u.	1
Unique reflections	5463 (780)
Completeness (%)	99.9 (100)
R_{meas}[b]	0.070 (0.524)
R_{pim}[c]	0.026 (0.190)
R_{merge}	0.064 (0.487)
CC(1/2)	0.998 (0.832)
Multiplicity	24.1 (4.36)
I/sig(I)	7.0 (7.4)
B_{Wilson} (Å^2)	53.75
Software used for integration	XDS
Software used for scaling	Scala
DATA REFINEMENT	
R_{cryst}[d]/ R_{free}[e]	0.236 / 0.276
No. Reflections used for R_{free} (%)	5
R.m.s.d. bonds (Å)	0.013
R.m.s.d. angles (º)	1.34
B protein (Å^2)	62.5
B solvent (Å^2)	50.0
Software used for refinement	PHENIX/REFMAC/PDB_REDO
Refinement method	ML/TLS

[a] Values in parentheses are for the highest resolution shell.

[b] $$R_{meas} = \frac{\sum_h \sqrt{\frac{n_h}{n_h - 1}} \sum_i^{n_h} \left| \hat{I}_h - I_{h,i} \right|}{\sum_h \sum_i^{n_h} I_{h,i}} \text{ with } \hat{I}_h = \frac{1}{n_h} \sum_i^{n_h} I_{h,i}$$

[c] $$R_{pim} = \sum_{hkl} \sqrt{\frac{1}{N-1}} \sum_i \left| I_i(hkl) - \overline{I(hkl)} \right| / \sum_{hkl} \sum_i I_i(hkl)$$

Where I (hkl) is the mean intensity of multiple I_i (*hkl*) observations of the symmetry-related reflections, N is the redundancy, n_h is the multiplicity, $\hat{I}_h$ is the average intensity and $I_{h,i}$ is the observed intensity.

[d] $R_{cryst} = \Sigma \, |F_o - F_c| \, / \, \Sigma \, F_o$

[e] R_{free} is the cross-validation R_{factor} for the test set of reflections (5 %) which are omitted in the refinement process.

The MyoA PDZ crystals belong to space group $I4_122$ with unit cell dimensions of a = b = 79.11, c = 60.49 Å. The final structure (figure 3.6) was refined to a resolution of 2.15 Å and R_{factor} and R_{free} of 23.6% and 27.6%, respectively. The data collection

and refinement statistics are summarized in table 3.2. The overall structure of MyoA PDZ is similar to other PDZ domains (Lee and Zheng 2010), consisting of five β strands (βA–βE) and two α-helices (αA and αB) (figure 3.6).

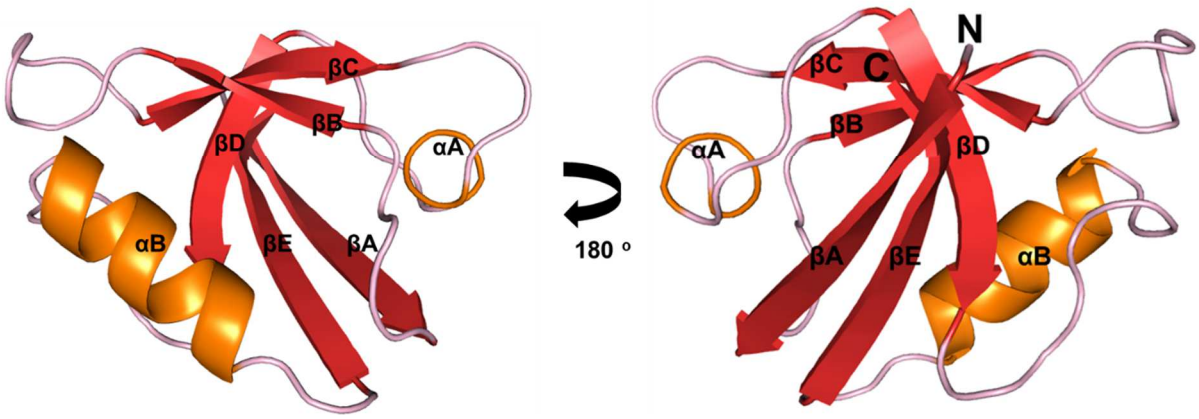

Figure 3.6: Overall structure of myopodin A PDZ domain. Secondary structures of PDZ2, α-helices, and β-strands are labeled and numbered according to their position in the sequence.

MyoA PDZ complexes with VPS18 and ACTN2 (α-actinin 2) C-terminal peptides co-crystalization was carried out under the same conditions of the pre-crystallization A1 solution. These crystals grew in 5 days (figure 3.7). MyoA PDZ complex with synemin peptide crystallization was obtained with the condition 17 (100 mM tris pH 8.5, 0.2 M Lithium sulfate monohydrate and 30% w/v Polyethylene glycol 4,000) from crystal screen I (Hampton Research) and grew in 3 days.

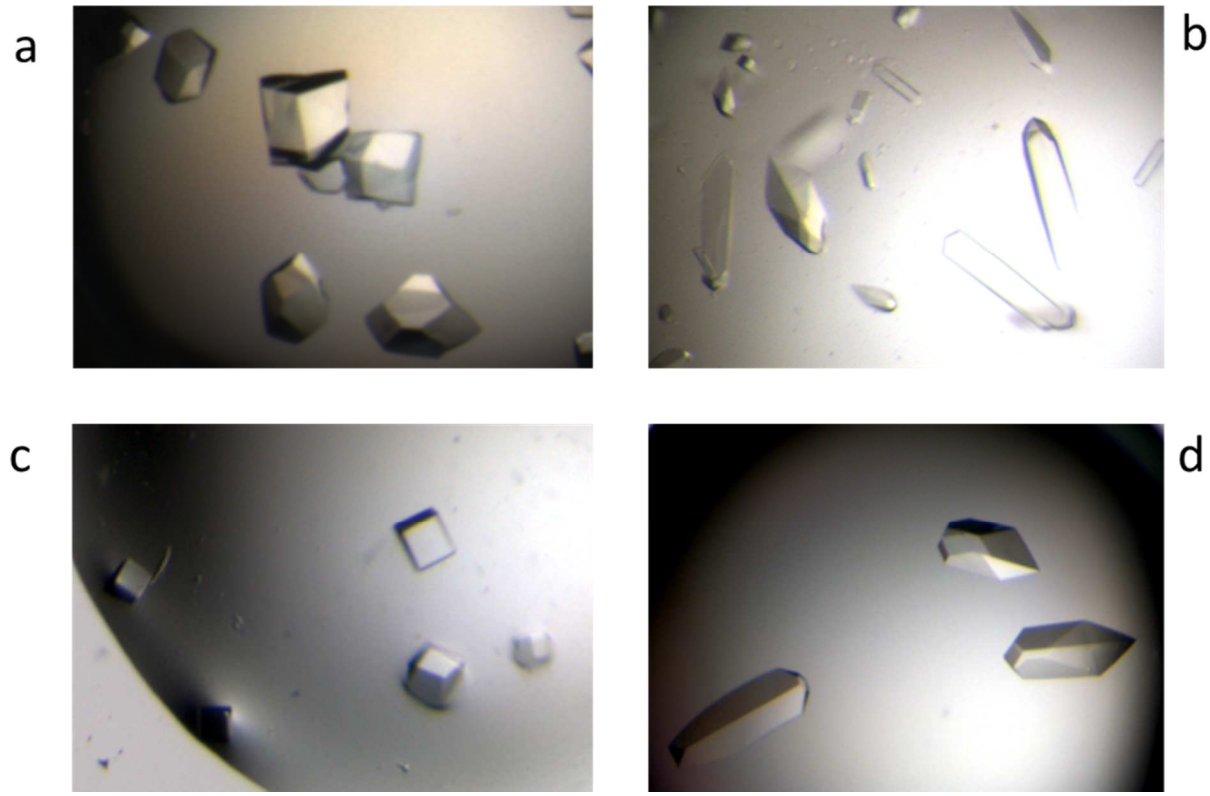

Figure 3.7: Crystal images. Crystals of MyoA PDZ (a), and in complex with synemin (b), VPS18 (c) and ACTN2 (d) peptides.

3.2. Myopodin A PDZ domain/synemin complex structure and interaction studies

3.2.1. Isothermal titration calorimetry of MyoA PDZ and synemin

In order to characterize further the binding of MyoA PDZ to synemin peptide the affinity by ITC was measured. For the ITC, synemin peptide 250 μM was injected into 25 μM a solution of MyoA PDZ. Data were plotted and analyzed using a single binding site model with the MicroCal Origin software. The titration curve of synemin C-terminal peptide is shown in figure 3.8 and the binding affinity of 0.75 μM ± 0.10 μM (dissociation constant, K_d) was determined with a stoichiometry of approximately 1. Synemin C-terminal PDZ binding motif peptide (EENDGHWF) does not fit exactly into any of the PDZ classes, but has characteristics similar to PDZ class III (-X-[D/E/K/R]-X-Φ), for example, the histidine in the synemin peptide at position P-2 is positively charged, and arginine and lysine residues are also present in the PDZ class III position P-2. This PDZ class presents low μM affinity for synemin peptide.

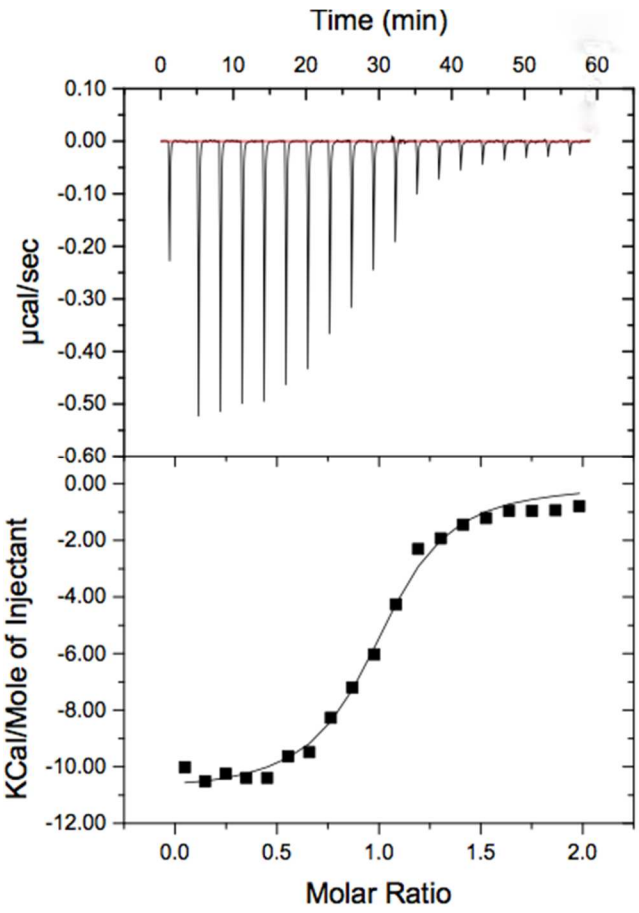

MyoA PDZ x synemin (EENDGHWF)

K_d = 0.75 µM ± 0.10 µM

Syringe: 250 µM synemin

Cell: 25 µM MyoA PDZ

N: 0.987 ±0.0138 sites

ΔH -10.92± 0.19 kcal/mol

ΔS -8.66 cal/mol/deg

Figure 3.8: Isothermal titration calorimetry of MyoA PDZ with synemin peptide. ITC titration of MyoA PDZ with synemin peptide was performed at 25ºC in 20 mM potassiun phosphate buffer, pH 7.0, 100 mM NaCl, and 1 mM TCEP. Shown, from top to bottom, are the raw titration data of synemin peptide injected into MyoA PDZ, and the integrated heat measurements for the titration. The first injection peak was discarded because of the backlash effect. The stoichiometry number (N) was obtained for the data set by fitting a standard 1:1 interaction. The data were plotted and analyzed using a single binding site model with the MicroCal Origin software.

3.2.2. Structure determination Myo PDZ/synemin complex

The MyoA PDZ in pure water in presence of 3 mM synemin peptide was submitted to a pre-crystallization test and an optimal concentration of 10 mg/ml (~ 1mM) to start the co-crystallization trials was observed. Initial crystallization trials in 96-well format were set up using commercially available crystallization screens. Crystals appeared in a crystallization condition containing 100 mM tris pH 8.5, 0.2 M Lithium sulfate monohydrate and 30% w/v Polyethylene glycol 4,000.

Table 3.3 Data collection and refinement statistics of MyoA PDZ/synemin complex

DATA COLLECTION	
Source	ESRF
Wavelength (Å)	0.933
Resolution (Å)	31.55 – 1.9 (2.0 - 1.9)
Space group	$I4_122$
Unit cell (Å)	a = b = 77.65, c = 63.09
Molecules / a.u.	1
Unique reflections	7782 (1033)
Completeness (%)	98.6 (92.2)
R_{meas}[b]	0.085 (0.660)
R_{pim}[c]	0.033 (0.328)
R_{merge}	0.078 (0.567)
CC(1/2)	0.997 (0.769)
Multiplicity	5.7 (3.5)
I/sig(I)	11.4 (1.6)
B_{Wilson} (Å^2)	42.02
Software used for integration	XDS
Software used for scaling	Scala
DATA REFINEMENT	
R_{cryst}[d]/ R_{free}[e]	0.201 / 0.233
No. Reflections used for R_{free} (%)	5
R.m.s.d. bonds (Å)	0.008
R.m.s.d. angles (º)	1.17
B protein (Å^2)	40.1
B solvent (Å^2)	51.1
B peptide (Å^2)	40.6
Software used for refinement	PHENIX/REFMAC/PDB_REDO
Refinement method	ML/TLS

[a] Values in parentheses are for the highest resolution shell.

[b] $$R_{meas} = \frac{\sum_h \sqrt{\frac{n_h}{n_h - 1}} \sum_i^{n_h} \left| \hat{I}_h - I_{h,i} \right|}{\sum_h \sum_i^{n_h} I_{h,i}} \text{ with } \hat{I}_h = \frac{1}{n_h} \sum_i^{n_h} I_{h,i}$$

[c] $$R_{pim} = \sum_{hkl} \sqrt{\frac{1}{N-1}} \sum_i \left| I_i(hkl) - \overline{I(hkl)} \right| / \sum_{hkl} \sum_i I_i(hkl)$$

Where I (hkl) is the mean intensity of multiple I_i (*hkl*) observations of the symmetry-related reflections, N is the redundancy, n_h is the multiplicity, $\hat{I}_h$ is the average intensity and $I_{h,i}$ is the observed intensity.

[d] $R_{cryst} = \Sigma |F_o - F_c| / \Sigma F_o$

[e] R_{free} is the cross-validation R_{factor} computed for the test set of reflections (5 %) which are omitted in the refinement process.

Diffraction data were collected using the beamline BM14 at ESRF (Grenoble,France). The MyoA PDZ/synemin complex crystals (figure 3.7 b) belong to space group $I4_122$ with unit cell dimensions of a = b = 77.65, c = 63.09 Å and 1

molecule in the asymmetric unit. The structure was solved by molecular replacement using BALBES (Long, Vagin et al. 2008) and PDLIM5 PDZ domain as search model (PDB code: 2UZC) (Elkins, Gileadi et al. 2010).The structure was refined to a resolution of 1.9 Å with R_{factor} and R_{free} of 20.1% and 23.3% respectively. The data collection and refinement statistics are summarized in table 3.3.

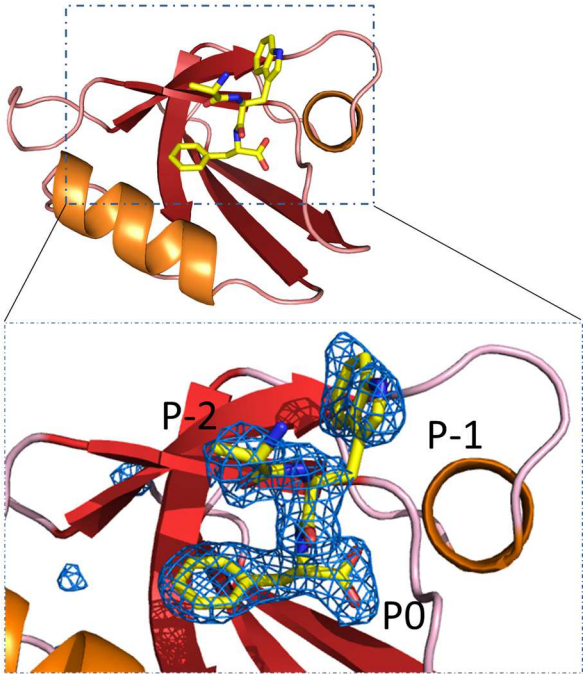

Figure 3.9: The structure of MyoA PDZ/synemim complex. PDZ domain structure with synemin peptide OMIT map calculated with σ_A-weighted ($2mF_o$ - DF_c) exp($i\varphi_c$) coefficients contoured at 1 σ level.

In the final solved model 3 out of 8 residues of the synemin peptide could be clearly seen in the electron density map (phenylalanine P0, tryptophan P-1 and histidine P-2 main chain) (figure 3.9 inset). Judging by the conformational of the histidine P-2, the rest of the peptide is apparently in a perpendicular orientation, i.e. the non-canonical conformation.

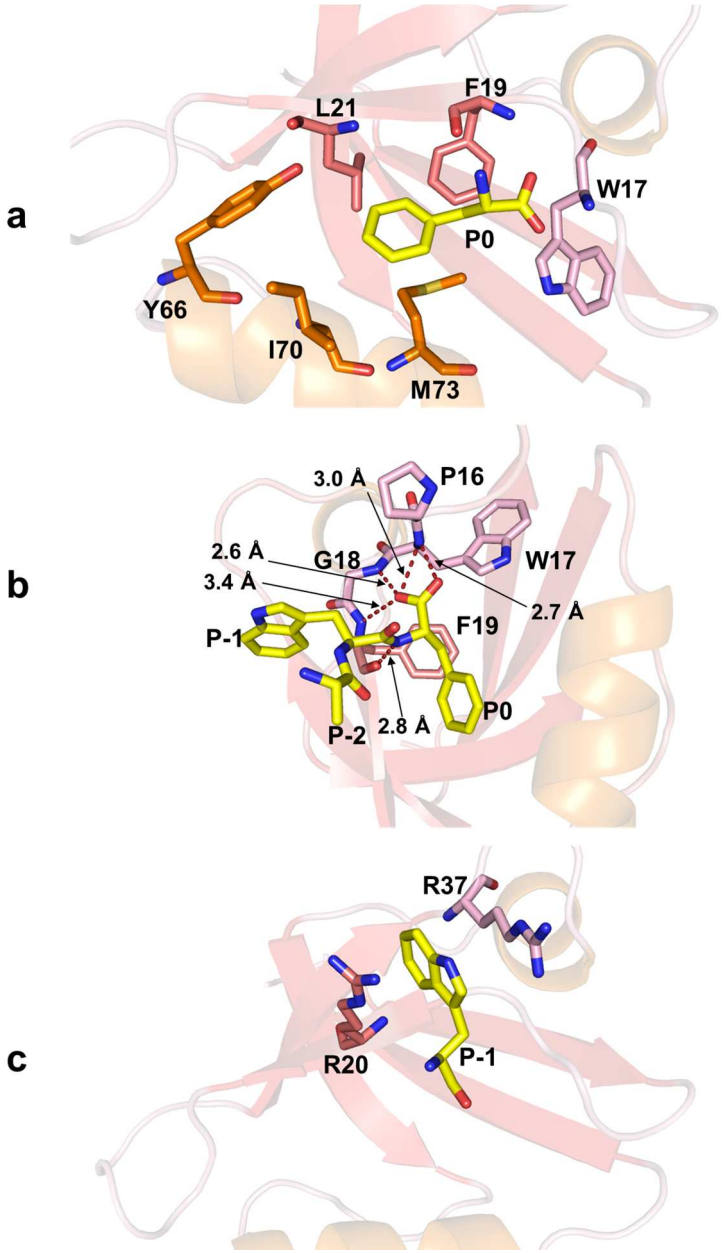

Figure 3.10: Structural basis for the binding affinity and specificity of MyoA PDZ domain/synemin peptide complex. (a) Interaction mode of the amino acid residue at position 0 (P0) of synemin C-terminal (peptide in yellow), interaction in detail to MyoA PDZ hydrophobic pocket. (b) The carboxylate-binding loop of the MyoA PDZ (Pro16–Phe19). (c) Interaction mode of the amino acid residue at position -1 (P-1) of synemin peptide mediated by the arginine stacking (Arg20 and Arg37).

Phenylalanine P0 and tryptophan P-1 peptide residues adapt the classical PDZ/peptide binding mode. The phenylalanine P0 side chain occupies the hydrophobic pocket, which is composed of Trp 17, Phe 19, Leu 21, Tyr 66, Ile 70 and Met 73 (figure 3.10a). The hydrophobic pocket is a primary interaction point, its size and volume will influence the affinity and selectivity to accommodate different ligand residues at the P0 position (Lee, Park et al. 2011). The carboxylate-binding loop

(Pro16, Trp 17, Gly18 and Phe 19) docks the peptide phenylalanine P0 carboxylate end and the amine group promotes the main polar interactions (figure 3.10b). The tryptophan P-1 side chain is stabilized in its position being sandwiched by two arginine residues (figure 3.10c). Guanidinium group of Arg20 is parallel to the tryptophan side chain, promoting a cation-π stacking interaction, and the Arg37 three hydrophobic methylene groups interact with the tryptophan indole aromatic hydrophobic group.

3.3. Myopodin A PDZ domain/VPS18 complex structure and interaction studies

3.3.1. Isothermal titration calorimetry of MyoA PDZ and VPS18

In order to characterize further the binding of MyoA PDZ to VPS18 peptide the affinity was measured by ITC. For the ITC, 500 μM VPS18 peptide was injected into a 25 μM solution of MyoA PDZ. Data were plotted and analyzed using a single binding site model with the MicroCal Origin software. The titration curve of VPS18 C-terminal peptide is shown in figure 3.11 and the binding affinity of 8.84 μM ± 0.86 μM (dissociation constant, K_d) was determined with a stoichiometry of approximately 1. VPS18 C-terminal PDZ binding motif peptide (EEEQLSWL) is classified as PDZ class I (-X-[S/T]-X-Φ), with a lower affinity observed in the ITC experiment compared with synemin peptide PDZ class III interaction.

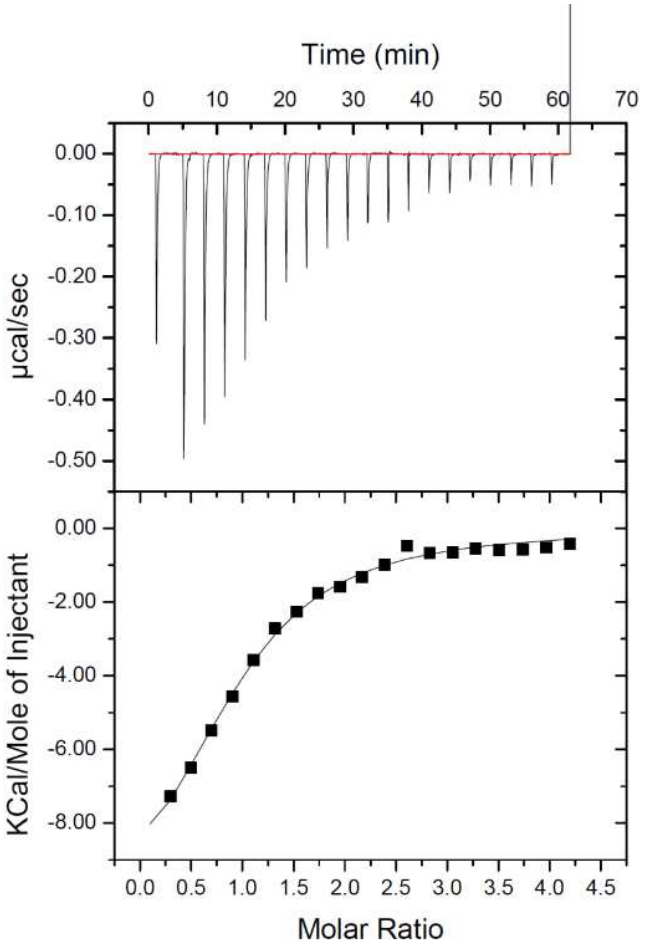

MyoA PDZ x VPS18 (EEEQLSWL)

K_d = 8.84 µM ± 0.86 µM

Syringe: 500 µM VPS18

Cell: 25 µM MyoA PDZ

N: 0.930 ± 0.0470 sites

ΔH -11.64 ± 0.76 kcal/mol

ΔS -16.1 cal/mol/deg

Figure 3.11: Isothermal titration calorimetry of MyoA PDZ with VPS peptide. ITC titration of MyoA PDZ with VPS18 peptide was performed at 25ºC in 20 mM potassiun phosphate buffer, pH 7.0, 100 mM NaCl, and 1 mM TCEP. Shown, from top to bottom, are the raw titration data of VPS18 peptide injected into MyoA PDZ, and the integrated heat measurements for the titration. The first injection peak was discarded because of the backlash effect. The stoichiometry number (N) was obtained for the data set by fitting a standard 1:1 interaction. The data were plotted and analyzed using a single binding site model with the MicroCal Origin software.

3.3.2. Structure determination Myo PDZ/VPS18 complex

The MyoA PDZ in pure water in presence of 3 mM VPS18 peptide was submitted to a pre-crystallization test and an optimal concentration of 10 mg/ml (~ 1mM) was observed. Crystals were already observed where we have the protein in water using the PCT condition A1 (100 mM tris pH 8.5, ammonium sulfate 2.0 M).

Table 3.4 Data collection and refinement statistics of MyoA PDZ/VPS18 complex

DATA COLLECTION	
Source	ESRF
Wavelength (Å)	0.933
Resolution (Å)	39.80 – 2.35 (2.48 – 2.35)
Space group	$I4_122$
Unit cell (Å)	a = b = 79.61,c = 63.86
Molecules / a.u.	1
Unique reflections	4508 (649)
Completeness (%)	99.9 (99.8)
R_{meas}[b]	0.039 (0.499)
R_{pim}[c]	0.015 (0.189)
R_{merge}	0.036 (0.461)
CC(1/2)	1.000 (0.893)
Multiplicity	6.3 (6.7)
I/sig(I)	27.6 (3.9)
B_{Wilson} (Å^2)	70.03
Software used for integration	XDS
Software used for scaling	Scala
DATA REFINEMENT	
R_{cryst}[d]/ R_{free}[e]	0.207 / 0.250
No. Reflections used for R_{free} (%)	5
R.m.s.d. bonds (Å)	0.006
R.m.s.d. angles (º)	1.15
B protein (Å^2)	68.7
B solvent (Å^2)	66.4
B peptide (Å^2)	94.5
Software used for refinement	PHENIX/REFMAC/PDB_REDO
Refinement method	ML/TLS

[a] Values in parentheses are for the highest resolution shell.

[b] $$R_{meas} = \frac{\sum_h \sqrt{\frac{n_h}{n_h - 1}} \sum_i^{n_h} \left| \hat{I}_h - I_{h,i} \right|}{\sum_h \sum_i^{n_h} I_{h,i}} \text{ with } \hat{I}_h = \frac{1}{n_h} \sum_i^{n_h} I_{h,i}$$

[c] $$R_{pim} = \sum_{hkl} \sqrt{\frac{1}{N-1}} \sum_i \left| I_i(hkl) - \overline{I(hkl)} \right| / \sum_{hkl} \sum_i I_i(hkl)$$

Where I (hkl) is the mean intensity of multiple I_i (*hkl*) observations of the symmetry-related reflections, N is the redundancy, n_h is the multiplicity, $\hat{I}_h$ is the average intensity and $I_{h,i}$ is the observed intensity.

[d] $R_{cryst} = \Sigma |F_o - F_c| / \Sigma F_o$

[e] R_{free} is the cross-validation R_{factor} computed for the test set of reflections (5 %) which are omitted in the refinement process.

Diffraction data were collected using the beamline BM14 at ESRF (Grenoble, France). The MyoA PDZ/VPS18 complex crystals (Figure 3.7 c) belong to space group $I4_122$ with unit cell dimensions of a = b = 79.61, c = 63.86 Å and 1 molecule in the

assimetric unit. The structure was solved by molecular replacement using MyoA PDZ/synemin complex structure as a search model and was refined to a resolution of 2.35 Å with R_{factor} and R_{free} of 20.7% and 25.0% respectively. The data collection and refinement statistics are summarized in table 3.4.

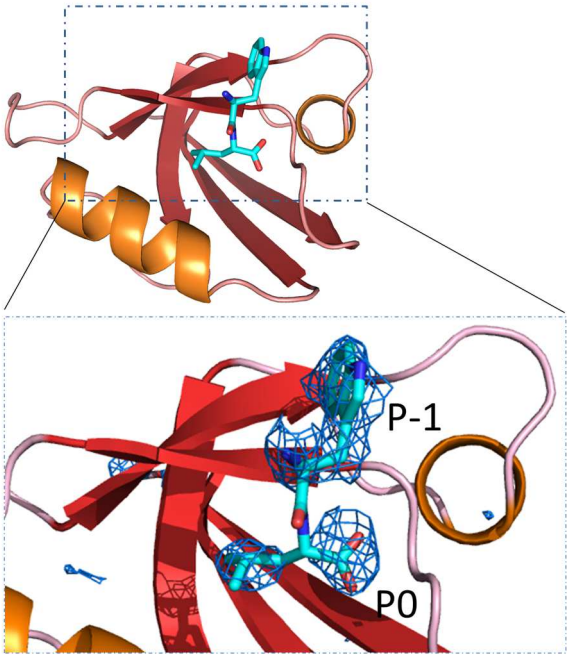

Figure 3.12: Structure of MyoA PDZ/VPS18 complex. PDZ domain structure with VPS18 peptide OMIT map calculated with σ_A-weighted ($2mF_o$ - DF_c) exp($i\varphi_c$) coefficients contoured at 1 σ level.

In the final refined model, 2 out of 8 residues of the synemin peptide could be clearly seen in the electron density map (Leucine P0 and tryptophan P-1) (figure 3.12 inset). The last 2 residues from VPS18 PDZ binding motif present a compatible conformation as observed in MyoA PDZ/synemin complex.

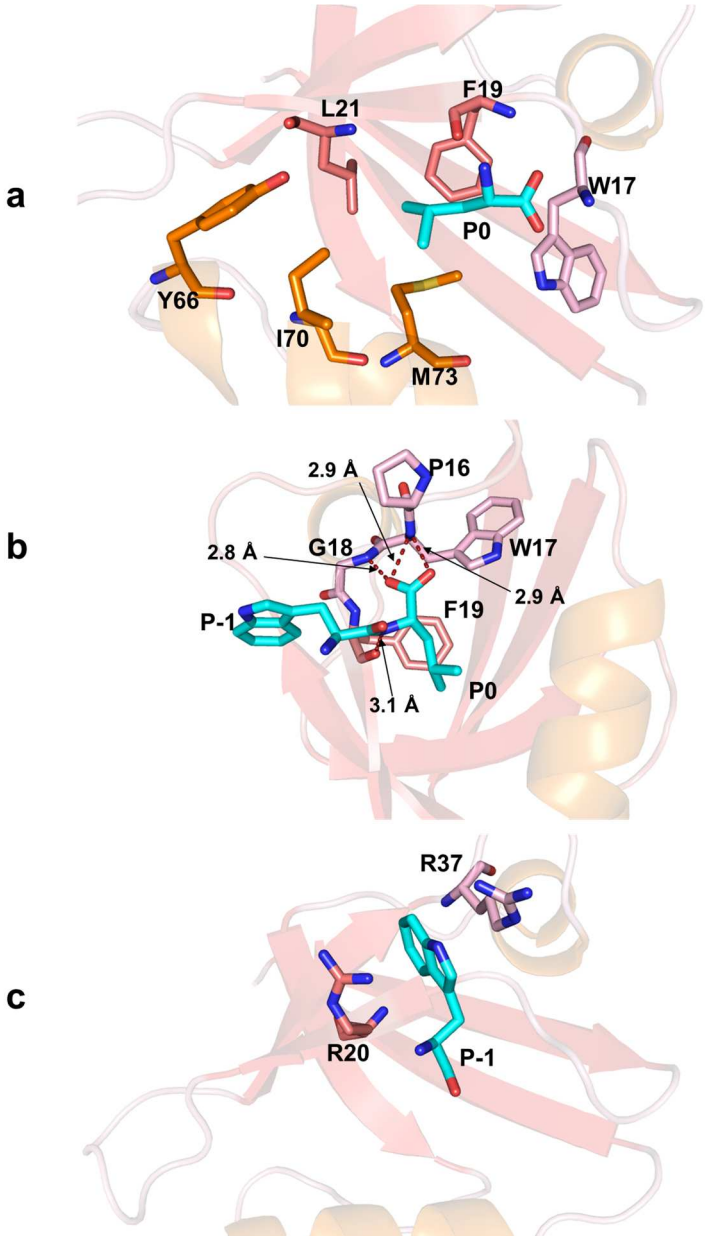

Figure 3.13: Structural basis for the binding affinity and specificity of MyoA PDZ domain/VPS18 peptide complex. (a) Interaction mode of the amino acid residue at position 0 (P0) of VPS18 C-terminal (peptide in cyan), interaction in detail to MyoA PDZ hydrophobic pocket. (b) The carboxylate-binding loop of the MyoA PDZ (Pro16–Phe19). (c) Interaction mode of the amino acid residue at position -1 (P-1) of VPS18 peptide mediated by the arginine stacking (Arg20 and Arg37).

Leucine P0 and tryptophan P-1 peptide residues still display the classical PDZ/peptide binding mode. The leucine P0 side chain occupies the hydrophobic pocket, which is composed of Trp 17, Phe 19, Leu 21, Tyr 66, Ile 70 and Met 73 (figure 3.13a). The hydrophobic pocket is a primary interaction point, but the leucine P0 from VPS18 does not occupy the same volume and does not interact closely with the major part of the hydrophobic residues, compared with phenylalanine P0 from synemin,

which might be the primary residue for the decrease affinity. The carboxylate-binding loop (Pro16, Trp 17, Gly18 and Phe 19) docks the leucine P0 carboxylate, which forms one polar interaction with main chain of Gly18 residue (figure 3.13b). The tryptophan P-1 side chain follows the same model observed in synemin binding, where the tryptophan is stabilized by an arginine packing promoted by 2 arginine residues (figure 3.13c). Arg20 is oriented in a parallel form to the tryptophan side chain, promoting a cation-π interaction in a stacked conformation, and the Arg37 three hydrophobic methylene groups interact hydrophobically with the tryptophan indole functional group.

3.4. Myopodin A PDZ domain/ACTN2 complex structure and interaction studies

3.4.1. Isothermal titration calorimetry of MyoA PDZ and ACTN2

In order to further characterize the binding of MyoA PDZ to α-actinin 2 (ACTN2) peptide, the affinity was measured by ITC. For the ITC, ACTN2 peptide 1.0 mM was injected into a solution of MyoA PDZ 50 μM. Data were plotted and analyzed using a single binding site model with the MicroCal Origin software. The titration curve of ACTN2 C-terminal peptide is shown in figure 3.14, but, unexpectedly, ITC measurements revealed only an extremely weak interaction with the peptide, with a curve that makes the interpretation impossible. ACTN2 C-terminal PDZ binding motif peptide (ALYGESDL) is classified as PDZ class I (-X-[S/T]-X-Φ). This class of interaction proved to have a decreased affinity as observed with VPS18 peptide. However, due tothe very low affinity observed for this complex, it was not possible to calculate the affinity for this interaction. The structure of the complex should deliver additional information to explain this difference between myopodin PDZ domain binding partners.

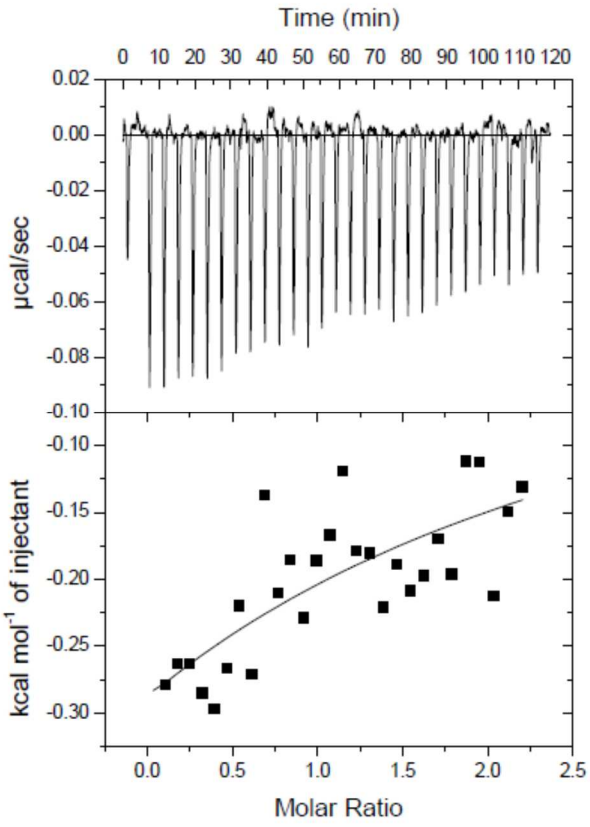

Figure 3.14: α-actinin 2 carboxy-terminal peptide binding to MyoA PDZ ITC analysis testing the interaction of peptide ALYGESDL. While a trend in the titration curve hints at a weak binding affinity it interaction cannot be reliably determined by ITC measurement.

3.4.2. Structure determination Myo PDZ/ACTN2 complex

The MyoA PDZ in pure water in presence of 3 mM ACTN2 peptide was submitted to a pre-crystallization test and an optimal concentration of 10 mg/ml (~ 1mM) was observed. Crystals were readily observed using the PCT condition A1 (100 mM tris pH 8.5, ammonium sulfate 2.0 M).

Table 3.5 Data collection and refinement statistics of MyoA PDZ/ACTN2 complex

DATA COLLECTION	
Source	ESRF
Wavelength (Å)	0.933
Resolution (Å)	39.63 – 1.95 (2.06 – 1.95)
Space group	$I4_122$
Unit cell (Å)	a = b = 79.27, c = 63.60
Molecules / a.u.	1
Unique reflections	7624 (1076)
Completeness (%)	99.6 (99.2)
R_{meas} [b]	0.074 (0.505)
R_{pim} [c]	0.023 (0.148)
R_{merge}	0.070 (0.483)
CC(1/2)	0.999 (0.941)
Multiplicity	10.6 (11.4)
I/sig(I)	11.8 (4.8)
B_{Wilson} (Å^2)	42.65
Software used for integration	XDS
Software used for scaling	Scala
DATA REFINEMENT	
R_{cryst} [d] / R_{free} [e]	0.209 / 0.227
No. Reflections used for R_{free} (%)	5
R.m.s.d. bonds (Å)	0.003
R.m.s.d. angles (º)	0.78
B protein (Å^2)	39.8
B solvent (Å^2)	56.4
B peptide (Å^2)	45.7
Software used for refinement	PHENIX/REFMAC/PDB_REDO
Refinement method	ML/TLS

[a] Values in parentheses are for the highest resolution shell.

[b] $$R_{meas} = \frac{\sum_h \sqrt{\frac{n_h}{n_h - 1}} \sum_i^{n_h} \left| \hat{\mathrm{I}}_h - \mathrm{I}_{h,i} \right|}{\sum_h \sum_i^{n_h} \mathrm{I}_{h,i}} \text{ with } \hat{I}_h = \frac{1}{n_h} \sum_i^{n_h} \mathrm{I}_{h,i}$$

[c] $$R_{pim} = \sum_{\mathrm{hkl}} \sqrt{\frac{1}{N-1}} \sum_i \left| \mathrm{I}_i(hkl) - \overline{\mathrm{I}(\mathrm{hkl})} \right| / \sum_{\mathrm{hkl}} \sum_i \mathrm{I}_i(hkl)$$

Where I (hkl) is the mean intensity of multiple I_i (*hkl*) observations of the symmetry-related reflections, N is the redundancy, n_h is the multiplicity, $\hat{I}_h$ is the average intensity and $I_{h,i}$ is the observed intensity.

[d] $R_{cryst} = \Sigma \, |F_o - F_c| \, / \, \Sigma \, F_o$

[e] R_{free} is the cross-validation R_{factor} computed for the test set of reflections (5 %) which are omitted in the refinement process.

Diffraction data were collected using the beamline ID23-2 ESRF (Grenoble, France). The MyoA PDZ/VPS18 complex crystals (figure 3.7 d) belong to space group $I4_122$ with unit cell dimensions of a = b = 79.27, c = 63.60 Å and 1 molecule in the

asymmetric unit. The structure was solved by molecular replacement using MyoA PDZ/synemin complex structure as a search model and was refined to a resolution of 1.95 Å with R_{factor} and R_{free} of 20.9% and 22.7% respectively. The data collection and refinement statistics are summarized in table 3.5.

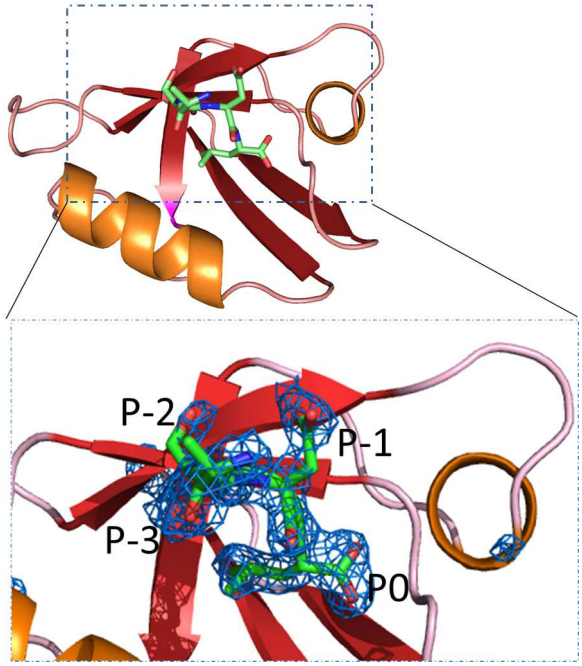

Figure 3.15: Structure of MyoA PDZ/ACTN2 complex PDZ domain structure with ACTN2 peptide OMIT map calculated with σ_A-weighted ($2mF_o$ - DF_c) exp($i\varphi_c$) coefficients contoured at 1 σ level.

In the final refined model, 4 out of 8 residues of the ACTN2 peptide can clearly be seen in the electron density map (leucine P0, aspartate P-1, serine P-2 and glutamate P-3 main chain) (figure 3.15 inset). As observed in MyoA PDZ/synemin complex, the conformational position of the residue P-2 and P-3 shows a perpendicular orientation in a non-canonical conformation. Since the rest of the peptide is not interacting, it could have an increased dynamic and consequently weak electron density.

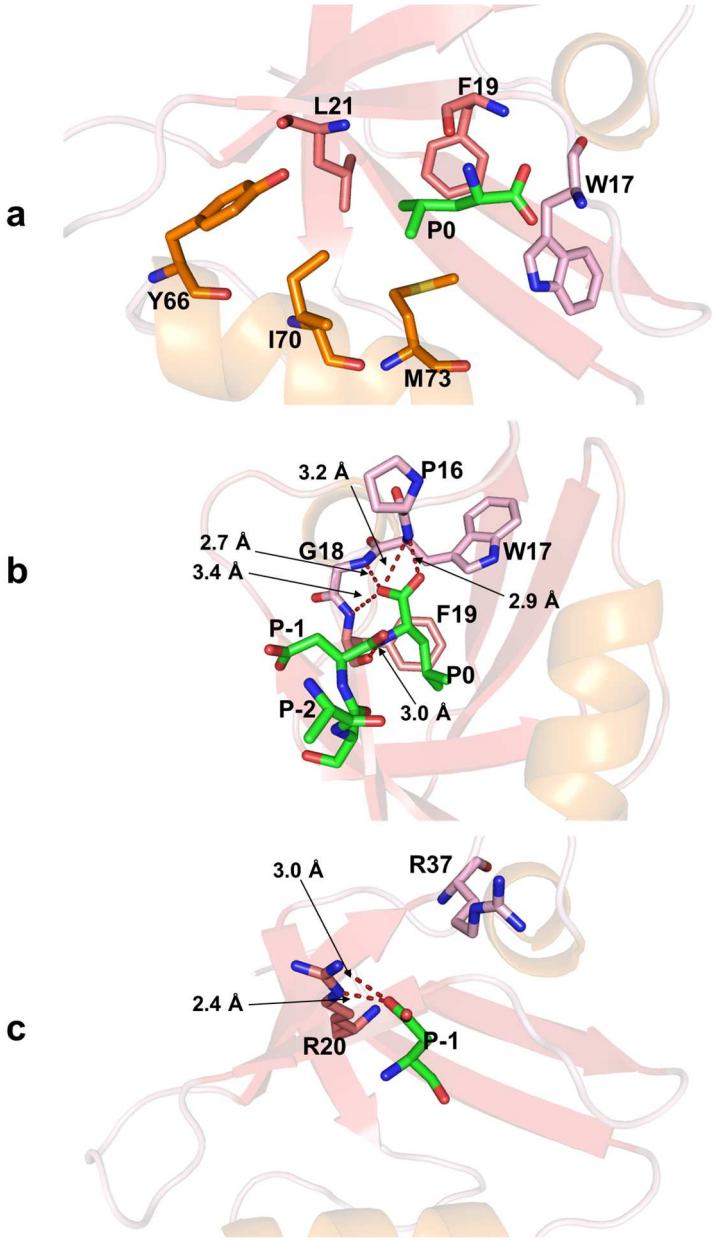

Figure 3.16: Structural basis for the binding affinity and specificity of MyoA PDZ domain/ACTN2 peptide complex. (a) Interaction mode of the amino acid residue at position 0 (P0) of ACTN2 C-terminal (peptide in green), interaction in detail to MyoA PDZ hydrophobic pocket. (b) The carboxylate-binding loop of the MyoA PDZ (Pro16–Phe19). (c) Interaction mode of the aspartate at position -1 (P-1) of VPS18 peptide mediated by electrostatic interactions with the Arg20.

Leucine P0 and aspartate P-1 peptide residues interact with the PDZ/peptide in classical mode mode. The leucine P0 side chain is occupying the hydrophobic pocket (figure 3.16a) as observed in MyoA PDZ/VPS18 complex. This primary interaction point stipulates a similar pattern of interactions as observed for leucine P0 hydrophobic residues of VPS18, and seems to be the primary source for different affinities. The carboxylate-binding loop (Pro16, Trp 17, Gly18 and Phe 19) docks the leucine P0

carboxylate group. These interactions are similar to those observed in the other complexes, since they are established to the main chain of the carboxylate-binding loop (figure 3.16b) and therefore sequence independent. The aspartate P-1 side chain does not follow the same model observed in the previous complexes, but interaction only with the guanidinium group of Arg20 (figure 3.16c).

3.5. MyoA PDZ crystal packing influence in the peptide binding site.

The apo structure of the myopodin solved PDZ domain reassembles the main features for a typical PDZ fold, with 5 β-strands forming an antiparallel β-barrel and 2 α-helices. In addition, the PDZ domain was co-crystallized with different peptides from 3 binding partners (synemin, VPS18 and ACTN2). All these solved structures present the same space group and unit cell dimensions. However, myopodin PDZ domain showed interaction with different PDZ/peptide biding motif classes. For class I interaction for α-actinin 2 (ACTN2) and VPS18 was observed, and for class III interaction for synemin. The apo structure of MyoA PDZ is very similar to MyoA PDZ in complex to the peptides (RMSD: 0.43, 0.41 and 2.13 $Å^2$ for synemin, VPS18 and ACTN2 complexes, for 84 equivalent Cα atoms). However, the most accentuated differences map to the residue side chains that compose the peptide binding pocket. These side chains change conformations to accommodate the PDZ binding motif from the binding partners. This is evident in the peptide binding pocket residues Tyr66, Ile70 and Met 73 from α-helix 2. Another structural difference is in the residues responsible for the arginine packing (Arg20 and Arg37) to the peptide binding, specifically the residue P-1 of the peptide (figure 3.17).

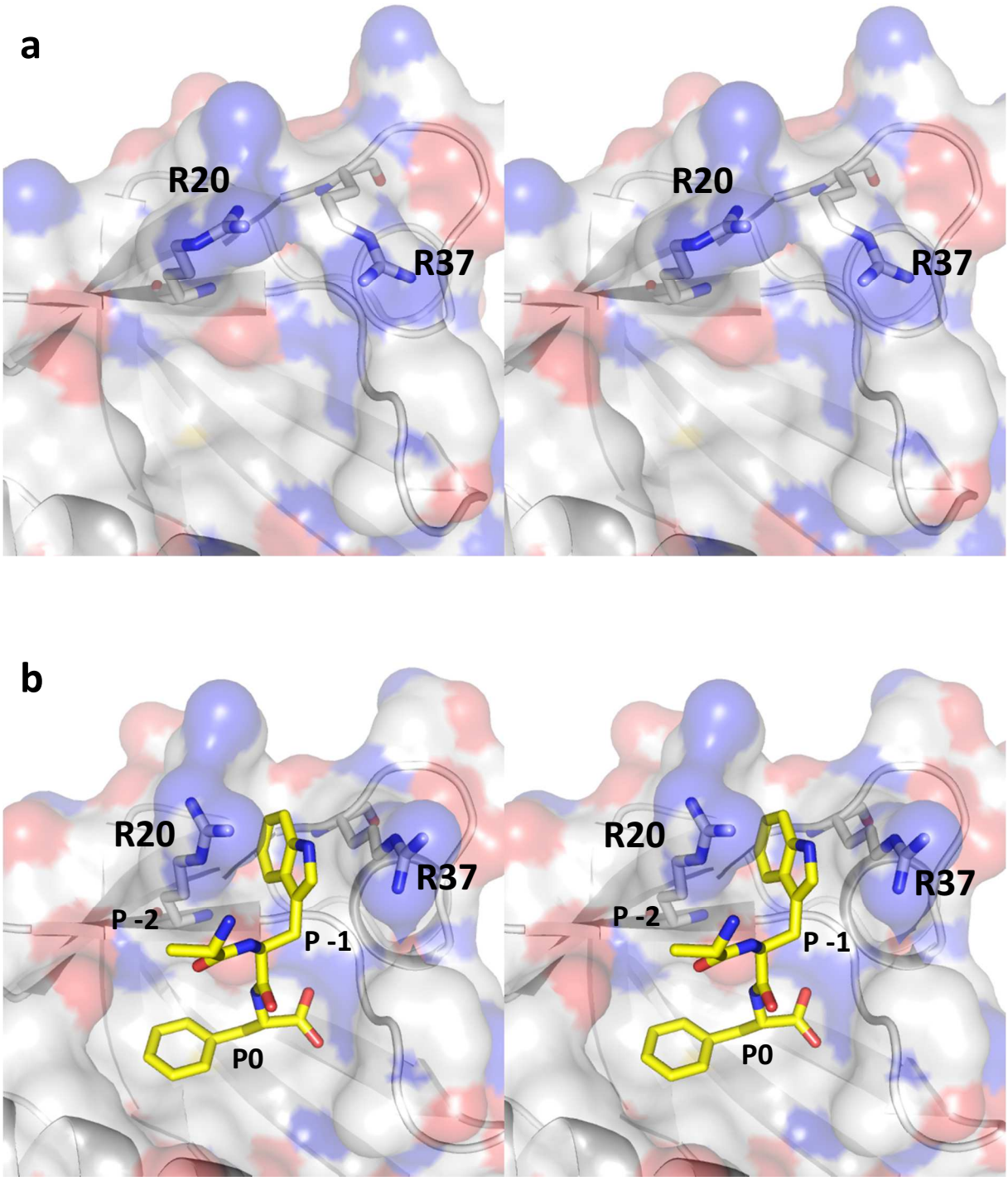

Figure 3.17: Arginine 20 and 37 side chain shift upon peptide binding. Stereo view of the apo PDZ domain (a) and the partial synemin peptide in the peptide binding pocket (b), representing how these arginine residues change conformation upon peptide accommodation.

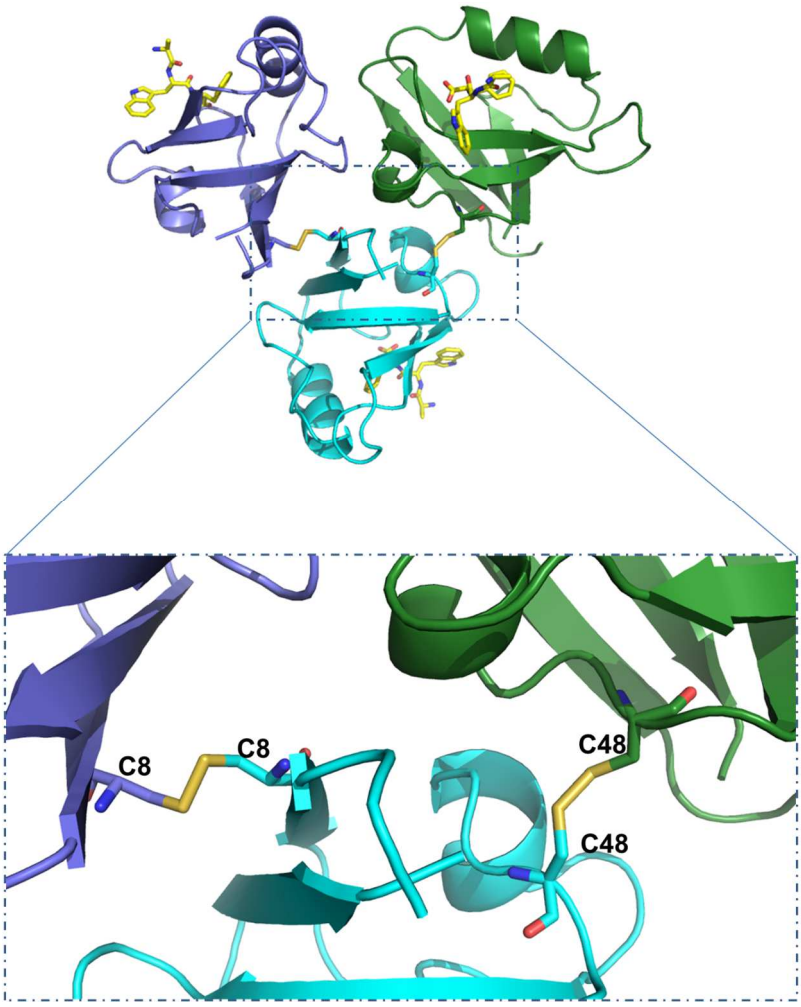

Figure 3.18: MyoA PDZ Crystal lattice arrangement representation. The crystal lattice is governed by PDZ intermolecular CYS-CYS interactions shown in detail in the image inset.

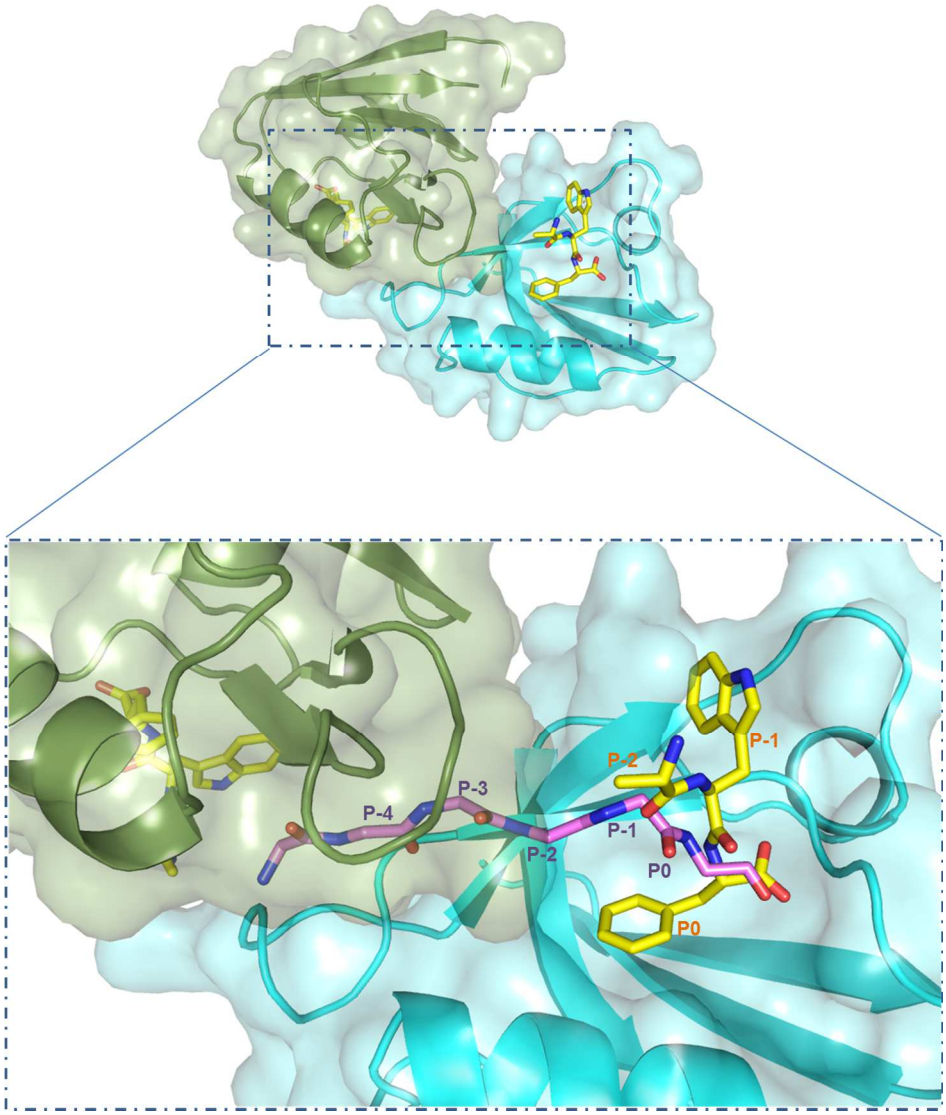

Figure 3.19: Crystal contact interface of MyoA PDZ-synemin structure. For the sake of simplicity, Myo A PDZ-synemin complex is used as an example of what can be seen in Myo A PDZ-VPS18 and Myo A PDZ-actinin 2 complexes. The peptide binding pocket from one MyoA PDZ molecule (green surface) is partially occupied by other MyoA PDZ molecule (cyan surface) from neighboring crystal lattice. On the bottom panel, the representation of a peptide bound in a canonical fashion (pink) to PDZ (PDB code: 3QGL) indicates the region of potential clashes between amino acid residues of the peptides (position -2 (P-2) to -4 (P-4)) and MyoA PDZ molecule binding pocket. Such MyoA PDZ crystal contact interface could lead to a perpendicular way of binding of synemin peptide (yellow).

In the MyoA PDZ domain/peptide structures presented here, only 3, 2, and 4 residues of synemin, VPS18 and ACTN2, respectively, could be observed due to the clash within the crystal packing contacts between the symmetry related molecules. Intermolecular disulfide bonds govern the crystal lattice formation. The Cys8 and Cys48 form disulfide bonds with the other two neighboring PDZ molecules (figure 3.18). This crystal arrangement can be observed in apo PDZ domain crystals and in

all peptide/PDZ domain complex crystals. The interface of the crystal contact clashes with the N-terminal part of peptides from the neighboring protein complex. This clash generates a partial impediment in peptide binding pocket, and consequently prevents the canonical binding for the PDZ binding motif. The MyoA PDZ crystallized in complex with the peptides from the binding partners showed a different conformation compared with PDZ/peptides complexes in a typical canonical orientation (figure 3.19). The peptide residues P0 present an interaction with the hydrophobic binding pocket and carboxylate-binding loop as described before in the literature for other PDZ domains, the rest of the bound peptide does not engage in a typical β-sheet augmentation with the PDZ β-strand, but display a perpendicular orientation.

3.6. Nuclear magnetic resonance spectroscopy for native and complex PDZ

In all our crystallographic models for MyoA PDZ in complex with peptides, we observe the non-canonical perpendicular conformation, but there are still some questions over the fact that this peptide conformation is present only in the crystal lattice, which alternates to a canonical conformation in solution. To investigate the true nature of the binding between the PDZ and its binding partner peptides, we performed NMR experiments using the MyoA PDZ complex with synemin peptide. Synemin presents the highest affinity to MyoA PDZ and saturated the peptide binding site with a molar ratio of 1.5 (1mM of Myo PDZ to 1.5 mM of synemin peptide). This concentration, no further significant changes in the shifts were observed.

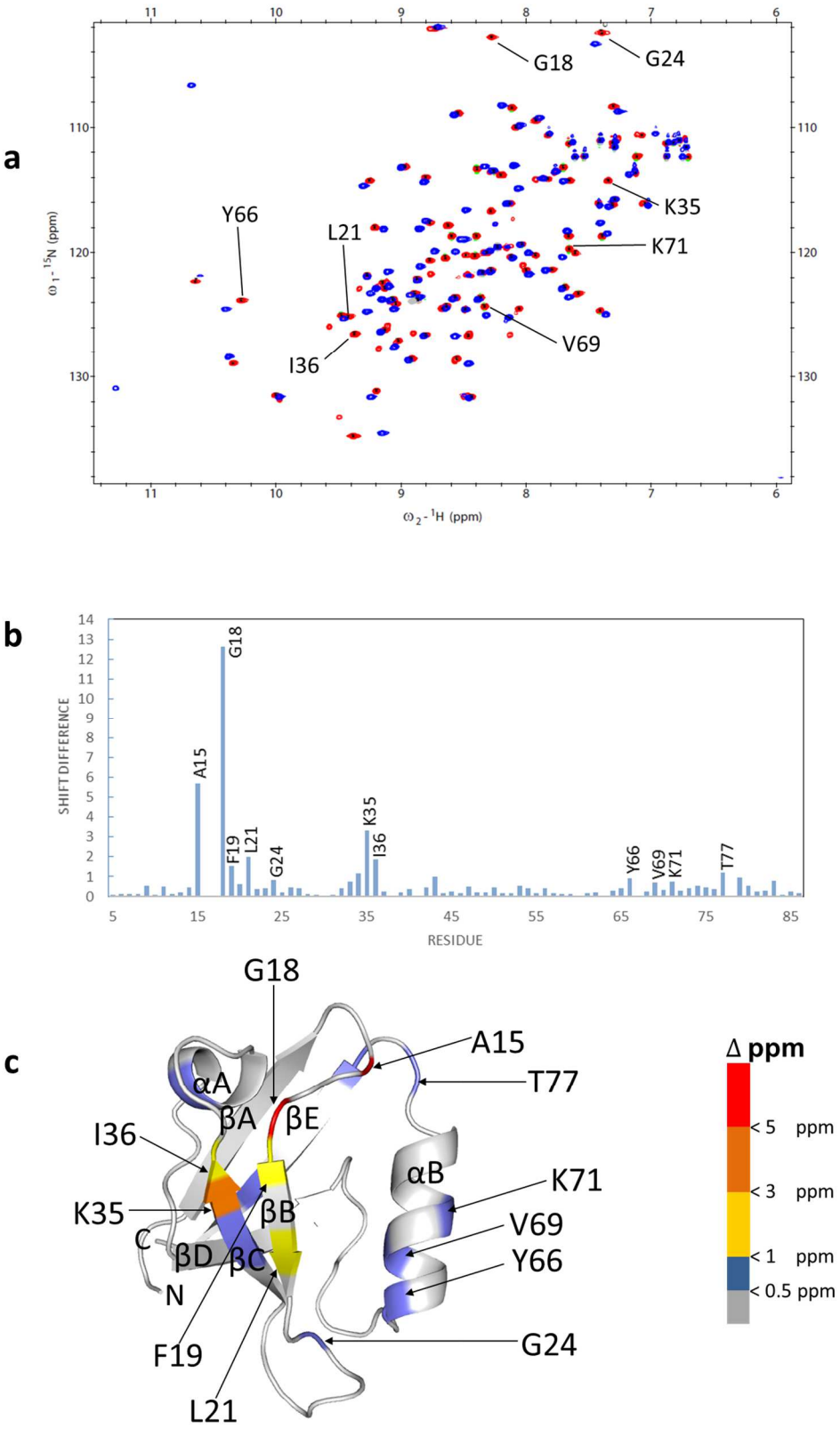

Figure 3.20: Structural changes of MyoA PDZ upon synemin peptide binding. (a) Overlay plot of the ^{1}H-^{15}N HSQC data of the free (red) and bound (blue) MyoA PDZ. (b) Chemical shifts differences > 1 ppm indicate synemin peptide binding to MyoA PDZ. (c) X-ray structure of MyoA PDZ displaying amino acid residues with significant chemical shift differences upon peptide binding experiment.

The overlay plot of the 1H-15N correlation maps were recorded for the free and bound forms of the 15N-labelled MyoA PDZ (figure 3.20a). This data allowed the detection of the effects on MyoA PDZ peptide binding pocket upon peptide interaction. The combined chemical shift changes of amides were calculated using the equation $\sqrt{(\Delta\delta^{15}\mathrm{N})^2 + (5\Delta\delta^{1}H)^2}$.

Structural changes were mapped based on the extent to which each peak moved in the bound state relative to the free state, and chemical shifts larger than 1 ppm are considered as indication of a change of chemical environment due the peptide binding (figure 3.20b). The residues with chemical shift changes enclose the peptide binding pocket to the carboxylate-binding loop and hydrophobic pocket (Gly18, Phe19 and Val 69). Moreover, shifts of Tyr66 side chains of α-helix B and shifts due to the β-sheet augmentation for the β-strand B Leu21 typical of for canonical peptide-binding site of the PDZ domain, are observed.

3.7. Myopodin central domain interaction studies

3.7.1 Myopodin central domain and filamin C constructs

The central domain construct of myopodin named MyoA CD (amino acid residues 664-916), is one of the independent sites of interactions to α-actinin 2, which also binds to filamin C and actin. In addition, one phosphomimetic central domain mutant was designed and named MyoA CD Mut, (S902D, S906D, S910D) to study the effects of a potential phosphorylation in the interactions (figure 3.21).

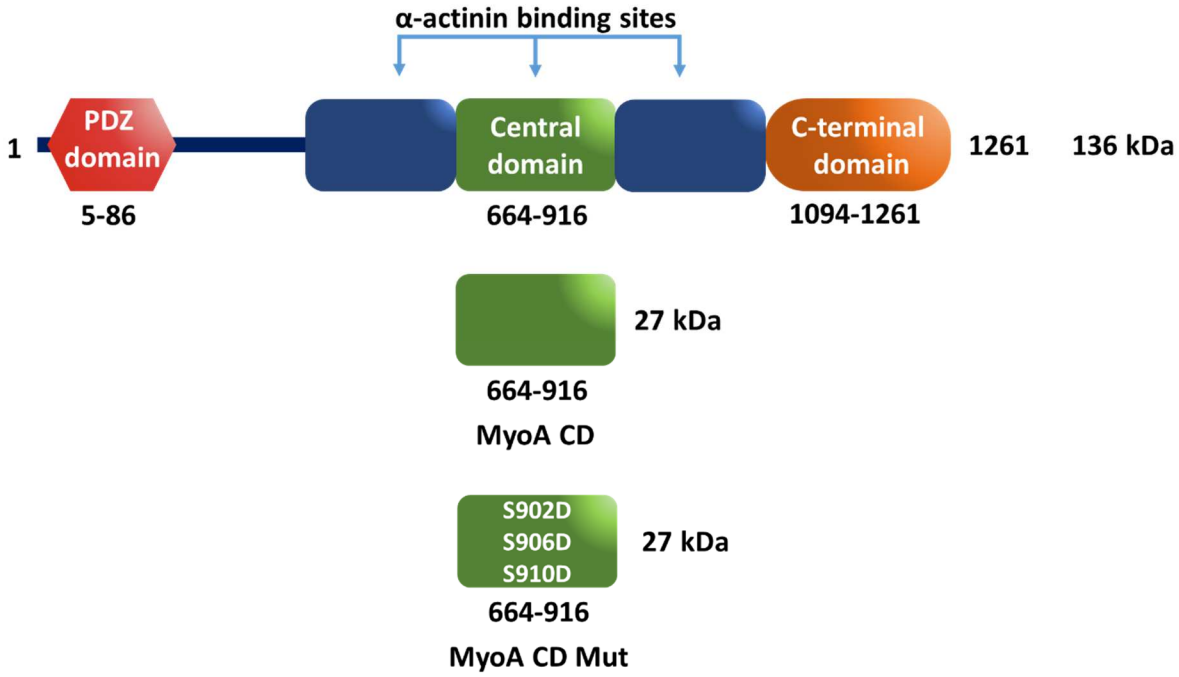

Figure 3.21. **Schematic illustration of myopodin A, an isoform with 1261 residues and 136 kDa**. The MyoA CD and MyoA CD Mut constructs contain the PDZ domain located in the amino-terminus (664-916).

The filamin C construct was designed to cover the mapped region of interaction to myopodin, the Ig domains d20-21. However, the constructs of the domain d20 alone and the domains d20-21 are unstable and present aggregation and degradation. To avoid this problem the designed constructs for the interaction assays present an extension in the N-terminal region, and additionally include the domains d19 and d18. The construct FLNc d18-21 (figure 3.22) becomes Suitable for purification without disturbing aggregation products.

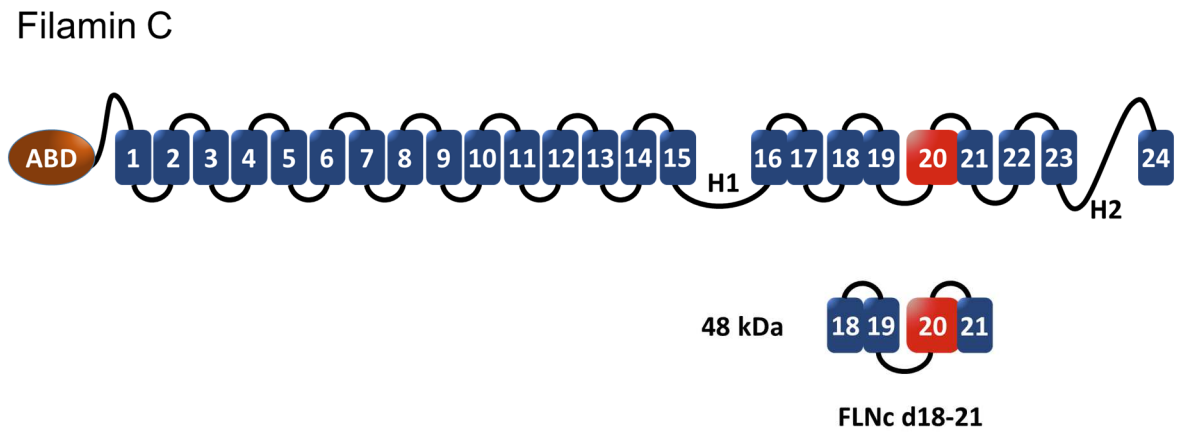

Figure 3.22. **Schematic illustration of filamin C.** The FLNc d18-21 construct (1952-2041aa) which contains the domains d20 and d21, the binding site to myopodin central domain.

3.7.2 Purification of recombinant myopodin central domain and filamin C constructs

MyoA CD and MyoA CD Mut constructs were expressed in Rosetta 2 (DE3) pLysS competent *E. coli* cells. Protein samples were initially purified by affinity chromatography with a HisTrap FF crude column (GE Healthcare) (figure 3.23a and 3.24 a). After His-tag cleavage by 3C protease, samples were introduced into a HiTrap Q FF ion exchange chromatography (GE Healthcare) (figure 3.23b and 3.24b). Unbound fractions were collected and further purified using a Superdex 75 16/60 gel filtration column (GE Healthcare) (figure 3.23c and 3.24c). The fractions of the peak corresponding to the MoyA PDZ were collected and further analyzed by SDS-PAGE to measure the purity of samples (Figure 3.23 and 3.24).

The FLNc d18-21 construct was expressed in BL21 (DE3) competent *E. coli* cells. Protein samples were initially purified by affinity chromatography with a HisTrap FF crude column (GE Healthcare) (figure 3.25a). Eluted fractions were collected and further purified using a Superdex 75 16/60 gel filtration column (GE Healthcare) (figure 3.25b). The size exclusion chromatography profile shows two major peaks; the first one is an aggregation product of FLNc d18-21, which can be separate from the native form in the second peak. The fractions of the second peak corresponding to the FLNc

d18-21 free of aggregation products were collected and further analyzed by SDS-PAGE to measure the purity of samples (figure 3.25).

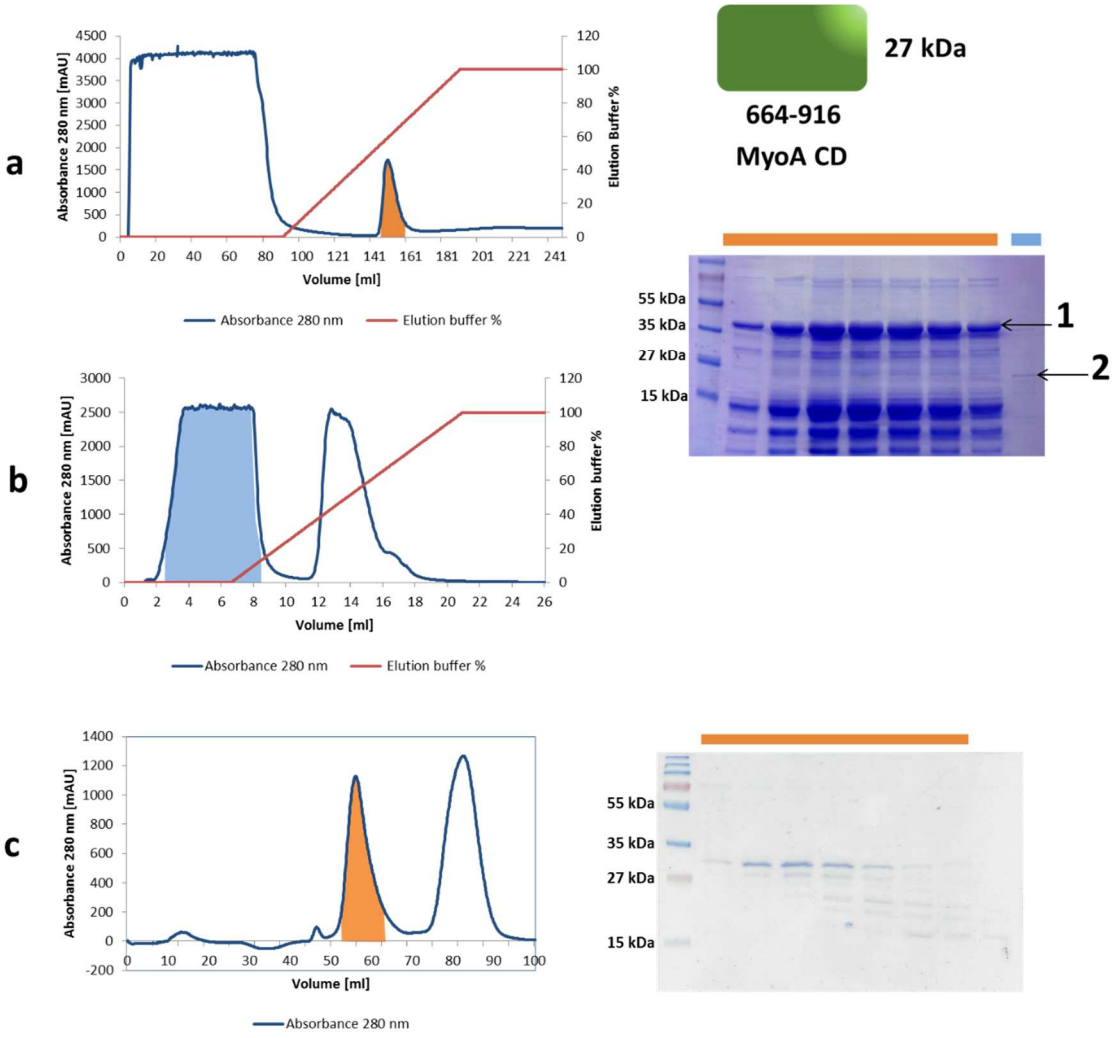

Figure 3.23: Purification of MyoA CD. (a) Elution profile of HisTrap with MyoA CD collected in the retained fraction (1). (b) The cleaved sample (2) is loaded into a HiTrap Q FF and the protein is collected in the flow through fraction. (c) In addition, the sample was applied in a superdex 75 16/600 and eluted with 55 ml elution volume. The purification steps and fractions were analyzed by SDS-PAGE. The gel (18% of acrylamide) was stained with Coomassie brilliant blue.

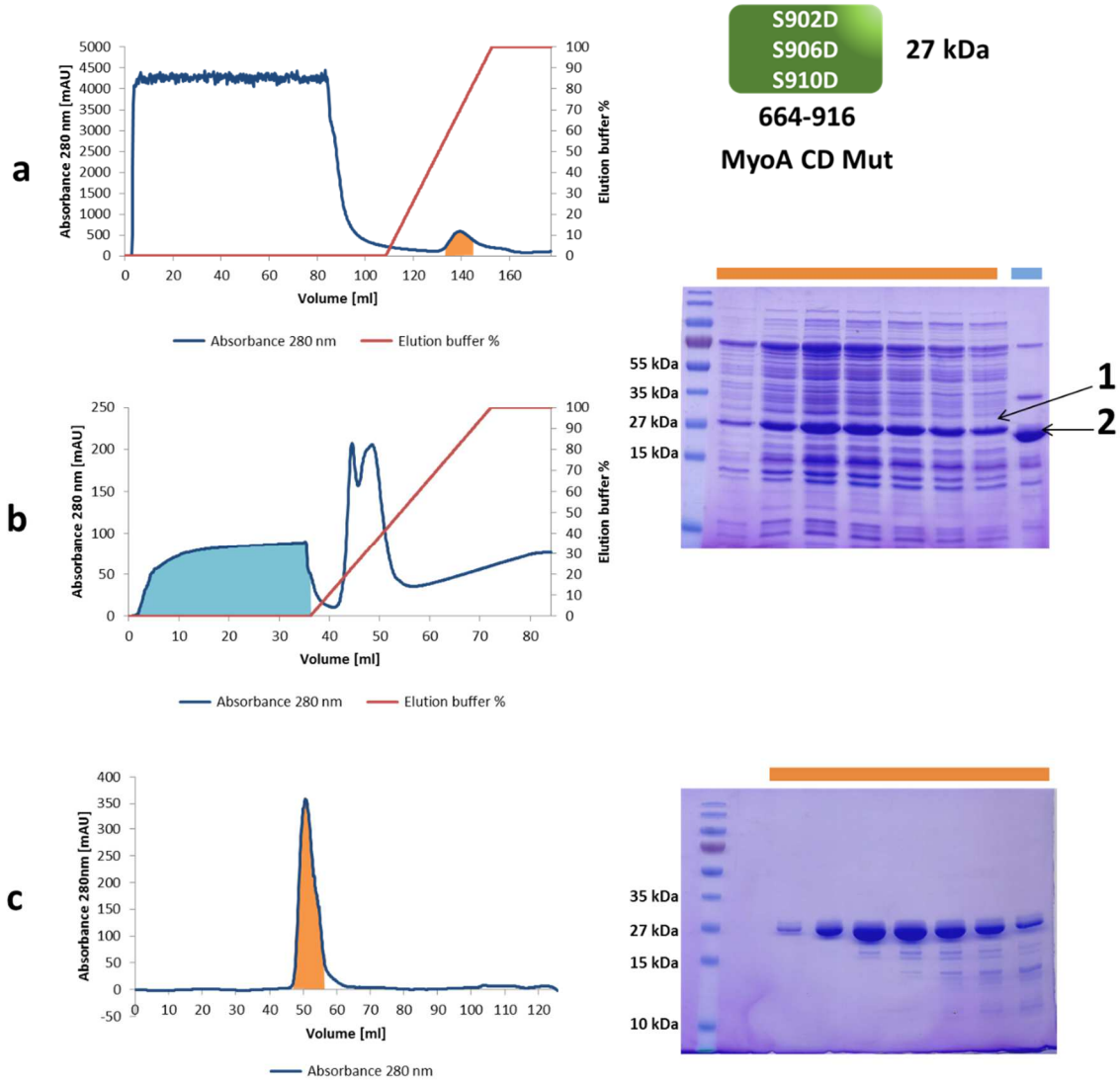

Figure 3.24: Purification of MyoA CD Mut. (a) Elution profile of HisTrap with MyoA CD Mut collected in the retained fraction (1). (b) The cleaved sample (2) is loaded into a HiTrap Q FF and the protein is collected in the flow through fraction. (c) In addition, the sample was applied in a superdex 75 16/600 and eluted with 53 ml elution volume. The purification steps and fractions were analyzed by SDS-PAGE. The gel (18% of acrylamide) was stained with Coomassie brilliant blue.

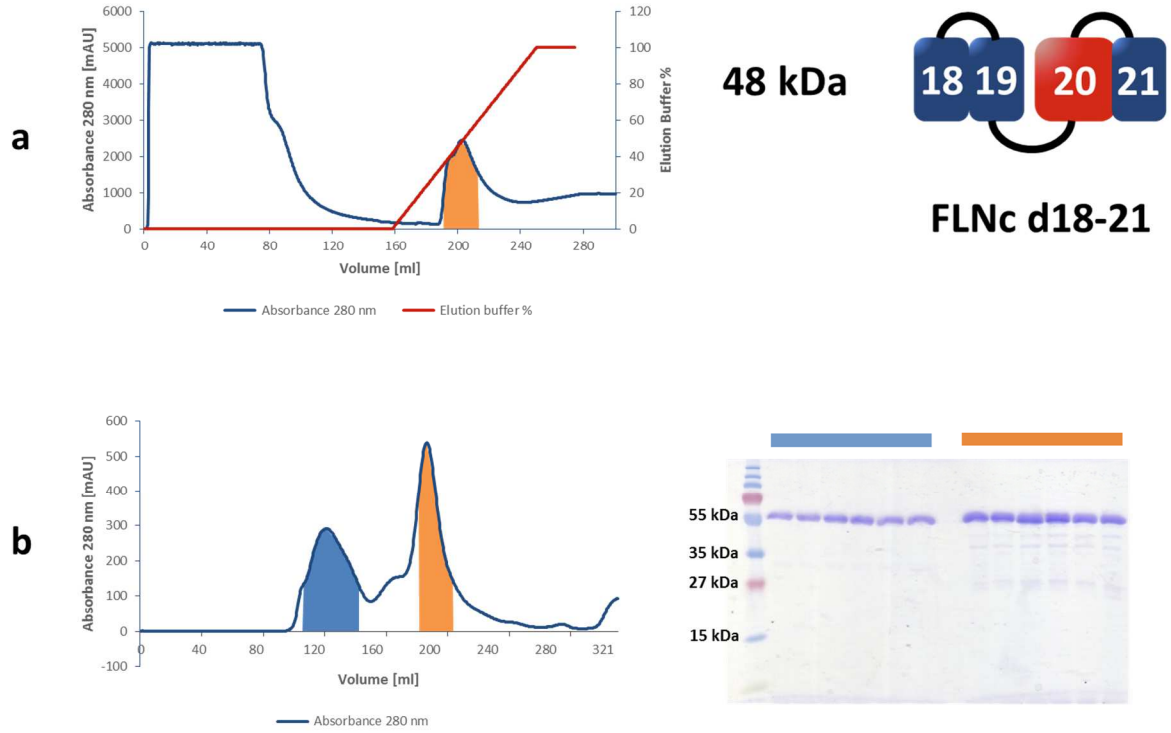

Figure 3.25: Purification of The FLNc d18-21**.** (a) Elution profile of HisTrap with The FLNc d18-21 collected in the retained fraction, (b) applied in a superdex 75 16/600 and the final purified protein (orange peak) was collected free of the aggregation products (blue peak). The purification steps and fractions were analyzed by SDS-PAGE. The gel (18% of acrylamide) was stained with Coomassie brilliant blue.

3.7.3. Myo CD oligomerization state influence in F-actin bundling in reducing conditions

3.7.3.1. Linnemann, A., Vakeel, P., Bezerra, E., Orfanos, Z., Djinovic-Carugo, K., van der Ven, P. F., Kirfel, G., and Furst, D. O. (2013) Myopodin is an F-actin bundling protein with multiple independent actin-binding regions J. Muscle Res. Cell Motil. 34, 61– 69

J Muscle Res Cell Motil (2013) 34:61–69
DOI 10.1007/s10974-012-9334-5

ORIGINAL PAPER

Myopodin is an F-actin bundling protein with multiple independent actin-binding regions

Anja Linnemann · Padmanabhan Vakeel · Eduardo Bezerra · Zacharias Orfanos · Kristina Djinović-Carugo · Peter F. M. van der Ven · Gregor Kirfel · Dieter O. Fürst

Received: 18 April 2012 / Accepted: 28 November 2012 / Published online: 9 December 2012

Abstract The assembly of striated muscle myofibrils is a multistep process in which a variety of proteins is involved. One of the first and most important steps in myofibrillogenesis is the arrangement of thin myofilaments into ordered I-Z-I brushes, requiring the coordinated activity of numerous actin binding proteins. The early expression of myopodin prior to sarcomeric α-actinin, as well as its binding to actin, α-actinin and filamin indicate an important role for this protein in actin cytoskeleton remodelling with the precise function of myopodin in this process yet remaining to be resolved. While myopodin was previously described as a protein capable of cross-linking actin filaments into thick bundles upon transient transfections, it has remained unclear whether myopodin alone is capable of bundling actin, or if additional proteins are involved. We have therefore investigated the in vitro actin binding properties of myopodin. High speed cosedimentation assays with skeletal muscle actin confirmed direct binding of myopodin to F-actin and showed that this interaction is mediated by at least two independent actin binding sites, found in all myopodin isoforms identified to date. Furthermore, low-speed cosedimentation assays revealed that not only full length myopodin, but also the fragment containing only the second binding site, bundles microfilaments in the absence of accessory proteins. Ultrastructural analysis demonstrated that this bundling activity resembled that of α-actinin. Biochemical experiments revealed that bundling was not achieved by myopodin's ability to dimerize, indicating the presence of two individual F-actin binding sites within the second binding segment. Thus full length myopodin contains at least three F-actin binding sites. These data provide further understanding of the mechanisms by which myopodin contributes to actin reorganization during myofibril assembly.

Keywords Myopodin · Synaptopodin 2 · Sarcomeric Z-disc · Actin-binding proteins · Actin cross-linking · Myofibrillogenesis

Electronic supplementary material The online version of this article (doi:10.1007/s10974-012-9334-5) contains supplementary material, which is available to authorized users.

A. Linnemann · P. Vakeel · Z. Orfanos · P. F. M. van der Ven (✉) · G. Kirfel · D. O. Fürst
Department of Molecular Cell Biology, Institute for Cell Biology, University of Bonn, Ulrich-Haberland-Str. 61a, 53121 Bonn, Germany
e-mail: pvdven@uni-bonn.de

Present Address:
A. Linnemann
Fraunhofer-Institute for Applied Information Technology FIT, BioMOS, Schloss Birlinghoven, 53754 St. Augustin, Germany

Present Address:
P. Vakeel
Division of Developmental Biology, Department of Pediatrics, Medical College of Wisconsin, Milwaukee, WI 53226, USA

E. Bezerra · K. Djinović-Carugo
Department for Structural and Computational Biology, Max F. Perutz Laboratories, University of Vienna, 1030 Vienna, Austria

K. Djinović-Carugo
Department of Biochemistry, Faculty of Chemistry and Chemical Technology, University of Ljubljana, 1000 Ljubljana, Slovenia

Introduction

Myopodin is a member of the podins, a protein family that further includes synaptopodin and tritopodin (also called

CHAP) (Chalovich and Schroeter 2010). While synaptopodin was initially detected in postsynaptic densities and in kidney podocytes (hence the name) (Mundel et al. 1997), both other podin proteins are mainly expressed in muscle cells. Myopodin is found in both smooth and striated muscle cells, whereas tritopodin is restricted to cross-striated muscle cells, where it is localized together with myopodin in the myofibrillar Z-disc (Beqqali et al. 2010; Claeys et al. 2009; Linnemann et al. 2010; Weins et al. 2001). A common function of all podins seems to be the organization of the actin cytoskeleton. A careful comparison of the temporal and spatial expression patterns of myopodin and the actin cross-linker α-actinin during early skeletal muscle cell differentiation revealed that myopodin expression precedes that of sarcomeric α-actinin in myofibril forming areas, thereby identifying myopodin as one of the first muscle-specific actin cytoskeleton-associated proteins in these structures (Linnemann et al. 2010).

Both, synaptopodin and myopodin were previously shown to bind actin filaments (Mundel et al. 1997; Weins et al. 2001; Kremerskothen et al. 2005). An additional important feature of all podins is their direct binding to other actin-associated proteins such as α-actinin (Asanuma et al. 2005; Kremerskothen et al. 2005; Linnemann et al. 2010; Weins et al. 2001; Beqqali et al. 2010), while myopodin was shown to bind filamin (Linnemann et al. 2010).

Transient transfection of full length mouse myopodin or of defined myopodin fragments into eukaryotic cells induced the formation of actin cables in the cytoplasm and the nucleus (Weins et al. 2001), implying that myopodin might directly bind and bundle actin filaments. Alternatively, this activity might also occur via α-actinin and filamin, two ligands of actin and myopodin (Linnemann et al. 2010). Along those lines, a mixture of two fesselin isoforms (a protein later identified as avian myopodin) was shown to induce actin gel formation in vitro (Leinweber et al. 1999), indicating that at least one of these proteins is able to bundle F-actin. An identification of the actual binding regions, however, was not possible. In summary, while there is no doubt about the F-actin-binding capacity of myopodin, a definite identification of precise F-actin binding region(s) of myopodin and the mechanisms underlying its actin bundling activity has so far not been provided.

In the experiments described in this report we have analyzed several recombinant fragments of the human myopodin isoform (GenBank: CAZ66141.1) that is expressed in skeletal muscle (Linnemann et al. 2010) for their capacity to directly bind or bundle actin filaments. Our results revealed that this isoform contains at least three independent actin-binding sites. These data significantly contribute to a better understanding of this protein's function, in both myofibril assembly and myofibrillar Z-disc stabilization.

Materials and methods

Design of cDNA constructs

DNA cloning was performed using standard procedures (Ausubel et al. 1995). For bacterial recombinant protein expression, myopodin cDNA fragments were amplified by PCR and cloned into the vectors pET23-T7 (Obermann et al. 1997) and pET23-myc respectively. In the latter vector the T7-tag in pET23-T7 was replaced by a myc-tag (Eulitz, van der Ven and Fürst, manuscript in preparation). For yeast two hybrid experiments, constructs encoding distinct portions of myopodin were cloned into modified pAct2 and pLex vectors (van der Ven et al. 2000) as prey and bait constructs, respectively.

Protein expression and purification

Protein expression was performed in *E. coli* BL21(DE3) Codon Plus cells (Stratagene, LaJolla, CA, USA). Bacteria were grown in LB medium supplemented with 100 mg/l carbenicillin and 34 mg/l chloramphenicol, and protein expression was induced at $OD_{600} = 0.6$ by addition of 0.5 mM IPTG. After 3 h at 30 °C, cells were harvested by centrifugation and stored at −20 °C until further use. Purification of His-tagged protein was performed essentially as described (Obermann et al. 1998). Briefly, bacterial cells were lysed by the addition of lysis buffer (50 mM sodium phosphate, pH 8.0, 300 mM NaCl, 10 mM imidazole, 1 mg/ml lysozyme). DNA was fragmented by sonification and cell debris sedimented by centrifugation (4,500 rpm, 30 min, 4 °C). The supernatant containing the soluble protein fraction was incubated with Ni^{2+}-NTA agarose beads (Qiagen) under constant agitation at 4 °C for 1 h. After filling the beads into a column, they were washed twice with washing buffer (50 mM sodium phosphate, pH 8.0, 300 mM NaCl, 20 mM imidazole) and bound protein was eluted with elution buffer (50 mM sodium phosphate, pH 8.0, 300 mM NaCl, 250 mM imidazole). Proteins were dialyzed against F-actin buffer (0.2 mM ATP, 1 mM EGTA, 2 mM $MgCl_2$, 100 mM KCl, 20 mM imidazol, pH 7.5) and stored on ice until use. Protein concentrations were determined as described (Pace et al. 1995).

Preparation of muscle actin

Muscle actin was purified from acetone powder prepared from chicken breast muscle essentially according to the protocol of Spudich and Watt (1971).

Actin cosedimentation assays

Cosedimentation assays were performed in F-actin buffer (see above). 5 μM G-actin was polymerized for 45 min at

room temperature in 70 µl of F-actin buffer with or without 0.5 mM β-mercaptoethanol. Purified myopodin fragments were added and the final volume was adjusted to 100 µl by the addition of F-actin buffer. After an incubation time of 45 min samples were centrifuged for 45 min at 4 °C at 100,000×*g* for high speed cosedimentation assays, or at 10,000×*g* for low speed cosedimentation experiments. Pellets and supernatants were separated; pellets were briefly rinsed with H_2O and resuspended in 100 µl F-actin buffer. 0.2 vol of 5× SDS sample buffer (5 mM EDTA, 30 % glycerol, 60 mM Tris/HCl, 15 % SDS, 7.5 % β-mercaptoethanol, 0.1 % bromophenol blue, pH 6.8) was added to the supernatants and resuspended pellets. Equal quantities of the samples were analyzed by SDS-PAGE, stained with Coomassie Brilliant Blue and protein amounts were quantified using the Odyssey Infrared Imaging System (LI-COR). Corresponding binding kinetics were determined via non-linear curve fitting using Graph Pad Prism4 assuming a 1:1 binding model.

Yeast two hybrid assays

To investigate whether myopodin is able to dimerize, cDNA fragments encoding distinct portions of myopodin were cloned into modified pAct2 and pLex vectors and cotransformed into L40 yeast cells. Growth on SD-LWH agar plates and activity of β-galactosidase were assayed as described (van der Ven et al. 2000).

Static light scattering (SLS)

SLS measurements were performed with an Agilent Technologies 1260 Infinity HPLC system equipped with MiniDAWN TREOS light-scattering detector (Wyatt Technology Corporation) and SHODEX refractive index detector. The data were analyzed with ASTRA software (Wyatt Technology Corporation). A Superdex 200 10/300 GL column (GE Healthcare) was equilibrated with 300 mM NaCl, 1 mM EDTA, 5 % glycerol (V/V), 50 mM Tris–HCl pH 8.0 or with 300 mM NaCl, 1 mM EDTA, 5 % glycerol (V/V), 50 mM Tris–HCl pH 8.0 and 1 mM DTT, for oxidizing and reducing conditions, respectively. Purified myopodin construct my 269–521 at a concentration of 200 µM, was applied to the column in the buffers described above.

Electron microscopy

To visualize F-actin bundles forming in the presence of different myopodin fragments, carbon-stabilized, formvar-coated nickel grids were incubated for 20 s face-down on a drop of suspensions containing in vitro polymerized F-actin with or without one of the myopodin fragments or α-actinin. Grids were washed for 15 s in F-actin buffer and subsequently negative staining was performed by incubating in 1 % (w/v) uranium acetate in water. After two 15 s washes, grids were drained and air-dried before imaging samples with a CM 120 transmission electron microscope (Philips, Eindhoven, The Netherlands).

Results

Myopodin contains multiple independent F-actin binding sites

Previous reports have claimed that myopodin interacts with actin filaments and proposed that it might bundle them (Leinweber et al. 1999; Weins et al. 2001). To investigate the molecular basis of this activity in vitro, we performed actin cosedimentation assays using skeletal muscle actin. To map potential F-actin binding regions within the myopodin molecule, we cloned and expressed different recombinant myopodin fragments (Fig. 1a), which were subsequently analyzed for their interaction with actin filaments. High speed cosedimentation assays clearly demonstrated that myopodin harbours at least two independent actin binding regions, since two large non-overlapping and non-homologous myopodin fragments (residues 10–268 and 269–521) both cosedimented with actin filaments (Fig. 1b, c). In contrast, the fragments my 1–138 and my 408–521 did not interact (Fig. 1b, c). All results were essentially identical in the presence or absence of β-mercaptoethanol. This localizes two actin-binding regions to amino acids 139–268 and 269–408, respectively. The quantitative analysis of three independent cosedimentation assays of each myopodin fragment showed that binding of my 269–521 to 1 µM F-actin was saturated at approximately 0.6 µM (Fig. 1c). The affinity of this fragment was therefore calculated to have a K_D of 3 µM. Unfortunately, all myopodin fragments containing the amino-terminal part of the protein, including fragments my 10–521 and 10–268 exhibited solubility problems and showed a minor degree of sedimentation even in the absence of F-actin (Fig. 1b), giving rise to non-saturated binding curves, hindering the calculation of precise molecular binding ratios and affinities (Fig. 1c). Taken together, our data point to a lower interaction affinity of the more amino-terminal actin-binding region.

Myopodin alone is capable of crosslinking actin filaments into thick bundles

Although myopodin was suggested to bundle actin filaments, an activity of this kind exerted directly by myopodin was not unequivocally demonstrated. Since our assays revealed at least two independent F-actin binding sites

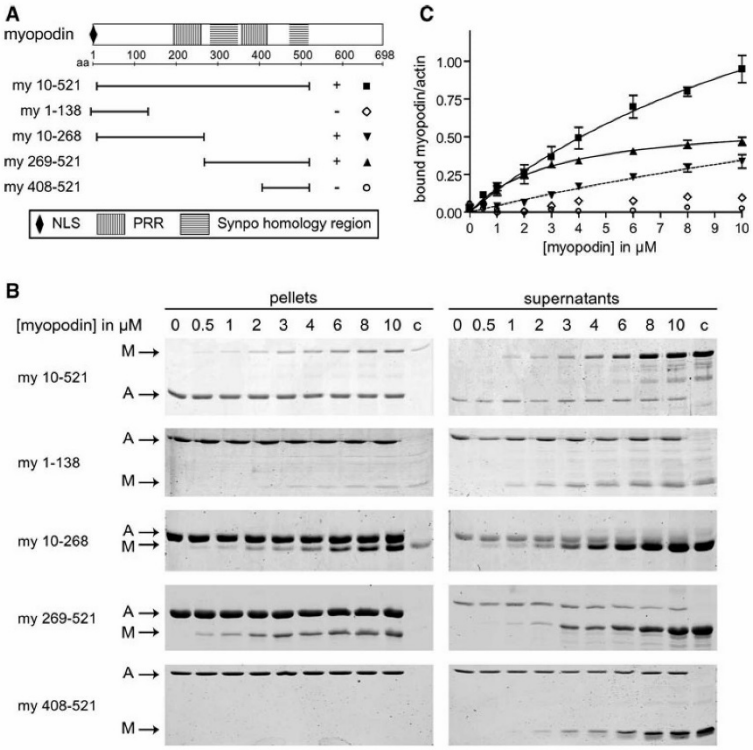

Fig. 1 Myopodin constructs used, and actin co-sedimentation assays. **a** Schematic representation of myopodin emphasizing its putative nuclear localization signal (NLS), particularly proline-rich regions (PRR) and regions that exhibit strong homology to synaptopodin, respectively. *Horizontal lines* below this sketch indicate relative positions of the myopodin fragments used. Precise construct borders are represented by their amino-acid numbers according to GenBank: CAZ66141.1. *Plus* or *minus* indicates binding or no binding to F-actin, respectively. The symbols on the right refer to the graphs shown in *panel C*. **b** F-actin co-sedimentation assays using the indicated myopodin constructs. Fragments my 10–521, my 10–268 and my 269–521 are coprecipitated with F-actin, while my 1–138 and my 408–521 are not. Controls without F-actin (*c*) contained 10 µM myopodin. Note that small amounts of all myopodin constructs containing the amino-terminus of the protein precipitated without F-actin. However, the addition of F-actin significantly increased the co-precipitated amount of my 10–268 and my 10–521. **c** Quantitative evaluation of all co-sedimentation assays performed by plotting the amount of myopodin fragment bound to actin versus the total amount of the respective myopodin construct. Note that my 269–521 (*upright triangle*) showed saturation binding kinetics. Both my 10–521 (*square*) and my 10–268 (*downward triangle*) bind less efficiently, but their tendency to precipitate precluded precise quantification of binding strengths. In contrast, my 1–138 (*diamond*) and my 408–521 (*circle*) did not bind F-actin

(see above), we tested whether myopodin alone was capable of bundling actin filaments. Therefore, low speed actin cosedimentation assays using skeletal muscle actin were performed. Indeed, myopodin fragment my 10–521 showed strong accumulation in the pellet together with increasing amounts of bundled actin, proving the ability of myopodin to directly crosslink actin filaments (Fig. 2). Interestingly, we found that the myopodin fragment my 269–521, which we assumed to harbour only one actin binding site, was also capable of crosslinking actin filaments (Fig. 2). In contrast, my 1–138, my 10–268 and my 408–521 were not cosedimented with F-actin in this assay (not shown).

Ultrastructural analysis of the F-actin/myopodin complexes revealed that the myopodin fragments my 10–521, my 240–521 and my 269–521 organized F-actin into densely packed bundles (Fig. 3b–d) that strongly resembled those obtained with α-actinin (Fig. 3a). Without myopodin (Fig. 3f) and with the fragments my 10–268 (Fig. 3e) or my 408–521 (not shown) no bundling was observed. All results were essentially identical under both reducing and oxidizing conditions.

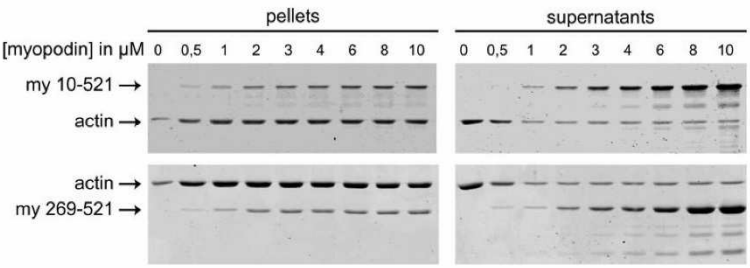

Fig. 2 Myopodin is a protein with a high capacity of bundling F-actin. Coomassie blue-stained SDS-polyacrylamide gels showing the results of low speed F-actin cosedimentation assays using myopodin constructs my 10–521 and my 269–521. Note that both fragments are capable of crosslinking F-actin, as demonstrated by the presence of large amounts of actin in the pellets

Is dimerization involved in myopodin's actin-bundling activity?

Actin bundling proteins either contain two independent F-actin binding sites (e.g. fascin), or they form dimers (e.g. α-actinin). To investigate the mechanism that enables myopodin fragment my 269–521 to bundle F-actin, we tested whether it was able to homodimerize. Indeed, yeast two hybrid assays indicated that myopodin fragment my 269–521 can interact with itself, whereas fragment my 269–414 cannot (Fig. 4b), indicating the presence of a dimerization site between amino acids 415 and 521. Biochemical experiments using the crosslinker EGS showed the tendency of my 269–521 to dimerize in vitro (Fig. 4c), but significant dimer amounts were only found under non-reducing conditions. Similarly, in size exclusion chromatography experiments under reducing conditions, my 269–521 eluted as a monomer with corresponding molecular mass of ~25 kDa, as measured with SLS (Fig. 4d). When the experiment was repeated with equilibration and elution buffer without DTT, a second peak was observed, corresponding to the molecular mass (55.6 kDa) of the dimeric protein (Fig. 4e). This condition was reversible by adding reducing agent to the size exclusion chromatography buffer (data not shown). These findings suggest that the actin bundling activity of my 269–521 is achieved by two independent F-actin binding sites within this fragment. The tendency to form dimers is most probably the result of an intermolecular interaction via a cysteine residue within this myopodin fragment. The data of the experiments described above are summarized in Fig. 5.

Discussion

Amongst the numerous cytoskeletal proteins investigated, myopodin is expressed as one of the earliest upon induction of myogenic differentiation (Linnemann et al. 2010; Weins et al. 2001). Remarkably, myopodin is distributed along stress fibres in a regular fashion even prior to α-actinin, the protein that has been considered to be the most prominent and important Z-disc component and constructor (Linnemann et al. 2010). Since it directly binds to α-actinin and filamin (Asanuma et al. 2005; Kremerskothen et al. 2005; Linnemann et al. 2010; Weins et al. 2001), myopodin seems to play a role as an organizer of early Z-discs of at least similar importance. For a more complete understanding of the biological function of myopodin it therefore occurred important to us to investigate its actin-binding and -bundling activity more intensively.

Our cosedimentation assays unequivocally identified non-overlapping F-actin binding regions which are part of all known myopodin isoforms. The strongest binding, more carboxy-terminally situated motif (amino acids 269–408), actually contains two binding sites and is in part identical to the mouse myopodin fragment 410–563 that previously has been reported to bind actin-containing structures in transfected cells (Weins et al. 2001). Since mouse myopodin fragment 506–643 was negative for binding to stress-fibres, the actual binding region was in fact narrowed down to residues 410–505 (Weins et al., 2001). An alignment of mouse and human myopodin reveals that part of this region (amino acids 410–466) is homologous to amino acids 356–408 of the human protein (Suppl. Fig. 1), indicating that at least one of the actual actin-binding sites might localize in this region. It should be noted however, that considering our current knowledge about the filamin and multiple α-actinin binding-sites of myopodin (Linnemann et al. 2010), transfection of myopodin fragments in cultured cells is not the most appropriate approach to unequivocally identify F-actin-binding sites. Interestingly, an alignment of one of the actin filament association regions of synaptopodin demonstrated a moderate level of similarity with a part of myopodin (313–416) that includes this region (Kremerskothen et al. 2005). In contrast, the sequence of the closely related protein tritopodin/CHAP shows only limited similarity to the regions harbouring the actin binding portions in myopodin. This is in line with the finding that tritopodin/CHAP does not bind to actin. Instead, its targeting to the actin cytoskeleton could specifically be attributed to its direct interaction with α-actinin (Beqqali et al. 2010).

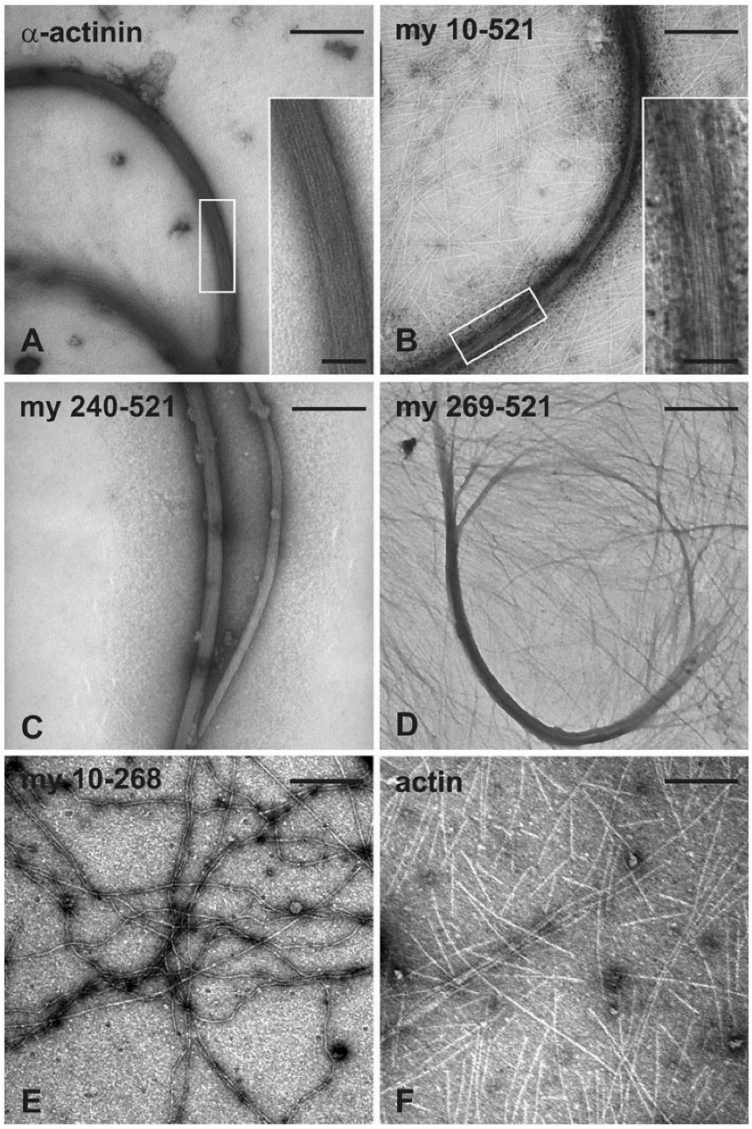

Fig. 3 Ultrastructural analysis of actin-bundling activity of myopodin fragments. Electron micrographs of negatively stained myopodin-actin bundles generated by the constructs my 10–521 (**b**), my 240–521 (**c**), and my 269–521 (**d**) respectively. All actin bundles strongly resemble those formed in the presence of the actin-bundling protein α-actinin that was used as a positive control (**a**). In contrast, construct my 10–268 (**e**) does not bundle actin filaments. Pure F-actin was used as a negative control (**f**). *Bars* 300 nm (**a**–**d**), 500 nm (**e**, **f**), 60 nm (*insets* in **a**, **b**)

For the myopodin fragment containing both binding sites close to the carboxy-terminus (amino acids my 269–521) we calculated a K_D value of approximately 3 μM, a number that almost precisely matches the binding strength reported for fesselin, the myopodin variant isolated from avian and mammalian smooth muscle tissue (Leinweber et al. 1999). It is also

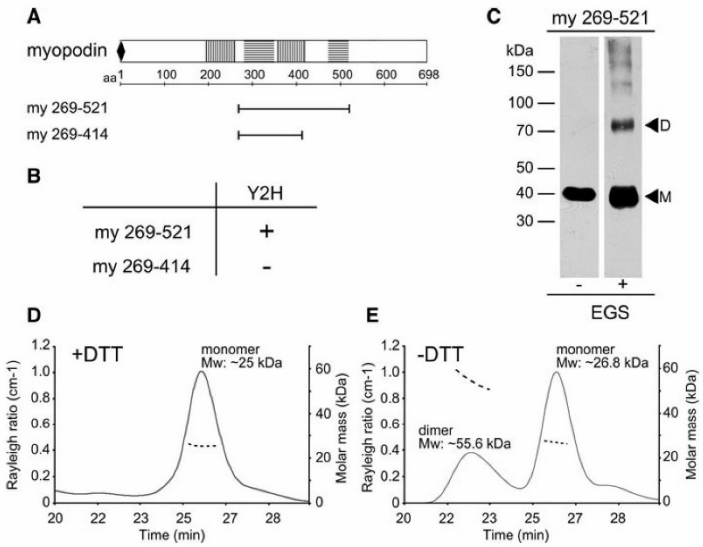

Fig. 4 Myopodin contains at least three independent F-actin binding-sites. **a** Position of myopodin constructs used for dimerization assays. **b** Summary of yeast two hybrid assays demonstrating that the construct my 269–521 seems to self-interact, whereas my 269–414 does not. **c** Dimer and multimer formation of my 269–521 demonstrated by chemical cross-linking using EGS. The SDS-PAGE lanes give a sample without EGS (−) and after incubation with EGS (+). *M* and *D* indicate positions of monomers and dimers, respectively. Note that only minor fraction of the construct is found as dimers, and that multimerization points to non-specific stickiness. **d**, **e** Size exclusion chromatography (SEC) profile of myopodin construct my 269–521. Experiments were performed under reducing conditions in the presence of DTT (**d**) or under oxidizing conditions in the absence of DTT (**e**). Proteins were eluted from the column: The *curves* show the measured Rayleigh ratio (*left axis*) and the dashed lines crossing the chromatogram profiles show the molecular masses determined using SEC on-line multi-angle laser light scattering (MALLS) and refractive index (RI) detection apparatus (*right axis*). Note that dimers are only observed under oxidizing conditions

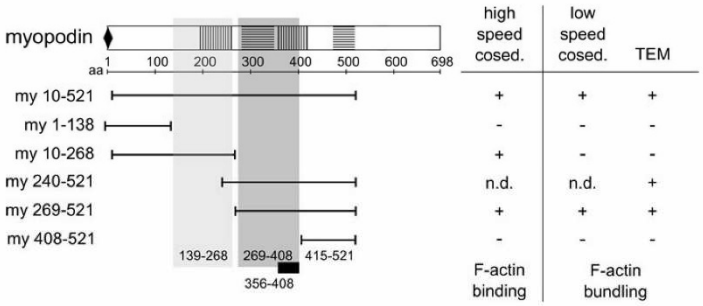

Fig. 5 Summary of F-actin binding and F-actin bundling data of human myopodin. The *molecular layout* and *scale bar* correspond to the illustration in Fig. 1. Shown are the constructs used in our F-actin-binding and -bundling experiments, and the results of the cosedimentation (cosed.) assays or transmission electronmicroscopal observation (TEM). The *vertical rectangles* indicate the positions of both identified weak (*light grey*) and strong (*dark grey*) F-actin-binding regions. The *small black bar* indicates the overlap (356–408) with the region of myopodin previously found to bind actin filaments upon expression in cultured cells (Weins et al., 2001). *Plus* or *minus* indicate binding or no binding to F-actin or bundling or no bundling of actin filaments, respectively

noteworthy that this binding strength is in the range of affinities reported for other actin binding domains. Although no K_D could be estimated for the second binding region, our results indicate that it binds significantly weaker. No quantitative binding data are available for the two microfilament association sites identified in synaptopodin (Kremerskothen et al. 2005).

In most proteins, F-actin-binding can be assigned to essentially globular domains, like the calponin homology domains (Gimona et al. 2002; Sjöblom et al. 2008; Stradal et al. 1998) or the myosin motor domain (Geeves and Holmes 2005; Ruppel and Spudich 1996). In contrast, the paradigm for proteins binding to multiple actin protomers along the thin filament are the alpha-helically structured tropomyosins (Perry 2001; Pittenger et al. 1994). Far less, however, is known about another group of side-binding, elongated proteins, which were proposed to be only weakly structured or unfolded if left alone, and which only adopt a defined structure upon binding to actin. Such a binding mode was first demonstrated for tropomodulin, which only forms stable α-helices upon binding to tropomyosin-actin (Kostyukova et al. 2000). Similarly, nebulin- and Xin-repeats apparently have a strong tendency to remain only unstably folded in solution, whereas their structure is stabilized by binding to actin filaments (Cherepanova et al. 2006; Lukoyanova et al. 2002; Pacholsky et al. 2004). An analysis of the primary sequences of the proteins of the podin family predicted that they are mostly unfolded (Chalovich and Schroeter 2010). Although this might suggest a mode of binding to the surface of actin filaments similar to that of nebulin and Xin-repeat proteins, a major difference is that in contrast to the podin proteins, the former are composed of multiple copies of short actin-binding peptide motifs (Jin and Wang 1991; Kruger et al. 1991; Labeit et al. 1991; Pacholsky et al. 2004; Trinick 1994). The actin-binding regions in myopodin however, are highly divergent and do not exhibit any similarity in their primary sequences, which also rules out the possibility that binding sites arose by a gene duplication event.

A further conspicuous feature of myopodin is its strong actin filament bundling activity in the absence of other F-actin-binding proteins. Myopodin/F-actin bundles are very tightly packed, most likely because the distances between the actin-binding motifs in myopodin are very short. In principle this activity could simply be achieved by the combination of multiple actin-binding regions in one myopodin protein, but we found indications that this effect is potentiated by its capability to dimerize. Biochemical experiments, however, showed that no compelling evidence for dimerization could be obtained under reducing conditions, indicating that the dimerization is caused by cysteine-based intermolecular interactions. Therefore, myopodin dimer formation in muscle cells may only occur under oxidative stress, enabling intermolecular protein disulfide formation (Brennan et al. 2004) but not under normal physiological (reducing) conditions.

The identified actin-binding regions are present in all known myopodin isoforms, including those expressed in tumour cells that were shown to be involved in tumour growth and metastasis (De Ganck et al. 2009; Esteban et al. 2012; Jing et al. 2004; Lin et al. 2001; Sanchez-Carbayo et al. 2003). Therefore, our data might help to better understand the role of myopodin in the specific alterations of actin filament organization associated with these processes.

It has been proposed that the high degree of flexibility of unstructured proteins like myopodin might facilitate binding to different partners, including components of signalling pathways (Chalovich and Schroeter 2010). Indeed, similarly to many other Z-disc proteins, myopodin has many interaction partners: in addition to binding to actin, α-actinin and filamin, myopodin also interacts with calmodulin, 14-3-3, zyxin and integrin linked kinase (Faul et al. 2005, 2007; Kolakowski et al. 2004; Linnemann et al. 2010; Pham and Chalovich 2006; Schroeter and Chalovich 2004; Shen et al. 2005; Weins et al. 2007; Yu and Luo 2006; Yu and Luo 2011). Both its observed multiple binding activities and its expression at the earliest stages of myocyte differentiation, suggest an important role of myopodin in the regulation of actin cytoskeleton remodelling that is linked to the membrane-associated formation of stress fibre-like structures as the initial sites of myofibril formation.

Acknowledgments We thank Mrs. U. Kukulies, A. Jünger-Leif, N. Thum-Schmitz, C. Mirschkorsch and Mr. C. Preiss for technical assistance. This work was supported by the German Research foundation: FOR1228 to D.O.F. and FOR 1352 to D.O.F. and K.D.C., and the German Ministry of Education and Research [MD-NET2, 01GM0887 to P.F.M.v.d.V. and D.O.F.].

References

Asanuma K, Kim K, Oh J, Giardino L, Chabanis S, Faul C, Reiser J, Mundel P (2005) Synaptopodin regulates the actin-bundling activity of alpha-actinin in an isoform-specific manner. J Clin Invest 115:1188–1198

Ausubel FM, Brent R, Kingston RE, Moore DD, Seidman JG, Smith JA, Struhl K (1995) Short protocols in molecular biology. Wiley, New York

Beqqali A, Monshouwer-Kloots J, Monteiro R, Welling M, Bakkers J, Ehler E, Verkleij A, Mummery C, Passier R (2010) CHAP is a newly identified Z-disc protein essential for heart and skeletal muscle function. J Cell Sci 123:1141–1150

Brennan JP, Wait R, Begum S, Bell JR, Dunn MJ, Eaton P (2004) Detection and mapping of widespread intermolecular protein disulfide formation during cardiac oxidative stress using proteomics with diagonal electrophoresis. J Biol Chem 279:41352–41360

Chalovich JM, Schroeter MM (2010) Synaptopodin family of natively unfolded, actin binding proteins: physical properties and potential biological functions. Biophys Rev 2:181–189

Cherepanova O, Orlova A, Galkin VE, van der Ven PFM, Fürst DO, Jin JP, Egelman EH (2006) Xin-repeats and nebulin-like repeats bind to F-actin in a similar manner. J Mol Biol 356:714–723

Claeys KG, van der Ven PFM, Behin A, Stojkovic T, Eymard B, Dubourg O, Laforet P, Faulkner G, Richard P, Vicart P, Romero

NB, Stoltenburg G, Udd B, Fardeau M, Voit T, Fürst DO (2009) Differential involvement of sarcomeric proteins in myofibrillar myopathies: a morphological and immunohistochemical study. Acta Neuropathol 117:293–307

De Ganck A, De Corte V, Bruyneel E, Bracke M, Vandekerckhove J, Gettemans J (2009) Down-regulation of myopodin expression reduces invasion and motility of PC-3 prostate cancer cells. Int J Oncol 34:1403–1409

Esteban S, Moya P, Fernandez-Suarez A, Vidaurreta M, Gonzalez-Peramato P, Sanchez-Carbayo M (2012) Diagnostic and prognostic utility of methylation and protein expression patterns of myopodin in colon cancer. Tumour Biol 33:337–346

Faul C, Hüttelmaier S, Oh J, Hachet V, Singer RH, Mundel P (2005) Promotion of importin α-mediated nuclear import by the phosphorylation-dependent binding of cargo protein to 14–3–3. J Cell Biol 169:415–424

Faul C, Dhume A, Schecter AD, Mundel P (2007) Protein kinase A, Ca^{2+}/calmodulin-dependent kinase II, and calcineurin regulate the intracellular trafficking of myopodin between the Z-disc and the nucleus of cardiac myocytes. Mol Cell Biol 27:8215–8227

Geeves MA, Holmes KC (2005) The molecular mechanism of muscle contraction. Adv Protein Chem 71:161–193

Gimona M, Djinović-Carugo K, Kranewitter WJ, Winder SJ (2002) Functional plasticity of CH domains. FEBS Lett 513:98–106

Jin JP, Wang K (1991) Nebulin as a giant actin-binding template protein in skeletal muscle sarcomere. Interaction of actin and cloned human nebulin fragments. FEBS Lett 281:93–96

Jing L, Liu L, Yu YP, Dhir R, Acquafondada M, Landsittel D, Cieply K, Wells A, Luo JH (2004) Expression of myopodin induces suppression of tumor growth and metastasis. Am J Pathol 164:1799–1806

Kolakowski J, Wrzosek A, Dabrowska R (2004) Fesselin is a target protein for calmodulin in a calcium-dependent manner. Biochem Biophys Res Commun 323:1251–1256

Kostyukova A, Maeda K, Yamauchi E, Krieger I, Maeda Y (2000) Domain structure of tropomodulin: distinct properties of the N-terminal and C-terminal halves. Eur J Biochem 267:6470–6475

Kremerskothen J, Plaas C, Kindler S, Frotscher M, Barnekow A (2005) Synaptopodin, a molecule involved in the formation of the dendritic spine apparatus, is a dual actin/alpha-actinin binding protein. J Neurochem 92:597–606

Kruger M, Wright J, Wang K (1991) Nebulin as a length regulator of thin filaments of vertebrate skeletal muscles: correlation of thin filament length, nebulin size, and epitope profile. J Cell Biol 115:97–107

Labeit S, Gibson T, Lakey A, Leonard K, Zeviani M, Knight P, Wardale J, Trinick J (1991) Evidence that nebulin is a protein-ruler in muscle thin filaments. FEBS Lett 282:313–316

Leinweber BD, Fredricksen RS, Hoffman DR, Chalovich JM (1999) Fesselin: a novel synaptopodin-like actin binding protein from muscle tissue. J Muscle Res Cell Motil 20:539–545

Lin F, Yu YP, Woods J, Cieply K, Gooding B, Finkelstein P, Dhir R, Krill D, Becich MJ, Michalopoulos G, Finkelstein S, Luo JH (2001) Myopodin, a synaptopodin homologue, is frequently deleted in invasive prostate cancers. Am J Pathol 159:1603–1612

Linnemann A, van der Ven PFM, Vakeel P, Albinus B, Simonis D, Bendas G, Schenk JA, Micheel B, Kley RA, Fürst DO (2010) The sarcomeric Z-disc component myopodin is a multiadapter protein that interacts with filamin and alpha-actinin. Eur J Cell Biol 89:681–692

Lukoyanova N, VanLoock MS, Orlova A, Galkin VE, Wang K, Egelman EH (2002) Each actin subunit has three nebulin binding sites: implications for steric blocking. Curr Biol 12:383–388

Mundel P, Heid HW, Mundel TM, Kruger M, Reiser J, Kriz W (1997) Synaptopodin: an actin-associated protein in telencephalic dendrites and renal podocytes. J Cell Biol 139:193–204

Obermann WMJ, Gautel M, Weber K, Fürst DO (1997) Molecular structure of the sarcomeric M band: mapping of titin and myosin binding domains in myomesin and the identification of a potential regulatory phosphorylation site in myomesin. EMBO J 16:211–220

Obermann WMJ, van der Ven PFM, Steiner F, Weber K, Fürst DO (1998) Mapping of a myosin-binding domain and a regulatory phosphorylation site in M-protein, a structural protein of the sarcomeric M band. Mol Biol Cell 9:829–840

Pace CN, Vajdos F, Fee L, Grimsley G, Gray T (1995) How to measure and predict the molar absorption coefficient of a protein. Protein Sci 4:2411–2423

Pacholsky D, Vakeel P, Himmel M, Löwe T, Stradal T, Rottner K, Fürst DO, van der Ven PFM (2004) Xin repeats define a novel actin-binding motif. J Cell Sci 117:5257–5268

Perry SV (2001) Vertebrate tropomyosin: distribution, properties and function. J Muscle Res Cell Motil 22:5–49

Pham M, Chalovich JM (2006) Smooth muscle alpha-actinin binds tightly to fesselin and attenuates its activity toward actin polymerization. J Muscle Res Cell Motil 27:45–51

Pittenger MF, Kazzaz JA, Helfman DM (1994) Functional properties of non-muscle tropomyosin isoforms. Curr Opin Cell Biol 6:96–104

Ruppel KM, Spudich JA (1996) Structure–function analysis of the motor domain of myosin. Annu Rev Cell Dev Biol 12:543–573

Sanchez-Carbayo M, Schwarz K, Charytonowicz E, Cordon-Cardo C, Mundel P (2003) Tumor suppressor role for myopodin in bladder cancer: loss of nuclear expression of myopodin is cell-cycle dependent and predicts clinical outcome. Oncogene 22:5298–5305

Schroeter M, Chalovich JM (2004) Ca^{2+}-calmodulin regulates fesselin-induced actin polymerization. Biochemistry 43:13875–13882

Shen X, Valencia CA, Szostak JW, Dong B, Liu R (2005) Scanning the human proteome for calmodulin-binding proteins. Proc Natl Acad Sci USA 102:5969–5974

Sjöblom B, Ylänne J, Djinović-Carugo K (2008) Novel structural insights into F-actin-binding and novel functions of calponin homology domains. Curr Opin Struct Biol 18:702–708

Spudich JA, Watt S (1971) The regulation of rabbit skeletal muscle contraction. I. Biochemical studies of the interaction of the tropomyosin-troponin complex with actin and the proteolytic fragments of myosin. J Biol Chem 246:4866–4871

Stradal T, Kranewitter W, Winder SJ, Gimona M (1998) CH domains revisited. FEBS Lett 431:134–137

Trinick J (1994) Titin and nebulin: protein rulers in muscle? Trends Biochem Sci 19:405–409

van der Ven PFM, Wiesner S, Salmikangas P, Auerbach D, Himmel M, Kempa S, Hayeß K, Pacholsky D, Taivainen A, Schröder R, Carpén O, Fürst DO (2000) Indications for a novel muscular dystrophy pathway. γ-filamin, the muscle-specific filamin isoform, interacts with myotilin. J Cell Biol 151:235–248

Weins A, Schwarz K, Faul C, Barisoni L, Linke WA, Mundel P (2001) Differentiation- and stress-dependent nuclear cytoplasmic redistribution of myopodin, a novel actin-bundling protein. J Cell Biol 155:393–404

Weins A, Schlondorff JS, Nakamura F, Denker BM, Hartwig JH, Stossel TP, Pollak MR (2007) Disease-associated mutant alpha-actinin-4 reveals a mechanism for regulating its F-actin-binding affinity. Proc Natl Acad Sci USA 104:16080–16085

Yu YP, Luo JH (2006) Myopodin-mediated suppression of prostate cancer cell migration involves interaction with zyxin. Cancer Res 66:7414–7419

Yu YP, Luo JH (2011) Phosphorylation and interaction of myopodin by integrin-link kinase lead to suppression of cell growth and motility in prostate cancer cells. Oncogene 30:4855–4863

Contribution to the manuscript:

As co-author of the manuscript, I expressed and purified wild type *E. coli* and biochemically characterized the my269-521 (MyoA CD). In addition, I applied this construct to size exclusion chromatography experiments under reducing conditions, with my269-521 eluted as a monomer with corresponding molecular mass of 25 kDa, as measured with SEC-MALLS. Repeating the experiment in oxidizing conditions, a second peak was observed, corresponding to the molecular mass of the dimeric protein. These pieces of evidence suggest how a myopodin oligomeric state could be modulated in a reducing and oxidizing environment.

3.7.4. Studies on the Myo CD/filamin complex

3.7.4.1. Studies of interactions of myopodin central domain with filamin C

The interaction between MyoA CD and FLNc d18-21 was measured by ITC. In order to quantify binding affinity, MyoA CD was titrated with FLNc d18-21/MyoA CD. Data were plotted and analyzed using a single binding site model with the MicroCal Origin software. The titration curve of FLNc d18-21 is shown in figure 3.26a and the dissociation constant of 1.65 ± 0.32 μM was determined with a stoichiometry of approximately 1.

I further carried out ITC to analyze the importance of the individual domains involved in the interaction. The posterior experiment was performed with the single Ig-like domain d21 titrated against MyoA CD. The titration curve is shown in figure 3.26b and the dissociation constant of 98 ± 30.6 μM was determined with a stoichiometry of approximately 1.

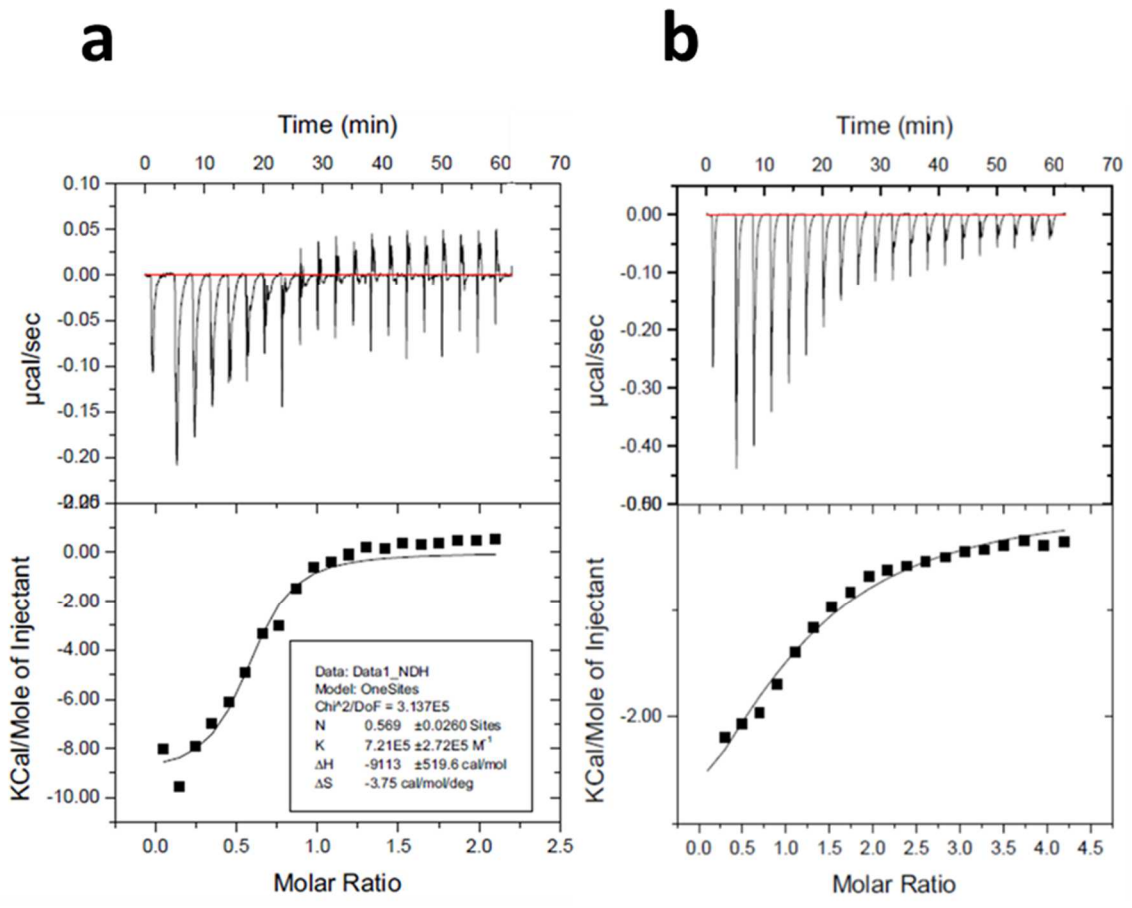

K_d: 1.65 ± 0.32 µM

Syringe: 400 µM FLNc d18-21

Cell: 40 µM MyoA CD

N: 0.547 ± 0.0293 sites

ΔH -9.70 ± 0.72 kcal/mol

ΔS -6.06 cal/mol/deg

K_d: 98 ± 30.6 µM

Syringe: 2.0 mM FLNc d21

Cell: 100 µM MyoA CD

N: 1.05 ± 0.0198 sites

ΔH -4.96 ± 1.17 kcal/mol

ΔS 1.72 cal/mol/deg

Figure 3.26: Isothermal titration calorimetry of MyoA CD with FLNc**.** ITC titrations of MyoA CD with (a) FLNc d18-21 and (b) FLNc d21 were performed at 25°C in 20 mM HEPES pH 7.4 and NaCl 150 mM and 1 mM TCEP. Shown, from top to bottom, are the raw titration data of FLNc d18-21 and (b) FLNc d21 injected into MyoA CD, and the integrated heat measurements for the titration. The first injection peak was discarded because of the backlash effect. The data were plotted and analyzed using a single binding site model with the MicroCal Origin software.

3.7.4.2. Studies of influence of phosphorylation on interaction of myopodin central domain with filamin C

Co-immunoprecipitation assays showed that myopodin central domain binds to filamin C Ig domain fragment d20-21 (Linnemann, van der Ven et al. 2010). We observed a dissociation constant (K_d) of 2.4 μM using microscale thermophoresis (MST) experiments (figure 3.27a) for central domain filamin C and Ig domain d18-21 complex. However, it was suggested that the phosphorylation of three serine sites (S902, S906 and S910) of the myopodin central domain regulates myopodin – filamin C interaction.

In order to evaluate the phosphorylation effect, phosphomimetic myopodin central domain mutant (MyoA CD Mut) was generated (S902D, S906D and S910D). From the MST experiment it was not possible to calculate FLNc d18-21 binding affinity constant for MyoA CD Mut (figure 3.27b), indicating that the MyoA CD Mut interacts with a very low affinity or does not interact at all with FLNc d18-21. This suggests a modulation of the interaction by myopodin phosphorylation in the central domain.

a

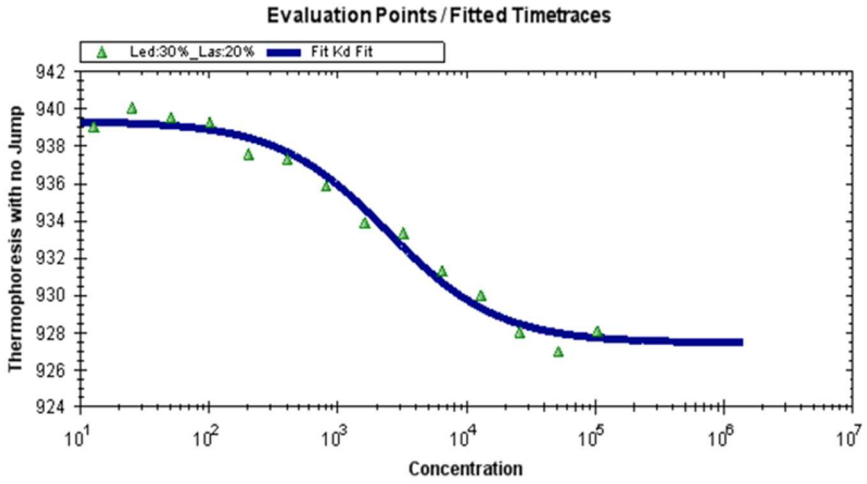

Led Power [%] :30 Laser Power [%] :20 **K_d : 2.4 µm**

Central domain x FLNC d18-21

b

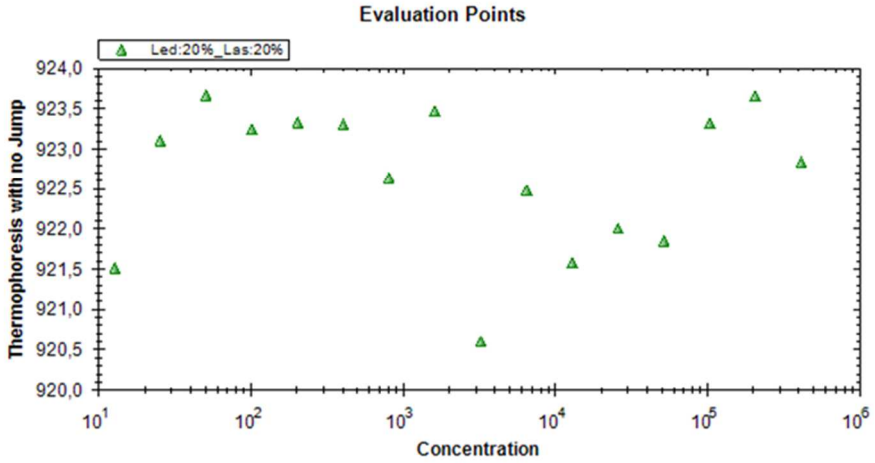

Led Power [%] :20 Laser Power [%] :20

Central domain phosphomimetic x FLNC d18-21

Figure 3.27: Microscale thermophoresis of MyoA CD and filamin C. Filamin C d18-21 was titrated into a fixed concentration of (**a**) Central domain and (**b**) phosphomimetic mutant (100 nM). Fitting of derived isotherms according to the law of mass action. The apparent K_d is 2.4 µM for myopodin central domain and no binding is observed for central domain phosphomimetic mutant.

4. Discussion

4.1. Structural basis for differential affinities of myopodin PDZ domain to Z-disc binding partners

It has been shown that myopodin is a multiadapter protein able to interact with several members of the Z-disc, such as actin (Mundel, Heid et al. 1997, Linnemann, Vakeel et al. 2013), α-actinin 2, filamin C (Linnemann, van der Ven et al. 2010) and zyxin (Yu and Luo 2006). A cardiac isoform of myopodin is expressed with a N-terminal PDZ domain, an important protein-protein interaction module that interacts with the C-terminal motif of its binding partners. Interactions with MyoA PDZ has already been observed for synemin (Vakeel 2006) and VPS18 (Ulbricht, Eppler et al. 2013). In our biochemical characterization of these interactions different dissociation constants were observed for the synemin and VPS18 peptides tested. Moreover, the predicted binding to C-terminal motif of α-actinin 2 was tested (Katzemich, Liao et al. 2013), but due to the apparent low affinity it was not possible to calculate the dissociation constant.

Paired comparison analysis of the X-ray structures shown in the figures 3.10, 3.13 and 3.16 were very helpful for understanding the differences of binding affinities of PDZ for the three peptides investigated here. In the PDZ-synemin complex a tryptophan residue at position -1 (P-1) from synemin peptide is stabilized by a close stacking of Arg20 and Arg37 residues of PDZ, whereas a bulky phenylalanine residue at position 0 (P0) is occupying a hydrophobic pocket formed by Trp17, Phe19, Val69, Ile70 and Met73 of PDZ domain (Figure 3B, left panel). All these interactions jointly lead to a stronger binding affinity of PDZ for synemin (K_d : 0.75 µM ± 0.10 µM) compared with K_d of 8.84 µM ± 0.86 µM found for VPS18 peptide. Thus, this lower affinity of PDZ for VPS18 peptide can be explained by the presence of a Leu residue at P0 instead of a Phe residue in the synemin peptide, which is partially buried in the hydrophobic pocket of PDZ domain. In the case of α-actinin 2 peptide, while a Leu residue at P0 assumes a similar mode of interaction seen for VPS18 peptide residue P0 (Figure 3A, right panel), at P-1 an Asp residue interacts only with Arg20 from PDZ (Figure 3B, right panel), which probably decreases the binding affinity of this peptide even more, compared to the other peptides.

The X-ray structures presented here reveal a non-conventional PDZ binding mode for all the peptides. This sort of binding can be explained by the analysis of the crystal packing contacts of these structures, which show symmetry related molecules tightly packed *via* disulfide bonds, causing sterical impediment for the binding of some residues from the peptides (figure 3.19). The non-conventional binding mode seen in our crystallographic structures can also be observed in NMR studies on the scaffold protein X11 (Mint family) PDZ domain (Long, Feng et al. 2005).

We used NMR experiments to investigate the binding mode of synemin peptide to MyoA PDZ domain in solution. For the sake of simplicity, Myo A PDZ-synemin complex was chosen as an example for our NMR studies, because it has higher binding affinity compared to the others. ^{15}N-labeled protein showed chemical shift changes during synemin peptide titration due to binding events. Interestingly, on one hand the binding mode for the peptide seen in the X-ray crystallography data is also identified in NMR experiments by inspection of the chemical shift related to Gly18 and Phe19. Chemical shifts of amino acids Gly18 and Phe19 are attributed to the canonical and non-canonical binding modes. On the other hand, chemical shifts of Leu21 (located at βB3) and Tyr66 (located at αB1) that are indicative of the canonical extended conformation (figure 3.20) can also be observed in our NMR experiments. Previous reports in the literature have demonstrated that residues of PDZ domain located at βB3 and αB1are involved in the peptide binding (residue at position -2), which are signatures of the presence of a canonical extended conformation (Sugi, Oyama et al. 2007, Elkins, Gileadi et al. 2010). Thus, our NMR data confirms that synemin peptide is bound in a canonical mode in solution, while the non-canonical binding observed in the X-ray structure data seems to be induced primarily by the crystal packing of the complex.

Interestingly, our crystallographic models capture one of the earliest steps of peptide interaction with PDZ, more specifically related to the position -1 and 0. Elkins and colleagues (2010) have already described and proposed the requirement of a non-canonical initial step for PDZ binding. Our data and paired comparison analysis of the X-ray structures of PDZ from PDLIM2 (Elkins, Gileadi et al. 2010) support their explanation. In addition, our NMR data reveal the peptide canonical interaction, as the final step of binding, where the peptide is oriented in an extended conformation, with the residue P-2 close to the binding site.

The combination of crystallographic and NMR data provides the understanding of the peptide binding mechanism in two distinct moments of the interaction and its specificity to different binding partners. The results generated here help us to understand the molecular basis of the differential affinities of synemin, VPS18 and α-actinin 2 for myopodin that seem to have an essential role in the interplay between the assembling and maintenance of Z-disc.

4.2. Myopdin PDZ domain binds different PDZ classes with different specificities

PDZ interaction characteristics regard the P0 and P-2 as main anchoring points for PDZ binding motif recognition. They are also associated with different classes of binding relative to ligand C-terminal sequence. Myopodin PDZ domain showed interaction with two distinct classes: interaction class I (-X-[S/T]-X-Φ) to VPS18 and ACTN2 peptide and a closely related class III (-X-[D/E/K/R]-X-Φ) to synemin peptide, where P-3 and P-1 represented by X could be any residue. Initially, it was thought the that residues represented by X would not have a relevant role in the interaction, contributing only with the hydrogen bonds from of the main chain. However, it was shown how residues from P-1 and P-3 could modulate both positively and negatively the specificity of the PDZ binding motif (Lee and Zheng 2010, Amacher, Cushing et al. 2014).

Our data suggest that the tryptophan -1 of synemin and VPS18 plays a specific role in that it not only contributes to the backbone affinity of the interaction with the peptide binding groove, but also to the specificity of the peptide binding. The tryptophan cation–π stacking between the peptide Trp at position P-1 and Arg20 promotes a pair of dipoles resulting in an electric quadrupole moment in the indole side-chain, resulting in a formation of a positively charged electrostatic surfaces on the indole ring plane and perpendicular negatively charged electron clouds (Dougherty 1996, Chan, Prenner et al. 2006). Concomitantly, the intrinsically hydrophobic indole group ring will interact with aliphatic portion of Arg37 side-chain (figure 3.10c and 3.13c) resulting in sandwiching the side chain of peptide Trp at position -1, therefore further stabilizing the interaction.

Carboxylate-binding loop

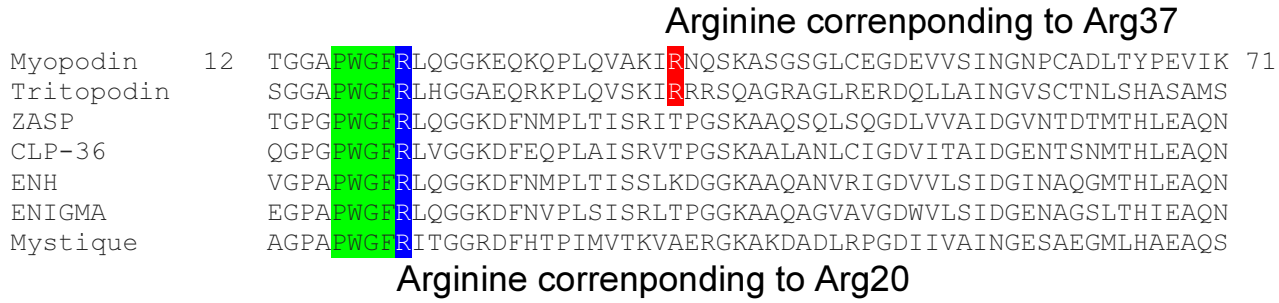

Figure 4.1: Myopodin PDZ domain alignment. PDZ domains from Z-disc proteins showing a conserved carboxylate-binding loop and adjacent arginine relative to the residue 20 in myopodin and the second arginine (Arg37) involved in the arginine packing conserved between myopodin and tritopodin. Carboxylate-binding loop highlighted in green, and residues corresponding to Arg20 and Arg37 in blue and red respectively.

The Arg20 from myopodin is conserved among PDZ domains from Z-disc proteins, adjacent to the carboxylate-binding loop (figure 4.1). This residue has already been identified as an involved in the predicted site to ACTN2 interaction (Kim, Kim et al. 2012, Katzemich, Liao et al. 2013). Based on the structural analysis of our myopodin PDZ domain complexes, and on conservation of this arginine residue in tritopodin we envisage a similar mode of interaction as in myopodin. The arginine corresponding to the myopodin Arg37 is also conserved, and is potentially able to interact with the other PDZ binding motifs with a higher specificity, such as myopodin.

4.3. PDZ domain drive myopodin to diverse cell processes in different moments

Myopodin is described as a multiadapter protein, colocalized with other members of the Z-disc, such as α-actinin 2 and filamin C (Linnemann, van der Ven et al. 2010), but this recent study also reports an additional binding site for α-actinin 2 *via* myopodin PDZ domain. This characteristics corroborates the idea that myopodin is anchored to the Z-disc, more precisely with α-actinin 2. Our data presented here show different affinities of myopodin PDZ domain to different binding partners.

Based on the localization/interactions reported in the literature and our data related to different affinities for myopodin PDZ domain we propose that myopodin PDZ domain could carry or anchor ligands involved in different cell events and moments and suggest a potential model for myopodin/α-actinin 2 assembling in the sarcomeric Z-disc. The early expression of myopodin during cardiomyocytes differentiation and its 3 independent α-actinin 2 binding sites have already been reported in detail (Linnemann, van der Ven et al. 2010). We propose that myopodin could be one of the initial α-actinin 2 binding partners during cardiomyocyte development, as described by Linnemann in 2010, where myopodin is colocalized with α-actinin 2 in immature myotubes. In addition, it was demonstrated by Lund in 2012 that the β-synemin isoform is preferentially associated with the Z-disc due to its interaction with α-actinin head and rod domain *via* synemin tail domain. An additional anchoring point provided by myopodin PDZ domain could favor this interaction. Synemin would compete for the PDZ domain from myopodin anchored to the Z-disc occupied first by the C-terminal residues from α-actinin EF hand domain 34 (figure 4.2 1). Our data show a higher affinity for synemin than α-actinin 2 C-terminus. This suggests that synemin could displace α-actinin 2 and occupy the PDZ binding site of myopodin (figure 4.2 2). Having myopodin as an initial anchoring point the local concentration of synemin at the Z-disc might increase and supply an optimal condition for α-actinin/synemin interaction.

The proteostasis of Z-disc components like filamin C is facilitated by chaperone assisted selective autophagy (CASA) complex under mechanical stress, the CASA component BAG3 is responsible for mobilizing filamin C in the degradation process (Arndt, Dick et al. 2010). BAG3 is colocalized with myopodin in the Z-disc and interacts *via* the N-terminal WW domain with the myopodin PPPY containing region (619-622 aa). Moreover, the participation of myopodin depend on the long isoforms which contain the N-terminal PDZ domain. Myopodin PDZ domain crosslinks CASA and HOPS complexes *via* vacuolar protein sorting 18 homolog subunit (VPS18), which is necessary for the autophagosomes formation (Ulbricht, Eppler et al. 2013). Our data presented here show that myopodin PDZ domain has a higher affinity for VPS18 compared with α-actinin 2 PDZ binding motif. This is compatible with reported behavior of myopodin being translocated from the Z-disc to autophagossome structures (Ulbricht, Eppler et al. 2013). VPS18 could act as an additional interaction point for myopodin, being able to displace α-actinin 2 from myopodin PDZ domain. This would

enable myopodin to participate in adult cardiomyocyte maintenance (figure 4.2 3), in HOPS/CASA autophagy process.

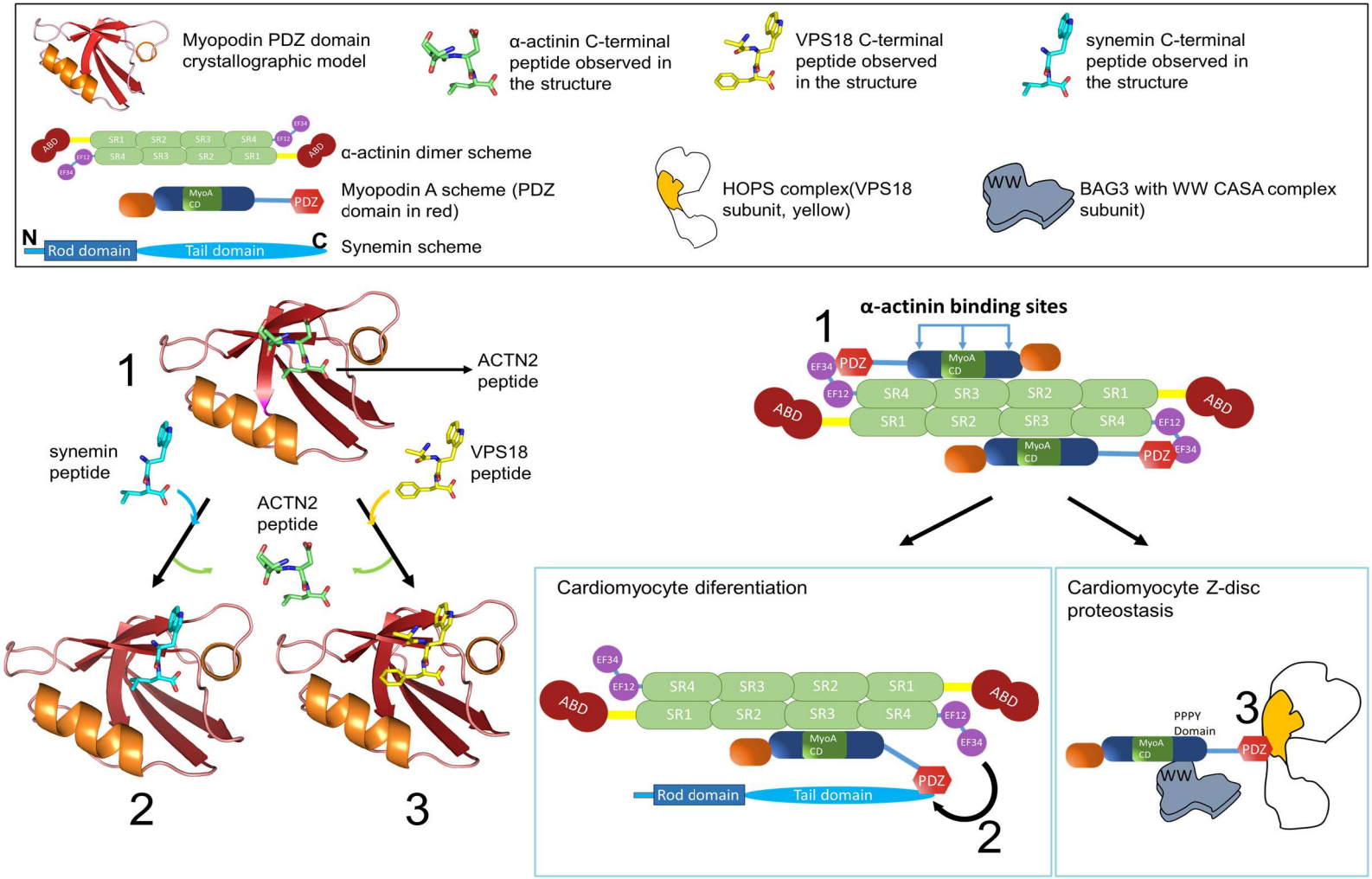

Figure 4.2: Myopodin regulation by PDZ domain proposed model. Myopodin anchored to the Z-disc via interactions with α-actinin 2. Including α-actinin 2 C-terminal domain to myopodin PDZ domain (1). During cardiomyocytes development, actinin C-terminal domain is displaced by synemin C-terminus (2). Recruitment of myopodin to CASA complex, via displacement of α-actinin 2 by HOPS subunit (VPS18) with contemporal interaction of BAG3 and PPPY region of myopodin(3).

4.4. Myopodin Central domain bundles F-actin *via* two actin-binding regions

Myopodin is described in the literature as an F-actin interaction binding partner (Weins, Schwarz et al. 2001), which presents multiple binding sites for F-actin filaments (Leinweber, Fredricksen et al. 1999). Myopodin interaction with F-actin was mapped using myopodin fragments. In this way 2 regions were identified which are able to interact with F-actin: the fragment my10-268 aa and my269-521 aa (sequence refers to the myopodin A isoform central domain 664-916 aa). In the same study it was demonstrated that the single fragment relative to myopodin central domain is able to dimerize and promote not only binding, but the bundling of F-actin filaments as well (Linnemann, Vakeel et al. 2013). However, in order to evaluate if dimerization is necessary for the actin bundling process we investigated conditions necessary for the dimer formation.

Using size exclusion chromatography coupled with a multiangle laser light-scattering detector, we were able to follow the formation of myopodin central domain dimerization, and showed that the dimeric form of the central domain could be observed restrictedly in oxidative conditions. This could be reversed by the addition of reducing agents, where only the monomeric form could be observed.

Since myopodin central domain monomer is still able to perform bundling of F-actin filaments under reducing conditions as demonstrated by Linnemann, 2013, these findings suggest that actin bundling activity of myopodin central domain is achieved by two independent F-actin binding sites. This information underlines that myopodin in a cardiomyocyte could be monomer under reducing environment or assume a dimeric state under oxidative stress.

4.5. Myopodin central domain interaction with filamin is modulated by myopodin phosphorylation

Linnemann reported the binding of myopodin central domain to filamin C in 2010. This interaction was mapped using filamin C Ig domain fragments d18-19, d18-21 and d20-21. The fragments containing the Ig domains d20-21 were mapped to host the interaction with myopodin. Using ITC we investigated the importance of the single domains involved in this interaction. For this approach, we used myopodin central domain against the single Ig domain d21 and the long fragment Ig domain d18-21.

Using ITC we observed a weak interaction of myopodin central domain with Ig domain d21 (K_d: 98 ± 30.6 μM), but this interaction increased dramatically with the experiment performed with the long construct composed of Ig domains d18-21 (K_d: 1.65 ± 0.32 μM). The latter observed binding value is in line with the data reported for this for this interaction using SAW (Linnemann, van der Ven et al. 2010). Furthermore, Linnemann at el. 2010 report the affinity of fln C d18-21 to myopodin was established to be $1.9\times10^{-6} \pm 0.8\times10^{-6}$ M. Taken together these results indicate that both, domain d20 and d21 are involved in the binding mechanism, but Ig domain d20 plays a fundamental role in the interaction.

```
                 859                                                ph  ph  ph    916
Myopodin         VGPSNELPGMSGRGAQLFAKRQSRMEKYVVDSDTVQ--AHAARAQSPTPSLPASWKYSSN
Tritopodin       SAGIPEPPRLQGRGGELFAKRQSRADRYVVEGTPGPGLGPRPRSPSPTPSLPPSWKYSPN
synaptopodin     PKPNQNLSEASGKGAELYARRQSRMEKYVIESSSHT--PELARCPSPTMSLPSSWKYPTN
```

Figure 4.3: Podin family central domain alignment. Myopodin central domain shows conserved serines (highlighted in red) among the podin family, which are potential phosphorylation sites.

In addition, this affinity for Ig domain d18-21 was replicated using micro scale thermophoresis, which corroborates the ITC experiment showing a dissociation constant of 2.4 μM. Moreover, we investigated a potential phosphorylation site located in the C-terminal portion of myopodin central domain, which is conserved among the members of the podin family. The phosphomimetic mutant of myopodin central domain shows how these potential phosphorylations (figure 4.3) could negatively modulate the interaction with filamin C (figure 3.27 b). This data suggest that phosphorylation of myopodin central domain acts as an important regulatory factor of filamin – myopodin interaction, where filamin C domain d20-21 could be released and become available to other Z-disc binding partners upon phosphorylation of Ser902, Ser906 and Ser910 in myopodin central domain.

5. Material and methods

5.1 Molecular cloning

Table 5.1 Oligonucleotide primers used for PCR

Name	Sequence
Primers for MyoA PDZ	
PDZ5F	5' CCAGGGGCCCGCCATGGATTTTATCTGCATTTCCATGAC
PDZ86R	5' GACCCGACGCGGTTATCTTTTGATGAGCATTTGGAGAG
Primers for MyoA CD	
CD664F	5' CCAGGGGCCCGCCATGTCTGAGCGAATAGCTTCCCGA
CD916R	5' GACCCGACGCGGTTAATTGGAGGAGTACTTCCAAC
Primers for MyoA CD Mut	
CDMUT916R	5' GACCCGACGCGGTTAATTTGGAGGAGTACTTCCAAT
Primers for FLNc Ig d18-21	
FLNC18-21F	5' AAGAAGGAGAACAACCATGAGGACCTCACAGCTGAATG
FLNC18-21R	5' GACCCGACCGCGGTCACAGGCACCACAAAGGGGCTG

Table 5.2 List of plasmids

	Name	tag	Resistance	Cleavage protease
Plasmid for MyoA PDZ	pETM14-LIC	N-term His-tag	kanamycin	PreScission
Plasmid for MyoA CD	p3NH-TrxA	N-term His-tag + TrxA	kanamycin	PreScission
Plasmid for MyoA CD Mut	pETM14-LIC	N-terminal His-tag	kanamycin	PreScission
Plasmid for FLNc Ig d18-21	pETM13-LIC	C-terminal His-tag	kanamycin	

Truncated construct inserts and linearized vectors were created *via* polymerase chain reaction (PCR) using plasmids containing full-length constructs as reaction templates. The PCR was prepared to a final volume of 25 µl containing 1 µl of each primer 10 µM (table 5.1), 12.5 µl of 2x (New England Biolabs) Phusion Flash Mastermix and 1 µl of template DNA (100 ng/µl). DNA was initially melted at 95°C for 2 minutes, then 30 cycles of 98°C for 30 s, 72°C for 20 s were performed followed by a final elongation step of 72°C for 10 min. Inserts PCR reactions were analyzed by agarose gel electrophoresis and purified using the Fermentas PCR purification kit according to the manufacturer's instructions. The linearized vectors were extracted from the gel using Fermentas gel extraction kit. These purified fragments of inserts and vectors have complementary overhang end sequences for ligation independent cloning. For the anneling procedure 0.02 pmol of the insert

DNA and 0.007 pmol of LIC prepared vector DNA incubated at 22°C for 10 minutes was needed (Aslanidis and de Jong 1990).

5.1.1. DNA Agarose Gel Electrophoresis

All the DNA samples were analyzed by DNA agarose gel electrophoresis at a concentration of 1.0 % w/v in 1x TAE buffer (40 mM tris (Trizma, Sigma), 4.7 %v/v acetic acid, 50mM EDTA pH 8.0) and 10 µl peqGREEN DNA dye (peqlab). The electrophoresis was carried out at 100V for 30 min and the DNA was visualized under UV light.

5.1.2. Bacterial transformation

The ligation mixture (table 5.2) was transformed into *E. coli* DH5α competent cells. Transformation was carried out by heat shock procedure. A 2 µl ligation mixture was added to 33 µl of DH5α competent cells and incubated for 15 min on ice. This was then followed by heat shock at 42°C for 60 s. Cells were then allowed to recover on ice for 2 min and 300 µl of LB media (Sigma-Aldrich) was added The culture was then incubated at 37°C with shaking for 1 h. This procedure was employed to positively transform selected plasmids into expression strains: *E. coli* BL21 (DE3) for MyoA PDZ and FLNc Ig 18-21; Rosetta 2 (DE3) pLysS for MyoA CD and MyoA CD Mut. The cells were subsequently plated out on LB-agar (LB and 1.5 % w/v agar) containing the appropriate antibiotic (kanamycin 50 µg/ml and for Rosetta 2 (DE3) pLysS chloramphenicol 34 µg/ml) and grown overnight at 37 °C during the process of cloning.

5.2. Expression of recombinant proteins and purification

5.2.1. Protein expression

Large scale expression of proteins carried out in auto-induction media ZYP-5052 (Studier 2005). A pre-culture of 20 ml LB containing the selective antibiotics was inoculated with the freshly transformed cells and grown overnight at 37 °C in a shaking incubator (180 rpm). The next day 1.0 ml of the inoculum was transferred into 2 liter flasks containing 500 ml of ZYP-5052 media (table 5.3) + antibiotics. The auto-induction cell growth and protein expression steps were carried out at 37°C for 6 h and at 18 °C overnight.

Table 5.3 ZYP-5052 media composition

Component	Final concentration
ZY	
Tryptone (Fluka analytical)	10 g/l
Yeast extract (Fluka analytical)	5.0 g/l
$MgSO_4$	1.0 mM
NPS	
$(NH_4)_2SO_4$	0.025 M
KH_2PO_4	0.05 M
Na_2HPO_4	0.05 M
5052	
Glycerol	0.5 %
Glucose	0.05 %
α-Lactose	0.2 %
Antibiotics	
Kanamycin	50 µg/ml
Chloraphenicol	34 µg/ml

Additionally, large scale expression of proteins used in NMR experiments were carried out in M9 Minimal Media. A pre-culture of 100 ml LB containing the selective antibiotics was inoculated with the freshly transformed cells and grown overnight at 37 °C in a shaking incubator (180 rpm). The next day 10 ml of the inoculum was transferred into 2 liter flasks containing 500 ml of M9 Minimal media (table 5.4). The

cells were grown in the medium until OD_{600} reached 0.7 A.U. At this point, IPTG at a final concentration of 0.2 mM was added and the temperature was set to 18 °C. The induction was carried out at 18 °C, under shaking (180 rpm) overnight (16 hours).

Table 5.4 M9 Minimal media composition (1 l)

Component	Amount
M9 Salt pH 7.4 (5x)	200 ml
Na_2HPO_4 (33.9 g)	
KH_2PO_4 (15.0 g)	
NaCl (2.5 g)	
*H_2O to 1 l	
1 M $MgSO_4$	2.0 ml
2 M $CaCl_2$	50 µl
Trace elements	10 ml
$CaCl_2$ * $2H_2O$ (0.6 g)	
$FeSO_4$ * $7H_2O$ (0.6 g)	
$MnCl_2$ * $4H_2O$ (0.115 g)	
$CoCl_2$ * $6H_2O$ (0.08 g)	
$ZnSO_4$ * $7H_2O$ (0.07 g)	
$CuCl_2$ * $2H_2O$ (0.03 g)	
H_3BO_3 (0.002 g)	
$(NH_4)_6MO_7O_{24}$ * $4H_2O$ (0.025 g)	
EDTA (0.5 g)	
*H_2O to 100 ml	
^{15}N NH_4Cl	1.0 g
^{13}C Glucose	3.0 g

5.2.2. Protein purification

Cell pellets were harvested by centrifugation (15 min at 5000 rpm at 4 °C, Sorvall RC 6+, F10S-4x1000 LEX rotor) and resuspended in the lysis buffer (20 mM tris pH 8.0, 500 mM NaCl, and 1.0 mM EDTA) with protease inhibitor mix (Complete, EDTA

free, Roche; 1 tablet/ 50 ml lysed solution). Subsequently, the cells were lysed by sonication (50% power for 3 x 3 min) on ice and centrifuged for 20 min at 18000 rpm at 4 °C (Sorvall RC 6+, F21S-8x50y rotor). The supernatant after centrifugation was used for the further purification steps on an AEKTA FPLC system (GE Healthcare) at 4 °C.

5.2.2.1. Purification of myopodin A PDZ domain construct(MyoA PDZ)

The lysed supernatant was purified by a HisTrap FF crude column (GE Healthcare) equilibrated in binding buffer (20 mM tris pH 8.0, 500 mM NaCl, 1.0 mM EDTA and 20 mM imidazole), using a gradient of imidazole for elution (20 mM tris pH 8.0, 500 mM NaCl, 1.0 mM EDTA and 20 - 500 mM imidazole). Major eluted fractions containing the desired proteins were pooled together with GST-3C protease (1.0 g protease for every 25 g of target protein) and dialyzed against the HisTrap binding buffer. The dialyzed samples were introduced again to HisTrap FF crude column (GE Healthcare). Unbound fractions were collected after second nickel-affinity chromatography, which were further purified using a Superdex 75 16/60 gel filtration column (GE Healthcare) and an in-line GSTrap HP column (GE Healthcare) in the SEC buffer (20 mM tris pH 8.0, 300 mM NaCl, 1.0 mM EDTA, 1.0 mM DTT and 5% glycerol).

5.2.2.2. Purification of myopodin A central domain constructs (MyoA CD and MyoA CD Mut)

The lysed supernatant was purified by a HisTrap FF crude column (GE Healthcare) equilibrated in binding buffer (20 mM tris pH 8.0, 500 mM NaCl, 1.0 mM EDTA and 20 mM imidazole), using a gradient of imidazole for elution (20 mM tris pH 8.0, 500 mM NaCl, 1.0 mM EDTA and 20 - 500 mM imidazole). Major eluted fractions containing the desired proteins were pooled together with GST-3C protease (1.0 g protease for every 25 g of target protein) and dialyzed against the ionic exchange chromatography binding buffer (20 mM tris pH 8.0, 1.0 mM EDTA, 1.0 mM DTT). The dialyzed samples were loaded into a HiTrap Q Sepharose FF. Unbound fractions were collected and further purified using a Superdex 75 16/60 gel filtration column (GE

Healthcare) and an in-line GSTrap HP column (GE Healthcare) in the SEC buffer (20 mM tris pH 8.0, 300 mM NaCl, 1.0 mM EDTA, 1.0 mM DTT and 5% glycerol).

5.2.2.3. Filamin C Ig d18-20 construct purification

The lysed supernatant was purified by a HisTrap FF crude column (GE Healthcare) equilibrated in binding buffer (20 mM tris pH 8.0, 500 mM NaCl, 1.0 mM EDTA and 20 mM imidazole), using a gradient of imidazole for elution (20 mM tris pH 8.0, 500 mM NaCl, 1.0 mM EDTA and 20 - 500 mM imidazole). Major eluted fractions containing the desired proteins were pooled together and further purified using a Superdex 200 26/60 gel filtration column (GE Healthcare) and an in-line GSTrap HP column (GE Healthcare) in the SEC buffer (20 mM tris pH 8.0, 300 mM NaCl, 1.0 mM EDTA, 1.0 mM DTT and 5% glycerol).

5.2.3. Protein concentration determination

The proteins were concentrated using a 3.0 kDa or 10 kDa MWCO Vivaspin turbo centrifugal concentrator (Sartorius stedim). The concentration of the protein samples was determined by measuring the protein absorbance by UV at 280 nm (Nanophotometer).The extinction coefficient (table 5.5) of the protein was calculated by the Protein Calculator v3.4 tool on the website (protcalc.sourceforge.net).

Table 5.5 Extinction coefficients of proteins

Name	Extinction coefficient ($M^{-1}cm^{-1}$)	Abs 0.1% (=1 g/l)
MyoA PDZ	6970	0.7832
MyoA CD	17780	0.6716
MyoA CD Mut	17780	0.6695
FLNc Ig d18-21	27310	0.5582

5.2.4. SDS-polyacrylamide gel electrophoresis

SDS-PAGE was used for the electrophoretic separation of proteins according to the method described by Laemmli (Laemmli 1970) to follow the purification of the constructs. Polyacrylamide gel of 12% and 15%, under denaturing conditions, was used in order to analyze the quality of the protein sample. The protein samples were mixed in a 1:1 ratio with 2x SDS loading buffer, boiled for 5 min at 95 °C and centrifuged before loading onto the gel. The gels ran at a fixed voltage (200 V) for 50 minutes and the gels were stained by Coomassie Brilliant Blue R-250 for 5 minutes and then destained using destaining solution (40% (v/v) ethanol, 7% (v/v) acetic acid).

5.3. Thermal shift assay (thermofluor)

Thermofluor experiments were performed with 5.0 µl samples composed of 50 µM protein samples and/or 1 mM peptide and 40 X Sypro Orange (Molecular Probes), which were added to a 96-well PCR plate. A 96 well plate with 20 µl of different buffers and salt concentrations (table 3.1) was used in order to screen the best condition. The plates were sealed with Optical-Quality Sealing Tape (Bio-Rad) and heated in an iCycler iQ Real Time PCR Detection System (Bio-Rad) from 20 to 95 °C in increments of 1 °C.

5.4. Static light scattering (SLS) using analytical SEC and MALLS

SLS was performed with a Superdex 200 10/300 GL column (GE Healthcare Life Sciences) equilibrated with the SEC buffer (20 mM tris pH 8.0, 300 mM NaCl, 1.0 mM EDTA and 5% glycerol) in the presence or absence 1 mM DTT. The experiments were performed at 20 ºC with a flow rate of 0.5 ml/min with an Agilent Technologies 1260 Infinity HPLC. On-line MALLS detection was performed with a miniDAWN TREOS detector (Wyatt Technology) and a refractive index measurement using a Shodex RI-101 (Wyatt Technology) was used. Purified protein was applied to the column at a concentration of 200 µM.

5.5. Isothermal Titration Calorimetry (ITC)

MyoA PDZ constructs and the binding partners' peptides were dialyzed against the buffer (potassium phosphate 20 mM pH 7.0 and NaCl 100 mM). MyoA CD and filamin C were dialyzed against the buffer (20 mM HEPES pH 7.4 pH 7.4 and NaCl 150 mM). The dialysis was performed overnight at 4°C. 200 µl protein samples were injected in the sample cell and water was filled in the reference cell. 40 µl of peptide samples were inserted into the sample syringe for injection. ITC was performed at 25° C using iTC200 Microcalorimeter (MicroCal). The experimental parameters were as follows: 20 times of total injections, 240 sec of initial delay, and 800 rpm of stirring speed. Injection parameters were as follows: 2.0 µl of injection volume, 180 sec of spacing time, and 5 sec of filter period. For MyoA PDZ/α-actinin 2 peptide ITC experiment was performed using MicroCal VP-ITC Microcalorimeter at 25° C. 1.4 ml protein samples were injected into the sample cell and water was filled in the reference cell. 300 µl of peptide samples were inserted into the sample syringe for injection. The experiment was carried out with 30 times of total injections, 360 sec of initial delay, and 300 rpm of stirring speed. Injection parameters were as follows: 10 µl of injection volume, 240 sec of spacing time, and 2 sec of filter period. Thermodynamic parameters of each interaction were obtained by fitting the single-set of binding model or competitive binding model using Origin 7.

5.6. Microscale Thermophoresis (MST)

Microscale thermophoresis interaction studies were performed on the Monolith NT.115 (Nanotemper Technologies, Munich, Germany). MyoA CD and MyoA CD Mut were labeled using MO-L001 Monolith™ Protein Labeling Kit RED-NHS (Amine Reactive) and recovered at a concentration of 8 µM and 4 µM respectively and used as described (Wienken, Baaske et al. 2010, Jerabek-Willemsen, Wienken et al. 2011, Seidel, Dijkman et al. 2013). Solutions of unlabeled FLNc d18-21 was serially diluted from 414 µM to 12.6 nM in the presence of 100 nM concentrations of one of the labeled MyoA CD or MyoA CD Mut proteins. Measurements were performed at 25 °C in 20

mM HEPES pH 7.4, 150 mM NaCl, 0.5 mM tris (2-carboxyethyl)phosphine, 0.05% Tween, using 20% IR-laser power with 30% and 20% LED power for experiments with MyoA CD and MyoA CD Mut respectively, using Monolith™ NT.115 Hydrophilic Capillaries. The data were analyzed using with NT analysis software, v.1.4.27.

5.7. Nuclear magnetic resonance spectroscopy (NMR)

For NMR, cells were grown in M9 minimal medium at 37 °C supplemented with $^{15}NH_4Cl$ and ^{13}C-glucose. Labeled proteins were purified following the procedure described for unlabeled protein samples, except in the final gel filtration step where there was a buffer containing potassium phosphate 20 mM pH 7.0 and 100 mM NaCl was used. Prior to measurement, D_2O to a final concentration of 10% (v/v) was added to MyoA PDZ at 1 mM.

Three-dimensional triple-resinance NMR spectra of ^{15}N-^{13}C-labeled MyoA PDZ were recorded and used for sequential amino acid residue assignments. Then, ^{1}H-^{15}N heteronuclear single quantum coherence (HSQC) experiments on ^{15}N labeled MyoA PDZ were applied to map backbone amide 15N-1H chemical shift differences upon titration of an unlabeled synemin peptide.

NMR experiments were performed with a Varian Direct Drive 600 MHz spectrometer equipped with 1H/13C/15N triple resonance probes at 25 °C. Spectra were processed with NMRPipe (Delaglio, Grzesiek et al. 1995) and analyzed with Sparky software (Goddard and Kneller, UCSF). Chemical shifts observed in 15N-HSQC experiments were quantified as $\sqrt{(\Delta\delta^{15}\mathrm{N})^2 + (5\Delta\delta^{1}H)^2}$.

5.8. Crystallization and structure solution

5.8.1. Crystallization and Structure Determination of the MyoA PDZ

MyoA PDZ was dialyzed against deionized water to remove the storage buffer (20 mM tris pH 8.0, 300 mM NaCl. and glycerol 5%) for 2 h. Following this, the protein sample (10mg/ml) was submitted to Hampton Research PCT™ (Pre-Crystallization Test) using sitting-drop method at 22 °C. For the protein/peptide complex the protein

was in contact with 3 mM peptide overnight at 4 °C. Protein solution mixed was with an equal volume of the crystallization solution containing 100 mM tris pH 8.5, 2.0 M ammonium sulfate for MyoA PDZ and MyoA PDZ/VPS18, MyoA PDZ/ACTN2 complexes. For MyoA PDZ/synemin complex 100 mM tris pH 8.5, 0.2 M Lithium sulfate monohydrate and 30% w/v Polyethylene glycol 4,000 was used as crystallization condition. Crystals were transferred to the cryo-cooling solution containing 25% glycerol and flash frozen in liquid nitrogen. Diffraction data were collected at the beamlines BM14, ID23-1 and ID23-2 in ESRF (Grenoble, France), integrated with XDS (Kabsch 2010) and scaled with Scala in the CCP4 suite (Evans and Murshudov 2013). The structure was solved by molecular replacement using BALBES (Long, Vagin et al. 2008). Refinement was carried out using Phenix Refine (Afonine, Grosse-Kunstleve et al. 2012), REFMAC (Murshudov, Vagin et al. 1997) and PDB_REDO (Joosten, Womack et al. 2009) alternating with model adjustment by Coot (Emsley and Cowtan 2004). The figures of the molecules were generated using PyMOL Molecular Graphics System.

6. References

Afonine, P. V., R. W. Grosse-Kunstleve, N. Echols, J. J. Headd, N. W. Moriarty, M. Mustyakimov, T. C. Terwilliger, A. Urzhumtsev, P. H. Zwart and P. D. Adams (2012). "Towards automated crystallographic structure refinement with phenix.refine." Acta Crystallogr D Biol Crystallogr **68**(Pt 4): 352-367.

Alberts, B., A. Johnson, J. Lewis, M. C. Raff, K. Roberts and P. Walter (2002). Molecular biology of the cell. S.l., Garland Science.

Amacher, J. F., P. R. Cushing, L. Brooks, 3rd, P. Boisguerin and D. R. Madden (2014). "Stereochemical preferences modulate affinity and selectivity among five PDZ domains that bind CFTR: comparative structural and sequence analyses." Structure **22**(1): 82-93.

Amos, L. and A. Klug (1974). "Arrangement of subunits in flagellar microtubules." J Cell Sci **14**(3): 523-549.

Arndt, V., N. Dick, R. Tawo, M. Dreiseidler, D. Wenzel, M. Hesse, D. O. Furst, P. Saftig, R. Saint, B. K. Fleischmann, M. Hoch and J. Hohfeld (2010). "Chaperone-assisted selective autophagy is essential for muscle maintenance." Curr Biol **20**(2): 143-148.

Asanuma, K., K. Kim, J. Oh, L. Giardino, S. Chabanis, C. Faul, J. Reiser and P. Mundel (2005). "Synaptopodin regulates the actin-bundling activity of alpha-actinin in an isoform-specific manner." J Clin Invest **115**(5): 1188-1198.

Aslanidis, C. and P. J. de Jong (1990). "Ligation-independent cloning of PCR products (LIC-PCR)." Nucleic Acids Res **18**(20): 6069-6074.

Baldassarre, M., Z. Razinia, N. N. Brahme, R. Buccione and D. A. Calderwood (2012). "Filamin A controls matrix metalloproteinase activity and regulates cell invasion in human fibrosarcoma cells." J Cell Sci **125**(Pt 16): 3858-3869.

Beatham, J., R. Romero, S. K. Townsend, T. Hacker, P. F. van der Ven and G. Blanco (2004). "Filamin C interacts with the muscular dystrophy KY protein and is abnormally distributed in mouse KY deficient muscle fibres." Hum Mol Genet **13**(22): 2863-2874.

Bellin, R. M., T. W. Huiatt, D. R. Critchley and R. M. Robson (2001). "Synemin may function to directly link muscle cell intermediate filaments to both myofibrillar Z-lines and costameres." J Biol Chem **276**(34): 32330-32337.

Bellin, R. M., S. W. Sernett, B. Becker, W. Ip, T. W. Huiatt and R. M. Robson (1999). "Molecular characteristics and interactions of the intermediate filament protein synemin. Interactions with alpha-actinin may anchor synemin-containing heterofilaments." J Biol Chem **274**(41): 29493-29499.

Beqqali, A., J. Monshouwer-Kloots, R. Monteiro, M. Welling, J. Bakkers, E. Ehler, A. Verkleij, C. Mummery and R. Passier (2010). "CHAP is a newly identified Z-disc protein essential for heart and skeletal muscle function." J Cell Sci **123**(Pt 7): 1141-1150.

Blanchard, A., V. Ohanian and D. Critchley (1989). "The structure and function of alpha-actinin." J Muscle Res Cell Motil **10**(4): 280-289.

Blanchoin, L., R. Boujemaa-Paterski, C. Sykes and J. Plastino (2014). "Actin dynamics, architecture, and mechanics in cell motility." Physiol Rev **94**(1): 235-263.

Braun, T. and M. Gautel (2011). "Transcriptional mechanisms regulating skeletal muscle differentiation, growth and homeostasis." Nat Rev Mol Cell Biol **12**(6): 349-361.

Brocker, C., A. Kuhlee, C. Gatsogiannis, H. J. Balderhaar, C. Honscher, S. Engelbrecht-Vandre, C. Ungermann and S. Raunser (2012). "Molecular architecture of the multisubunit homotypic fusion and vacuole protein sorting (HOPS) tethering complex." Proc Natl Acad Sci U S A **109**(6): 1991-1996.

Burns, R. G. (1991). "Alpha-, beta-, and gamma-tubulins: sequence comparisons and structural constraints." Cell Motil Cytoskeleton **20**(3): 181-189.

Caldwell, J. E., S. G. Heiss, V. Mermall and J. A. Cooper (1989). "Effects of CapZ, an actin capping protein of muscle, on the polymerization of actin." Biochemistry **28**(21): 8506-8514.

Chalovich, J. M. and M. M. Schroeter (2010). "Synaptopodin family of natively unfolded, actin binding proteins: physical properties and potential biological functions." Biophysical Reviews **2**: 181-189.

Chan, D. I., E. J. Prenner and H. J. Vogel (2006). "Tryptophan- and arginine-rich antimicrobial peptides: structures and mechanisms of action." Biochim Biophys Acta **1758**(9): 1184-1202.

Claeys, K. G., P. F. van der Ven, A. Behin, T. Stojkovic, B. Eymard, O. Dubourg, P. Laforet, G. Faulkner, P. Richard, P. Vicart, N. B. Romero, G. Stoltenburg, B. Udd, M. Fardeau, T. Voit and D. O. Furst (2009). "Differential involvement of sarcomeric proteins in myofibrillar myopathies: a morphological and immunohistochemical study." Acta Neuropathol **117**(3): 293-307.

Colucci-Guyon, E., M. M. Portier, I. Dunia, D. Paulin, S. Pournin and C. Babinet (1994). "Mice lacking vimentin develop and reproduce without an obvious phenotype." Cell **79**(4): 679-694.

Cowburn, D. (1997). "Peptide recognition by PTB and PDZ domains." Curr Opin Struct Biol **7**(6): 835-838.

De Ganck, A., V. De Corte, A. Staes, K. Gevaert, J. Vandekerckhove and J. Gettemans (2008). "Multiple isoforms of the tumor suppressor myopodin are simultaneously transcribed in cancer cells." Biochem Biophys Res Commun **370**(2): 269-273.

Delaglio, F., S. Grzesiek, G. W. Vuister, G. Zhu, J. Pfeifer and A. Bax (1995). "NMRPipe: a multidimensional spectral processing system based on UNIX pipes." J Biomol NMR **6**(3): 277-293.

DePianto, D. and P. A. Coulombe (2004). "Intermediate filaments and tissue repair." Exp Cell Res **301**(1): 68-76.

Desai, A. and T. J. Mitchison (1997). "Microtubule polymerization dynamics." Annu Rev Cell Dev Biol **13**: 83-117.

Dey, P., J. Togra and S. Mitra (2014). "Intermediate filament: structure, function, and applications in cytology." Diagn Cytopathol **42**(7): 628-635.

Djinovic-Carugo, K., M. Gautel, J. Ylanne and P. Young (2002). "The spectrin repeat: a structural platform for cytoskeletal protein assemblies." FEBS Lett **513**(1): 119-123.

dos Remedios, C. G., D. Chhabra, M. Kekic, I. V. Dedova, M. Tsubakihara, D. A. Berry and N. J. Nosworthy (2003). "Actin binding proteins: regulation of cytoskeletal microfilaments." Physiol Rev **83**(2): 433-473.

Dougherty, D. A. (1996). "Cation-pi interactions in chemistry and biology: a new view of benzene, Phe, Tyr, and Trp." Science **271**(5246): 163-168.

Doyle, D. A., A. Lee, J. Lewis, E. Kim, M. Sheng and R. MacKinnon (1996). "Crystal structures of a complexed and peptide-free membrane protein-binding domain: molecular basis of peptide recognition by PDZ." Cell **85**(7): 1067-1076.

Du, A., J. M. Sanger and J. W. Sanger (2008). "Cardiac myofibrillogenesis inside intact embryonic hearts." Dev Biol **318**(2): 236-246.

Elkins, J. M., C. Gileadi, L. Shrestha, C. Phillips, J. Wang, J. R. Muniz and D. A. Doyle (2010). "Unusual binding interactions in PDZ domain crystal structures help explain binding mechanisms." Protein Sci **19**(4): 731-741.

Elkins, J. M., E. Papagrigoriou, G. Berridge, X. Yang, C. Phillips, C. Gileadi, P. Savitsky and D. A. Doyle (2007). "Structure of PICK1 and other PDZ domains obtained with the help of self-binding C-terminal extensions." Protein Sci **16**(4): 683-694.

Emsley, P. and K. Cowtan (2004). "Coot: model-building tools for molecular graphics." Acta Crystallogr D Biol Crystallogr **60**(Pt 12 Pt 1): 2126-2132.

Evans, L., T. Mitchison and M. Kirschner (1985). "Influence of the centrosome on the structure of nucleated microtubules." J Cell Biol **100**(4): 1185-1191.

Evans, P. R. and G. N. Murshudov (2013). "How good are my data and what is the resolution?" Acta Crystallogr D Biol Crystallogr **69**(Pt 7): 1204-1214.

Fanning, A. S. and J. M. Anderson (1996). "Protein-protein interactions: PDZ domain networks." Curr Biol **6**(11): 1385-1388.

Frank, D. and N. Frey (2011). "Cardiac Z-disc signaling network." J Biol Chem **286**(12): 9897-9904.

Frank, D., C. Kuhn, H. A. Katus and N. Frey (2006). "The sarcomeric Z-disc: a nodal point in signalling and disease." J Mol Med (Berl) **84**(6): 446-468.

Fuchs, E. and K. Weber (1994). "Intermediate filaments: structure, dynamics, function, and disease." Annu Rev Biochem **63**: 345-382.

Furst, D. O., L. G. Goldfarb, R. A. Kley, M. Vorgerd, M. Olive and P. F. van der Ven (2013). "Filamin C-related myopathies: pathology and mechanisms." Acta Neuropathol **125**(1): 33-46.

Gontier, Y., A. Taivainen, L. Fontao, A. Sonnenberg, A. van der Flier, O. Carpen, G. Faulkner and L. Borradori (2005). "The Z-disc proteins myotilin and FATZ-1 interact with each other and are connected to the sarcolemma via muscle-specific filamins." J Cell Sci **118**(Pt 16): 3739-3749.

Guharoy, M., B. Szabo, S. Contreras Martos, S. Kosol and P. Tompa (2013). "Intrinsic structural disorder in cytoskeletal proteins." Cytoskeleton (Hoboken) **70**(10): 550-571.

Herrmann, H. and U. Aebi (2000). "Intermediate filaments and their associates: multi-talented structural elements specifying cytoarchitecture and cytodynamics." Curr Opin Cell Biol **12**(1): 79-90.

Hillier, B. J., K. S. Christopherson, K. E. Prehoda, D. S. Bredt and W. A. Lim (1999). "Unexpected modes of PDZ domain scaffolding revealed by structure of nNOS-syntrophin complex." Science **284**(5415): 812-815.

Holmes, W. B. and C. L. Moncman (2008). "Nebulette interacts with filamin C." Cell Motil Cytoskeleton **65**(2): 130-142.

Inoue, S. and E. D. Salmon (1995). "Force generation by microtubule assembly/disassembly in mitosis and related movements." Mol Biol Cell **6**(12): 1619-1640.

Ishida, T. and K. Kinoshita (2007). "PrDOS: prediction of disordered protein regions from amino acid sequence." Nucleic Acids Res **35**(Web Server issue): W460-464.

Ishikawa, H., R. Bischoff and H. Holtzer (1968). "Mitosis and intermediate-sized filaments in developing skeletal muscle." J Cell Biol **38**(3): 538-555.

Jelen, F., A. Oleksy, K. Smietana and J. Otlewski (2003). "PDZ domains - common players in the cell signaling." Acta Biochim Pol **50**(4): 985-1017.

Jerabek-Willemsen, M., C. J. Wienken, D. Braun, P. Baaske and S. Duhr (2011). "Molecular interaction studies using microscale thermophoresis." Assay Drug Dev Technol **9**(4): 342-353.

Joosten, R. P., T. Womack, G. Vriend and G. Bricogne (2009). "Re-refinement from deposited X-ray data can deliver improved models for most PDB entries." Acta Crystallogr D Biol Crystallogr **65**(Pt 2): 176-185.

Jordan, M. A. and L. Wilson (2004). "Microtubules as a target for anticancer drugs." Nat Rev Cancer **4**(4): 253-265.

Kabsch, W. (2010). "Xds." Acta Crystallogr D Biol Crystallogr **66**(Pt 2): 125-132.

Karsenti, E., F. Nedelec and T. Surrey (2006). "Modelling microtubule patterns." Nat Cell Biol **8**(11): 1204-1211.

Katzemich, A., K. A. Liao, S. Czerniecki and F. Schock (2013). "Alp/Enigma family proteins cooperate in Z-disc formation and myofibril assembly." PLoS Genet **9**(3): e1003342.

Kennedy, M. B. (1995). "Origin of PDZ (DHR, GLGF) domains." Trends Biochem Sci **20**(9): 350.

Khaymina, S. S., J. M. Kenney, M. M. Schroeter and J. M. Chalovich (2007). "Fesselin is a natively unfolded protein." J Proteome Res **6**(9): 3648-3654.

Kim, E. and M. Sheng (2004). "PDZ domain proteins of synapses." Nat Rev Neurosci **5**(10): 771-781.

Kim, J., I. Kim, J. S. Yang, Y. E. Shin, J. Hwang, S. Park, Y. S. Choi and S. Kim (2012). "Rewiring of PDZ domain-ligand interaction network contributed to eukaryotic evolution." PLoS Genet **8**(2): e1002510.

Knoll, R., M. Hoshijima, H. M. Hoffman, V. Person, I. Lorenzen-Schmidt, M. L. Bang, T. Hayashi, N. Shiga, H. Yasukawa, W. Schaper, W. McKenna, M. Yokoyama, N. J. Schork, J. H. Omens, A. D. McCulloch, A. Kimura, C. C. Gregorio, W. Poller, J. Schaper, H. P. Schultheiss and K. R. Chien (2002). "The cardiac mechanical stretch sensor machinery involves a Z disc complex that is defective in a subset of human dilated cardiomyopathy." Cell **111**(7): 943-955.

Kontrogianni-Konstantopoulos, A., M. A. Ackermann, A. L. Bowman, S. V. Yap and R. J. Bloch (2009). "Muscle giants: molecular scaffolds in sarcomerogenesis." Physiol Rev **89**(4): 1217-1267.

Kremerskothen, J., C. Plaas, S. Kindler, M. Frotscher and A. Barnekow (2005). "Synaptopodin, a molecule involved in the formation of the dendritic spine apparatus, is a dual actin/alpha-actinin binding protein." J Neurochem **92**(3): 597-606.

Laemmli, U. K. (1970). "Cleavage of structural proteins during the assembly of the head of bacteriophage T4." Nature **227**(5259): 680-685.

Lammerding, J., P. C. Schulze, T. Takahashi, S. Kozlov, T. Sullivan, R. D. Kamm, C. L. Stewart and R. T. Lee (2004). "Lamin A/C deficiency causes defective nuclear mechanics and mechanotransduction." J Clin Invest **113**(3): 370-378.

Lange, S., E. Ehler and M. Gautel (2006). "From A to Z and back? Multicompartment proteins in the sarcomere." Trends Cell Biol **16**(1): 11-18.

Lange, S., M. Himmel, D. Auerbach, I. Agarkova, K. Hayess, D. O. Furst, J. C. Perriard and E. Ehler (2005). "Dimerisation of myomesin: implications for the structure of the sarcomeric M-band." J Mol Biol **345**(2): 289-298.

Lassar, A. B., S. X. Skapek and B. Novitch (1994). "Regulatory mechanisms that coordinate skeletal muscle differentiation and cell cycle withdrawal." Curr Opin Cell Biol **6**(6): 788-794.

Lazarides, E. and B. D. Hubbard (1976). "Immunological characterization of the subunit of the 100 A filaments from muscle cells." Proc Natl Acad Sci U S A **73**(12): 4344-4348.

Lebedev, A. A., A. A. Vagin and G. N. Murshudov (2008). "Model preparation in MOLREP and examples of model improvement using X-ray data." Acta Crystallogr D Biol Crystallogr **64**(Pt 1): 33-39.

Lee, H. J. and J. J. Zheng (2010). "PDZ domains and their binding partners: structure, specificity, and modification." Cell Commun Signal **8**: 8.

Lee, J. H., H. Park, S. J. Park, H. J. Kim and S. H. Eom (2011). "The structural flexibility of the shank1 PDZ domain is important for its binding to different ligands." Biochem Biophys Res Commun **407**(1): 207-212.

Leinweber, B. D., R. S. Fredricksen, D. R. Hoffman and J. M. Chalovich (1999). "Fesselin: a novel synaptopodin-like actin binding protein from muscle tissue." J Muscle Res Cell Motil **20**(5-6): 539-545.

Lin, F., Y. P. Yu, J. Woods, K. Cieply, B. Gooding, P. Finkelstein, R. Dhir, D. Krill, M. J. Becich, G. Michalopoulos, S. Finkelstein and J. H. Luo (2001). "Myopodin, a synaptopodin homologue, is frequently deleted in invasive prostate cancers." Am J Pathol **159**(5): 1603-1612.

Linnemann, A. (2010). Biochemische und zellbiologische Charakterisierung der Podin-Proteinfamilie als Adapterproteine des Aktinzytoskeletts in Muskelzellen, University of Bonn.

Linnemann, A., P. Vakeel, E. Bezerra, Z. Orfanos, K. Djinovic-Carugo, P. F. van der Ven, G. Kirfel and D. O. Furst (2013). "Myopodin is an F-actin bundling protein with multiple independent actin-binding regions." J Muscle Res Cell Motil **34**(1): 61-69.

Linnemann, A., P. F. van der Ven, P. Vakeel, B. Albinus, D. Simonis, G. Bendas, J. A. Schenk, B. Micheel, R. A. Kley and D. O. Furst (2010). "The sarcomeric Z-disc component myopodin is a multiadapter protein that interacts with filamin and alpha-actinin." Eur J Cell Biol **89**(9): 681-692.

Long, F., A. A. Vagin, P. Young and G. N. Murshudov (2008). "BALBES: a molecular-replacement pipeline." Acta Crystallogr D Biol Crystallogr **64**(Pt 1): 125-132.

Long, J. F., W. Feng, R. Wang, L. N. Chan, F. C. Ip, J. Xia, N. Y. Ip and M. Zhang (2005). "Autoinhibition of X11/Mint scaffold proteins revealed by the closed conformation of the PDZ tandem." Nat Struct Mol Biol **12**(8): 722-728.

Lund, L. M., J. P. Kerr, J. Lupinetti, Y. Zhang, M. A. Russell, R. J. Bloch and M. Bond (2012). "Synemin isoforms differentially organize cell junctions and desmin filaments in neonatal cardiomyocytes." FASEB J **26**(1): 137-148.

Luther, P. K. (1991). "Three-dimensional reconstruction of a simple Z-band in fish muscle." J Cell Biol **113**(5): 1043-1055.

Luther, P. K. (2009). "The vertebrate muscle Z-disc: sarcomere anchor for structure and signalling." J Muscle Res Cell Motil **30**(5-6): 171-185.

Ma, P. C., M. A. Rould, H. Weintraub and C. O. Pabo (1994). "Crystal structure of MyoD bHLH domain-DNA complex: perspectives on DNA recognition and implications for transcriptional activation." Cell **77**(3): 451-459.

Mundel, P., H. W. Heid, T. M. Mundel, M. Kruger, J. Reiser and W. Kriz (1997). "Synaptopodin: an actin-associated protein in telencephalic dendrites and renal podocytes." J Cell Biol **139**(1): 193-204.

Murshudov, G. N., A. A. Vagin and E. J. Dodson (1997). "Refinement of macromolecular structures by the maximum-likelihood method." Acta Crystallogr D Biol Crystallogr **53**(Pt 3): 240-255.

Pardo, J. V., J. D. Siliciano and S. W. Craig (1983). "A vinculin-containing cortical lattice in skeletal muscle: transverse lattice elements ("costameres") mark sites of attachment between myofibrils and sarcolemma." Proc Natl Acad Sci U S A **80**(4): 1008-1012.

Patrie, K. M., A. J. Drescher, A. Welihinda, P. Mundel and B. Margolis (2002). "Interaction of two actin-binding proteins, synaptopodin and alpha-actinin-4, with the tight junction protein MAGI-1." J Biol Chem **277**(33): 30183-30190.

Pollard, T. D. (1986). "Rate constants for the reactions of ATP- and ADP-actin with the ends of actin filaments." J Cell Biol **103**(6 Pt 2): 2747-2754.

Pollard, T. D., L. Blanchoin and R. D. Mullins (2000). "Molecular mechanisms controlling actin filament dynamics in nonmuscle cells." Annu Rev Biophys Biomol Struct **29**: 545-576.

Ponting, C. P. (1997). "Evidence for PDZ domains in bacteria, yeast, and plants." Protein Sci **6**(2): 464-468.

Razinia, Z., T. Makela, J. Ylanne and D. A. Calderwood (2012). "Filamins in mechanosensing and signaling." Annu Rev Biophys **41**: 227-246.

Remaut, H. and G. Waksman (2006). "Protein-protein interaction through beta-strand addition." Trends Biochem Sci **31**(8): 436-444.

Sanger, J. W., S. Kang, C. C. Siebrands, N. Freeman, A. Du, J. Wang, A. L. Stout and J. M. Sanger (2005). "How to build a myofibril." J Muscle Res Cell Motil **26**(6-8): 343-354.

Sanger, J. W., J. Wang, Y. Fan, J. White and J. M. Sanger (2010). "Assembly and dynamics of myofibrils." J Biomed Biotechnol **2010**: 858606.

Saras, J. and C. H. Heldin (1996). "PDZ domains bind carboxy-terminal sequences of target proteins." Trends Biochem Sci **21**(12): 455-458.

Sawyer, G. M. and A. J. Sutherland-Smith (2012). "Crystal structure of the filamin N-terminal region reveals a hinge between the actin binding and first repeat domains." J Mol Biol **424**(5): 240-247.

Schroeter, M. and J. M. Chalovich (2004). "Ca2+-calmodulin regulates fesselin-induced actin polymerization." Biochemistry **43**(43): 13875-13882.

Seidel, S. A., P. M. Dijkman, W. A. Lea, G. van den Bogaart, M. Jerabek-Willemsen, A. Lazic, J. S. Joseph, P. Srinivasan, P. Baaske, A. Simeonov, I. Katritch, F. A. Melo, J. E. Ladbury, G. Schreiber, A. Watts, D. Braun and S. Duhr (2013). "Microscale

thermophoresis quantifies biomolecular interactions under previously challenging conditions." Methods **59**(3): 301-315.

Studier, F. W. (2005). "Protein production by auto-induction in high density shaking cultures." Protein Expr Purif **41**(1): 207-234.

Styers, M. L., A. P. Kowalczyk and V. Faundez (2005). "Intermediate filaments and vesicular membrane traffic: the odd couple's first dance?" Traffic **6**(5): 359-365.

Sugi, T., T. Oyama, T. Muto, S. Nakanishi, K. Morikawa and H. Jingami (2007). "Crystal structures of autoinhibitory PDZ domain of Tamalin: implications for metabotropic glutamate receptor trafficking regulation." EMBO J **26**(8): 2192-2205.

Thompson, T. G., Y. M. Chan, A. A. Hack, M. Brosius, M. Rajala, H. G. Lidov, E. M. McNally, S. Watkins and L. M. Kunkel (2000). "Filamin 2 (FLN2): A muscle-specific sarcoglycan interacting protein." J Cell Biol **148**(1): 115-126.

Ulbricht, A., F. J. Eppler, V. E. Tapia, P. F. van der Ven, N. Hampe, N. Hersch, P. Vakeel, D. Stadel, A. Haas, P. Saftig, C. Behrends, D. O. Furst, R. Volkmer, B. Hoffmann, W. Kolanus and J. Hohfeld (2013). "Cellular mechanotransduction relies on tension-induced and chaperone-assisted autophagy." Curr Biol **23**(5): 430-435.

Vakeel, P. (2006). Biochemical and cellular characterization of filamin binding proteins in cross striated muscle., Universität Potsdam.

van der Flier, A. and A. Sonnenberg (2001). "Structural and functional aspects of filamins." Biochim Biophys Acta **1538**(2-3): 99-117.

van der Ven, P. F., E. Ehler, P. Vakeel, S. Eulitz, J. A. Schenk, H. Milting, B. Micheel and D. O. Furst (2006). "Unusual splicing events result in distinct Xin isoforms that associate differentially with filamin c and Mena/VASP." Exp Cell Res **312**(11): 2154-2167.

van der Ven, P. F., W. M. Obermann, B. Lemke, M. Gautel, K. Weber and D. O. Furst (2000). "Characterization of muscle filamin isoforms suggests a possible role of gamma-filamin/ABP-L in sarcomeric Z-disc formation." Cell Motil Cytoskeleton **45**(2): 149-162.

van der Ven, P. F., S. Wiesner, P. Salmikangas, D. Auerbach, M. Himmel, S. Kempa, K. Hayess, D. Pacholsky, A. Taivainen, R. Schroder, O. Carpen and D. O. Furst (2000). "Indications for a novel muscular dystrophy pathway. gamma-filamin, the muscle-specific filamin isoform, interacts with myotilin." J Cell Biol **151**(2): 235-248.

van Eldik, W., A. Beqqali, J. Monshouwer-Kloots, C. Mummery and R. Passier (2011). "Cytoskeletal heart-enriched actin-associated protein (CHAP) is expressed in striated and smooth muscle cells in chick and mouse during embryonic and adult stages." Int J Dev Biol **55**(6): 649-655.

von Nandelstadh, P., M. Ismail, C. Gardin, H. Suila, I. Zara, A. Belgrano, G. Valle, O. Carpen and G. Faulkner (2009). "A class III PDZ binding motif in the myotilin and FATZ families binds enigma family proteins: a common link for Z-disc myopathies." Mol Cell Biol **29**(3): 822-834.

Wakelam, M. J. (1985). "The fusion of myoblasts." Biochem J **228**(1): 1-12.

Wang, J., N. Shaner, B. Mittal, Q. Zhou, J. Chen, J. M. Sanger and J. W. Sanger (2005). "Dynamics of Z-band based proteins in developing skeletal muscle cells." Cell Motil Cytoskeleton **61**(1): 34-48.

Weins, A., K. Schwarz, C. Faul, L. Barisoni, W. A. Linke and P. Mundel (2001). "Differentiation- and stress-dependent nuclear cytoplasmic redistribution of myopodin, a novel actin-bundling protein." J Cell Biol **155**(3): 393-404.

Wienken, C. J., P. Baaske, U. Rothbauer, D. Braun and S. Duhr (2010). "Protein-binding assays in biological liquids using microscale thermophoresis." Nat Commun **1**: 100.

Yu, Y. P. and J. H. Luo (2006). "Myopodin-mediated suppression of prostate cancer cell migration involves interaction with zyxin." Cancer Res **66**(15): 7414-7419.

Yu, Y. P., G. C. Tseng and J. H. Luo (2006). "Inactivation of myopodin expression associated with prostate cancer relapse." Urology **68**(3): 578-582.

Zhou, Q., P. Ruiz-Lozano, M. E. Martone and J. Chen (1999). "Cypher, a striated muscle-restricted PDZ and LIM domain-containing protein, binds to alpha-actinin-2 and protein kinase C." J Biol Chem **274**(28): 19807-19813.

7. Curriculum Vitae

Eduardo Henrique Salviano Bezerra

Max F. Perutz Laboratories, University of Vienna

Campus Vienna Biocenter 5, 1030, Vienna, Austria

Academic career:

B.S Federal University of Ceará (Dept. of Department of Biological Sciences, with honor), Fortaleza-Brazil
2004-2008 Dissertation title: Structural analysis and ligand investigation of a lectin from *Canavalia brasiliensis* seeds/ Supervisor: Prof. Benildo Sousa Cavada

M.S Federal University of Ceará (Dept. of Department of Biochemistry and Molecular Biology,), Fortaleza-Brazil
2008-2010 Structural analysis of ConBr reveals molecular correlation between the carbohydrate recognition domain and endothelial nitric oxide production / Supervisor: Prof. Benildo Sousa Cavada

Ph.D MFPL, University of Vienna (Dept. of Structural and Computational Biology), Austria
2011- Expected to complete the thesis in Jul 2015/Supervisor: Prof. Kristina Djinovic-Carugo

Seminar presentations:

Structural characterization and interaction studies of myopodin isoform A with Z-disc binding partners
15th Heart of Europe bio-crystallography (HEC) Meeting, Beilngries (Germany), 28-30 September 2012

Structural characterization and interaction studies of myopodin isoform A with Z-disc binding partners
17th Heart of Europe bio-crystallography (HEC) Meeting, Berlin (Germany), 25-27 September 2014

Publications:

Linnemann, A., Vakeel, P., Bezerra, E., Orfanos, Z., Djinović-Carugo, K., Van Der Ven, P.F.M., Kirfel, G., Fürst, D.O. Myopodin is an F-actin bundling protein with multiple independent actin-binding regions. (2013) Journal of Muscle Research and Cell Motility, 34 (1), pp. 61-69.

Delatorre, P., Rocha, B.A.M., Simões, R.C., Pereira-Júnior, F.N., Silva, H.C., Bezerra, E.H.S., Bezerra, M.J.B., Marinho, E.S., Gadelha, C.A.A., Santi-Gadelha, T., Farias, D.L., Assreuy, A.M.S., Marques-Domingos, G.F.O., Nagano, C.S., Cavada, B.S. Mass spectrometry and X-ray diffraction analysis of two crystal types of dioclea virgata lectin: An antinociceptive protein candidate to structure/function analysis. (2011)Applied Biochemistry and Biotechnology, 164 (6), pp. 741-754.

Bezerra, E.H.S., Rocha, B.A.M., Nagano, C.S., Bezerra, G.D.A., Moura, T.R.D., Bezerra, M.J.B., Benevides, R.G., Sampaio, A.H., Assreuy, A.M.S., Delatorre, P., Cavada, B.S. Structural analysis of ConBr reveals molecular correlation between the carbohydrate recognition domain and endothelial NO synthase activation. (2011) Biochemical and Biophysical Research Communications, 408 (4), pp. 566-570.

Assreuy, A.M.S., Fontenele, S.R., De Freitas Pires, A., Fernandes, D.C., Rodrigues, N.V.F.C., Bezerra, E.H.S., Moura, T.R., Do Nascimento, K.S., Cavada, B.S. Vasodilator effects of Diocleinae lectins from the Canavalia genus. (2009) Naunyn-Schmiedeberg's Archives of Pharmacology, 380 (6), pp. 509-521.

Figueiredo, J.G., Da Silveira Bitencourt, F., Beserra, I.G., Teixeira, C.S., Luz, P.B., Bezerra, E.H.S., Mota, M.R.L., Assreuy, A.M.S., De Queiroz Cunha, F., Cavada, B.S., De Alencar, N.M.N. Antinociceptive activity and toxicology of the lectin from Canavalia boliviana seeds in mice. (2009) Naunyn-Schmiedeberg's Archives of Pharmacology, 380 (5), pp. 407-414.

Vasconcelos, S.M.M., Lima, S.R., Soares, P.M., Assreuy, A.M.S., de Sousa, F.C.F., Lobato, R.d.F.G., Vasconcelos, G.S., Santi-Gadelha, T., Bezerra, E.H.S., Cavada, B.S., Patrocínio, M.C.A. Central action of Araucaria angustifolia seed lectin in mice. (2009) Epilepsy and Behavior, 15 (3), pp. 291-293.

Moura, T.R., Bezerra, G.A., Bezerra, M.J.B., Teixera, C.S., Bezerra, E.H.S., Benevides, R.G., Da Rocha, B.A.M., De Souza, L.A.G., Delatorre, P., Nagano, C.S., Cavada, B.S. Crystallization and preliminary X-ray diffraction analysis of the lectin from Canavalia boliviana Piper seeds. (2009) Acta Crystallographica Section F: Structural Biology and Crystallization Communications, 65 (3), pp. 213-215.

de Oliveira, T.M., Delatorre, P., da Rocha, B.A.M., de Souza, E.P., Nascimento, K.S., Bezerra, G.A., Moura, T.R., Benevides, R.G., Bezerra, E.H.S., Moreno, F.B.M.B., Freire, V.N., de Azevedo Jr., W.F., Cavada, B.S. Crystal structure of Dioclea rostrata lectin: Insights into understanding the pH-dependent dimer-tetramer equilibrium and the structural basis for carbohydrate recognition in Diocleinae lectins. (2008) Journal of Structural Biology, 164 (2), pp. 177-182.

Research Experience

Molecular biology and biochemistry, Molecular cloning, protein expression and purification with a variety of chromatographic techniques
Biophysics, ITC, CD spectroscopy, Dynamic Light Scattering, SEC-MALLS, Thermofluor
X-ray Crystallography, Protein crystallization, data processing and structure determination, data collection by synchrotron radiation at ESRF, EMBLand Diamond Light Source, software skill (CCP4, PHENIX, XDS, Coot, Pymol)

Structures:

Crystal structure of Crystal structure of a lectin from *Canavalia brasiliensis* seed (ConBr) complexed with alpha-aminobutyric acid (1.8 Å) by MR (2009)

Crystal structures of myopodin PDZ domain in complex with synemin peptide (1.9 Å), VPS18 peptide (2.35 Å) and ACTN2 peptide (1.95 Å) by MR (planned to submit to PDB in 2015)